5. RESULTS

The chemical, mineralogical, milling and flotation characteristics of the fourteen samples are compared in Table 5.1.

5.1 Chemical composition

The chemical compositions of the samples are reported in terms of major element oxide, sulphur, nickel, copper and platinum-group element contents (Table 5.1A to D). Cr_2O_3 contents for the fourteen samples vary between 20.05 and 34.58%. Note the relatively high TiO_2 contents of samples A4, B4 and C1.

Of particular interest are the relatively low sulphur and acid soluble copper and nickel values in samples from area C (C1 to C5) and, in the case of copper and sulphur, in samples B2, A2 and A5. Since copper occurs almost exclusively in sulphide minerals in the UG2 chromitite, total copper values are similar to acid soluble copper values (see analyses for samples A1 and C1). Total nickel values are considerably higher than acid soluble nickel indicating that most of the nickel occurs in phases other than sulphide minerals, probably predominantly in chromite (De Waal, 1975; Von Gruenewaldt, 1979), and to a lesser extent in silicate minerals. Curiously, although acid soluble nickel is low in samples from area C, total nickel values are similar or higher compared to the other samples. The Cu_{as}/Ni_{as}[+] ratio varies between 0.10 to 0.16, except for samples A3, B3, A4, B4 and C1 in which it is 0.20 or higher. As also observed by Smits (1988), very little of the cobalt appears to be present in acid soluble form.

Total PGE+Au[*] values range between 3.17 and 5.87 ppm with platinum the major PGE present at levels ranging between 2.13 and 3.34 ppm, representing between 55 and 67 per cent of the total PGE+Au. Palladium ranges from 0.66 to 2.05 ppm (21 to 36 per cent of the total PGE+Au) and rhodium between 0.33 and 0.61 ppm (9 to 11 per cent of the total PGE+Au).

[+] as = acid soluble
[*] Total PGE+Au refers to Σ(Pt,Pd,Rh,Au)

Table 5.1 *Chemical, mineralogical, milling and flotation characteristics of fourteen samples of UG2 chromitite.*

Sample locality	***An fw***	***Nor fw***	***Peg fw***		***Pothole***		***RPeg fw***	***Faulted***	***Faulted***	***Pothole***	***Nor fw***	***Faulted***	***Peg fw***	***An fw***
	A2	***B2***	***A1***	***B1***	***A3***	***B3***	***A4***	***B4***	***A5***	***C1***	***C2***	***C3***	***C4***	***C5***
A. Major element oxide composition (mass %)														
Cr_2O_3	29.10	20.90	29.33	25.05	33.80	30.70	34.50	32.90	27.70	34.58	31.80	32.40	31.20	33.80
Fe_2O_3	22.30	18.40	22.58	22.97	25.40	23.30	28.00	28.30	22.40	27.48	24.00	24.50	23.00	25.20
CaO	3.27	4.77	2.67	2.71	2.45	3.03	2.33	2.47	3.38	2.14	2.84	2.20	2.95	2.14
MgO	10.20	11.50	10.60	14.55	9.35	10.10	10.40	9.73	11.50	9.46	9.23	9.81	9.83	10.40
Al_2O_3	18.10	16.70	16.78	13.40	16.80	16.90	14.90	15.05	16.40	15.33	17.60	17.10	17.80	16.10
SiO_2	17.10	27.30	16.11	20.20	12.50	15.20	10.40	11.70	16.00	10.40	13.90	12.80	15.05	12.50
TiO_2	0.71	0.55	0.67	0.66	0.73	0.69	0.97	1.02	0.57	0.95	0.74	0.78	0.67	0.76
MnO	0.18	0.17	0.19	0.20	0.19	0.19	n.d.	0.21	0.23	0.21	0.19	0.19	0.19	0.20
Na_2O	n.d.	n.d.	0.64	0.60	n.d.	0.60	0.13	0.35	0.05	0.36	0.61	0.53	0.66	0.43
K_2O	n.d.	n.d.	0.12	0.16	n.d.	0.09	0.01	0.07	0.47	0.05	0.07	0.07	0.07	0.08
B. Cu, Ni, Co and S determined by chemical analysis														
S (%)	0.02	0.01	0.03	0.05	0.04	0.03	0.05	0.08	0.02	0.01	0.01	0.01	0.01	0.01
Ni_{total} *(ppm)* $^{+}$	1000	1000	1070	1450	1300	1150	1148	1335	914	1151	1400	1400	1300	1400
$Ni_{acid\ soluble}$ *(ppm)* $^{+}$	238	126	271	525	151	202	295	316	356	82	114	108	114	88
Co_{total} *(ppm)*	n.d.	n.d.	170	n.d.	n.d.	n.d.	n.d.	n.d.	n.d.	225	n.d.	n.d.	n.d.	n.d.
$Co_{acid\ soluble}$ *(ppm)*	n.d.	n.d.	28	n.d.	n.d.	n.d.	n.d.	n.d.	n.d.	<20	n.d.	n.d.	n.d.	n.d.
Cu_{total} *(ppm)*	n.d.	n.d.	75	n.d.	n.d.	n.d.	n.d.	n.d.	n.d.	60	n.d.	n.d.	n.d.	n.d.
$Cu_{acid\ soluble}$ *(ppm)*	48	42	73	95	107	91	109	170	44	57	45	47	30	35
$Ni_{acid\ soluble}/Ni_{total}$	0.29	0.30	0.39	0.50	0.34	0.35	0.48	0.42	0.38	0.24	0.22	0.21	0.20	0.20
$Cu_{acid\ soluble}/Ni_{acid\ soluble}$	0.20	0.33	0.25	0.18	0.71	0.45	0.37	0.54	0.12	0.70	0.40	0.44	0.26	0.40

An fw = Anorthosite footwall Nor fw = Norite footwall Peg fw = Pegmatoid footwal Pothole = Pothole edge RPeg fw = Replacement pegmatoid footwall Faulted = Faulted UG2

n.d. = not determined $^{+}$ Ni analyses performed on samples crushed to <2mm to avoid contamination by stainless steel

Table 5.1 continued *Chemical, mineralogical, milling and flotation characteristics of fourteen samples of UG2 chromitite*

Sample locality	***An fw***	***Nor fw***	***Peg fw***		***Pothole***		***RPeg fw***	***Faulted***	***Faulted***	***Pothole***	***Nor fw***	***Faulted***	***Peg fw***	***An fw***
	A2	***B2***	***A1***	***B1***	***A3***	***B3***	***A4***	***B4***	***A5***	***C1***	***C2***	***C3***	***C4***	***C5***
C. PGE content														
Pt (ppm)	2.13	2.04	3.08	2.42	3.67	2.81	3.05	3.34	3.13	3.03	2.97	3.25	2.90	3.06
Pd (ppm)	0.66	1.17	1.41	1.30	1.57	1.43	1.48	1.87	2.05	1.04	1.14	1.12	0.94	1.31
Rh (ppm)	0.35	0.33	0.43	0.37	0.61	0.43	0.46	0.53	0.52	0.45	0.47	0.55	0.47	0.50
Ru (ppm)	0.74	0.58	1.08	0.68	0.94	n.d.	n.d.	n.d.	n.d.	n.d.	n.d.	n.d.	n.d.	n.d.
Ir (ppm)	0.19	0.16	0.22	0.19	0.25	n.d.	n.d.	n.d.	n.d.	n.d.	n.d.	n.d.	n.d.	n.d.
Au (ppm)	0.04	0.02	0.07	0.03	0.02	0.05	0.04	0.07	0.05	<0.05	<0.05	<0.05	<0.05	<0.05
PGE+Au (ppm)	3.17	3.55	4.99	4.12	5.87	4.71	5.02	5.81	5.74	4.52	4.58	4.92	4.31	4.87
D. PGE distribution														
Pt (%)	67.14	57.35	61.72	58.74	62.52	59.54	60.75	57.48	54.53	67.04	64.85	66.06	67.29	62.83
Pd (%)	20.70	32.93	28.26	31.55	26.75	30.35	29.38	32.18	35.63	23.01	24.89	22.76	21.81	26.90
Rh (%)	11.06	9.15	8.62	8.98	10.39	9.13	9.06	9.12	9.06	9.96	10.26	11.18	10.90	10.27
E. Bulk modal analysis measured by image analysis. Precision determined at the 95% confidence level. Chromite content measured by image analysis (i.a.) is compared with chromite content calculated from Cr_2O_3 values.														
BMS (mass %)	0.10 ±0.03	0.11 ±0.05	0.13 ±0.02	0.17 ±0.04	0.11 ±0.02	0.15 ±0.08	0.18 ±0.04	0.15 ±0.02	0.09 ±0.08	0.03 ±0.01	0.07 ±0.03	0.04 ±0.01	0.04 ±0.01	0.04 ±0.02
Chromite (mass %)(IA)	64.6 ±1.2	50.1 ±3.8	65.7 ±1.1	58.3 ±1.9	71.9 ±2.7	62.4 ±2.9	70.5 ±6.8	68.8 ±1.5	54.3 ±2.7	75.9 ±1.2	71.4 ±2.1	67.3 ±2.2	67.7 ±2.3	65.3 ±4.2
Chromite (mass %) (calc)	67.9	48.8	68.4	58.4	78.9	71.6	80.5	76.8	64.6	80.7	74.2	75.6	72.8	78.9
Difference	3.3	-1.3	2.7	0.2	6.9	9.2	10.0	8.0	10.3	4.8	2.8	8.3	5.1	13.5
Silicate (mass %)	35.3 ±0.7	49.8 ±2.4	34.1 ±0.7	41.6 ±1.2	28.0 ±1.7	37.4 ±1.9	29.4 ±4.4	31.1 ±1.0	45.6 ±1.9	24.1 ±0.7	28.5 ±1.3	32.7 ±1.4	32.2 ±1.4	34.6 ±2.7

An fw = Anorthosite footwall Nor fw = Norite footwall Peg fw = Pegmatoid footwal Pothole = Pothole edge RPeg fw = Replacement pegmatoid footwall Faulted = Faulted UG2

n.d. = not determined PGE+Au =Σ(Pt,Pd,Rh,Au) BMS=base-metal sulphide

Table 5.1 continued *Chemical, mineralogical, milling and flotation characteristics of fourteen samples of UG2 chromitite*

Sample locality	***An fw***	***Nor fw***	***Peg fw***		***Pothole***		***RPeg fw***	***Faulted***	***Faulted***	***Pothole***	***Nor fw***	***Faulted***	***Peg fw***	***An fw***
	A2	***B2***	***A1***	***B1***	***A3***	***B3***	***A4***	***B4***	***A5***	***C1***	***C2***	***C3***	***C4***	***C5***
F. Relative proportions of sulphide minerals (volume %). Precision determined at the 95% confidence level.														
Chalcopyrite	27 ±4	29±6	24±4	25±5	28±8	19±5	26±10	15±1	23±8	43±9	32±15	54±13	34±10	49±6
Pentlandite	52±3	48±6	49±4	45±4	46±7	55±9	51±8	46±7	71±8	2±1	5±3	5±2	5±5	5±6
Pyrrhotite	13±4	4±2	19±3	29±7	14±4	25±5	22±5	35±7	6±4	-	1±1	2±3	5±5	0±2
Pyrite	8±1	16±5	8±1	1±1	11±6	1±1	1±0	3±2	-	11±8	31±13	15±16	16±4	20±5
Millerite	-	2±1	-	-	-	-	-	-	-	43±6	32±7	24±10	41±9	26±1
G. Sulphide modal composition in mass %, calculated from E and F. Precision determined at the 95% confidence level.														
Chalcopyrite	0.02 ±0.01	0.03 ±0.02	0.03 ±0.01	0.04 ±0.01	0.03 ±0.01	0.02 ±0.02	0.04 ±0.02	0.02 ±0.00	0.01 ±0.01	0.01 ±0.00	0.01 ±0.01	0.02 ±0.01	0.01 ±0.00	0.01 ±0.01
Pentlandite	0.05 ±0.02	0.05 ±0.02	0.07 ±0.02	0.08 ±0.02	0.05 ±0.01	0.07 ±0.05	0.09 ±0.02	0.07 ±0.01	0.07 ±0.03	0.00 ±0.00	0.00 ±0.00	0.00 ±0.00	0.00 ±0.00	0.00 ±0.00
Pyrrhotite	0.01 ±0.01	0.00 ±0.00	0.02 ±0.01	0.04 ±0.02	0.01 ±0.00	0.04 ±0.03	0.04 ±0.01	0.05 ±0.01	0.00 ±0.00	0.00 ±0.00	0.00 ±0.00	0.00 ±0.00	0.00 ±0.00	0.00 ±0.00
Pyrite	0.01 ±0.00	0.02 ±0.01	0.02 ±0.00	0.01 ±0.00	0.01 ±0.01	0.00 ±0.00	0.00 ±0.00	0.01 ±0.00	0.00 ±0.00	0.00 ±0.00	0.03 ±0.02	0.00 ±0.00	0.01 ±0.00	0.02 ±0.02
Millerite	0.00 ±0.00	0.00 ±0.00	0.00 ±0.00	0.00 ±0.00	0.00 ±0.00	0.00 ±0.00	0.00 ±0.00	0.00 ±0.00	0.00 ±0.00	0.01 ±0.01	0.02 ±0.01	0.01 ±0.00	0.02 ±0.01	0.01 ±0.00
H. Pentlandite/millerite ratio expressed as mass % pentlandite/(mass % pentlandite + mass % millerite)														
pn/(pn+mil)	0.998	0.935	0.996	1.000	0.997	0.998	0.999	0.999	1.000	0.045	0.043	0.156	0.038	0.129
I. S and acid soluble Cu, Ni, and Fe calculated from image analysis measurements														
S (%)	0.03	0.04	0.05	0.06	0.04	0.05	0.06	0.05	0.03	0.01	0.03	0.01	0.01	0.02
Cu (ppm)	78	99	93	137	106	77	134	69	47	31	50	69	39	37
Ni (ppm)	160	171	209	246	164	238	287	217	224	86	158	63	120	47
Fe in BMS (ppm)	241	250	306	387	269	324	427	297	280	30	50	67	38	38

An fw = Anorthosite footwall Nor fw = Norite footwall Peg fw = Pegmatoid footwal Pothole = Pothole edge RPeg fw = Replacement pegmatoid footwall Faulted = Faulted UG2

Table 5.1 continued. *Chemical, mineralogical and flotation characteristics of fourteen samples of UG2 chromitite.*

Sample locality	***An fw***	***Nor fw***	***Peg fw***		***Pothole***		***RPeg fw***	***Faulted***	***Faulted***	***Pothole***	***Nor fw***	***Faulted***	***Peg fw***	***An fw***
	A2	***B2***	***A1***	***B1***	***A3***	***B3***	***A4***	***B4***	***A5***	***C1***	***C2***	***C3***	***C4***	***C5***
J. Chromite equivalent circle diameter calculated from area measurements (µm)														
20th percentile	102	98	105	108	117	120	84	143	72	110	103	104	83	113
median	164	164	169	177	191	187	221	221	127	184	173	175	142	177
80th percentile	250	266	252	269	298	273	356	322	194	294	276	267	222	260
K. Relative proportions of silicate minerals (volume %)														
*Ca-Al-silicate**	n.d.	n.d.	66	n.d.	68	56	24	25	50	69	75	n.d.	66	n.d.
Mg-Fe-silicate+	n.d.	n.d.	30	n.d.	28	33	47	49	18	15	17	n.d.	30	n.d.
Phlogopite	n.d.	n.d.	2	n.d.	1	3	<1	<1	1	<1	1	n.d.	1	n.d.
Clinopyroxene	n.d.	n.d.	1	n.d.	<1	6	22	23	8	1	<1	n.d.	<1	n.d.
Quartz	n.d.	n.d.	<1	n.d.	<1	<1	<1	<1	1	3	1	n.d.	<1	n.d.
Chlorite	n.d.	n.d.	<1	n.d.	1	1	1	1	13	4	3	n.d.	1	n.d.
Amphibole	n.d.	n.d.	<1	n.d.	<1	<1	1	1	4	1	2	n.d.	1	n.d.
Albite	n.d.	n.d.	<1	n.d.	<1	<1	<1	<1	4	6	1	n.d.	1	n.d.
K-Al-silicate°	n.d.	n.d.	<1	n.d.	<1	<1	<1	<1	<1	1	<1	n.d.	<1	n.d.

An fw = Anorthosite footwall Nor fw = Norite footwall Peg fw = Pegmatoid footwal Pothole = Pothole edge RPeg fw = Replacement pegmatoid footwall Faulted = Faulted UG2

n.d. = not determined

* *Predominantly plagioclase. Also includes pumpellyite, prehnite and epidote, especially in samples from area C.*

\+ *Predominantly orthopyroxene, minor talc, and rarely serpentine and olivine*

° *K-feldspar and sericite*

Table 5.1 continued. *Chemical, mineralogical and flotation characteristics of fourteen samples of UG2 chromitite.*

Sample locality	***An fw***	***Nor fw***	***Peg fw***		***Pothole***		***RPeg fw***	***Faulted***	***Faulted***	***Pothole***	***Nor fw***	***Faulted***	***Peg fw***	***An fw***
	A2	***B2***	***A1***	***B1***	***A3***	***B3***	***A4***	***B4***	***A5***	***C1***	***C2***	***C3***	***C4***	***C5***
L. BMS mode of occurrence and grain size in feed samples crushed to <2mm (area %)														
BMS median ECD (μm)	32	30	32	30	39	33	45	38	17	19	21	22	22	17
Liberated BMS	24	12	16	13	21	2	2	8	3	8	18	15	18	11
Grain boundary	60	80	73	74	56	72	68	71	37	68	46	49	55	42
*Locked in oxide**	1	4	1	3	3	2	1	1	7	3	3	1	3	6
Locked in silicate•	15	5	11	10	19	24	29	20	53	20	33	36	24	41
Predicted BMS liberation+	84	92	89	87	78	74	70	79	40	76	64	64	73	53
M. Relative proportions of PGE minerals (PGEM) (volume %). Statistical uncertainty determined at the 90% confidence level and reported as absolute variation.														
Number of grains	543	471	1766	426	433	420	420	437	425	441	445	400	425	385
Pt-Pd-Ni-S	21±7	38±10	36±6	20±5	17±9	26±7	2±1	7±6	14±5	39±7	33±12	37±8	36±11	38±11
Pt-S	26±8	8±3	19±5	20±5	26±7	15±4	5±2	6±3	1±1	2±1	4±2	3±2	3±2	7±6
Pt-Rh-Cu- Ni-S	24±5	28±8	18±4	10±3	27±7	13±5	4±3	2±1	11±5	33±7	42±15	35±9	40±9	29±7
Ru-Os-Ir-S	23±6	17±6	19±4	27±7	22±6	29±7	31±8	33±8	30±9	22±7	16±6	20±9	18±5	23±8
PGE-Bi-Te	1±0	0±0	2±1	3±1	1±1	3±2	4±2	3±1	3±1	0±0	1±2	0±0	0±0	1±1
PGE-As-S	2±1	6±7	3±2	5±4	2±1	2±1	1±1	2±3	9±5	2±1	2±1	2±1	1±1	1±1
Pt-Fe alloy	2±1	0±0	2±1	9±4	5±4	10±4	40±8	45±9	17±9	0±0	0±0	0±0	0±0	0±0
Other non-sulphide PGEM	1±1	2±1	2±1	7±2	1±1	3±2	14±5	2±2	17±5	2±1	2±1	3±1	2±1	2±2

An fw = Anorthosite footwall Nor fw = Norite footwall Peg fw = Pegmatoid footwal Pothole = Pothole edge RPeg fw = Replacement pegmatoid footwall Faulted = Faulted UG2

n.d. = not determined

ECD = equivalent circle diameter

* May also be at oxide-oxide grain boundaries

• May also be at silicate-silicate grain boundaries

+ Predicted BMS liberation = area % BMS at grain boundaries+liberated BMS

Table 5.1 continued. *Chemical, mineralogical and flotation characteristics of fourteen samples of UG2 chromitite*

Sample locality	***An fw***	***Nor fw***	***Peg fw***		***Pothole***		***RPeg fw***	***Faulted***	***Faulted***	***Pothole***	***Nor fw***	***Faulted***	***Peg fw***	***An fw***
	A2	***B2***	***A1***	***B1***	***A3***	***B3***	***A4***	***B4***	***A5***	***C1***	***C2***	***C3***	***C4***	***C5***
N. PGE mineral (PGEM) modal composition (volume %).														
Total non-sulphide PGEM	7	11	12	32	11	24	84	77	81	5	6	7	4	5
O. PGE mineral median equivalent circle diameter (ECD) (µm) in feed samples at <2mm														
By number	2.6	2.2	2.5	1.8	2.8	1.9	1.8	2.5	1.8	2.9	2.9	2.8	2.9	2.7
By area	5.6	8.0	7.2	4.2	5.5	3.9	3.9	6.2	3.0	6.3	10.2	9.4	8.1	5.3
P. PGE mineral mode of occurrence in feed samples at <2mm (area %). Statistical uncertainty determined at the 90% confidence level and reported as absolute variation.														
Number of grains	334	257	665	228	184	214	199	199	196	179	205	189	207	192
Liberated PGEM	13±7	11±9	7±6	11±6	10±7	1±1	1±1	-	-	9±10	3±3	14±13	19±16	-
Locked in BMS	23±8	24±8	26±9	32±8	27±14	26±8	27±8	40±19	7±4	7±4	8±5	0±0	12±8	6±4
Locked in chromite	7±4	4±3	2±1	9±10	3±2	12±9	12±10	6±5	8±5	2±2	4±3	6±3	5±3	7±4
Locked in silicate	6±3	10±10	2±1	10±5	12±5	5±2	10±6	12±6	44±9	42±11	40±17	29±11	34±10	44±12
BMS/Gangue GB	44±10	42±14	57±10	30±8	31±10	53±10	40±10	30±12	25±9	20±8	37±21	25±12	16±8	19±7
Chromite/Silicate GB	7±4	10±8	6±5	8±4	17±8	4±2	10±6	11±6	16±5	20±9	8±5	26±10	15±7	23±8
Predicted PGEM liberation[+]	82	83	89	83	71	75	77	74	45	45	46	48	49	55
Q. Volume % PGE mineral associated with different base-metal sulphides in feed samples at <2mm														
Number of grains	241	236	512	174	90	71	157	127	54	54	62	34	49	51
Chalcopyrite	23	15	26	22	11	48	22	17	2	24	21	3	2	8
Pentlandite	60	61	49	74	67	38	72	68	98	2	8	32	2	43
Pyrrhotite	1	0	11	3	2	8	6	13	-	-	-	3	-	-
Pyrite	16	22	14	1	20	6	-	2	-	10	29	6	45	6
Millerite	-	2	-	-	-	-	-	-	-	45	31	35	41	41
Siegenite	-	0	-	-	-	-	-	-	-	20	11	21	10	2

An fw = Anorthosite footwall Nor fw = Norite footwall Peg fw = Pegmatoid footwal Pothole = Pothole edge RPeg fw = Replacement pegmatoid footwall Faulted = Faulted UG2

BMS = base-metal sulphide PGEM=platinum-group element mineral GB=grain boundary

Total Non-sulphide PGEM = (Pt-Fe alloy+PGE-As-S+PGE-Bi-Te+other non-sulphide PGEM)/Total PGEM (excluding laurite)

Predicted PGEM liberation = (liberated PGEM+PGEM at grain boundaries)+(PGEM assoaciated with BMS*predicted BMS liberation)

Table 5.1 continued. *Chemical, mineralogical and flotation characteristics of fourteen samples of UG2 chromitite*

Sample locality	*An fw*	*Nor fw*	*Peg fw*		*Pothole*		*RPeg fw*	*Faulted*	*Faulted*	*Pothole*	*Nor fw*	*Faulted*	*Peg fw*	*An fw*
	A2	*B2*	*A1*	*B1*	*A3*	*B3*	*A4*	*B4*	*A5*	*C1*	*C2*	*C3*	*C4*	*C5*
R. Median chromite grain diameter at 80%<75 µm based on area measurements														
Median ECD (µm)	44	38	40	41	36	38	37	41	32	42	39	41	n.d.	38
S. Median silicate grain diameter at 80%<75 µm based on area measurements														
Median ECD (µm)	39	35	34	35	34	32	31	35	30	36	32	34	n.d.	34
T. Cumulative BMS liberation and grain size at 80%<75 µm based on area measurements														
Median BMS ECD (µm)	13	12	10	12	10	10	11	10	7	7	11	9	9	2
0.8-1.0	95	100	96	99	87	92	70	99	69	48	91	88	84	33
0.6-0.8	95	100	96	99	87	92	70	99	69	48	91	88	84	33
0.4-0.6	95	100	96	99	87	98	92	99	69	58	91	88	84	33
0.2-0.4	95	100	96	99	90	100	95	99	69	78	91	88	84	46
U. PGE mineral mode of occurrence in feed samples at 80%<75µm. 90% confidence limits were calculated using resampling statistics (area %)														
Number of grains	185	193	619	187	217	190	211	217	216	236	185	191	203	183
Liberated PGEM	49±12	48±15	57±6	64±9	61±15	57±11	76±8	67±13	47±16	62±11	61±12	54±10	61±11	76±11
PGEM+Liberated BMS	28±9	38±15	30±6	18±8	9±5	26±9	16±6	25±14	0±0	6±4	7±6	5±3	5±4	0±0
PGM+(BMS)+Gangue	23±10	14±7	13±4	17±6	30±16	17±6	9±4	9±4	52±16	32±10	32±11	41±10	34±11	24±12
PGEM/(PGEM+BMS)	0.6	0.6	0.7	0.7	0.8	0.6	0.7	0.8	0.9	0.9	0.9	0.9	0.9	0.9
V. Combined liberation index of PGE-bearing particles in feed samples at 80%<75µm (area %). 90% confidence limits calculated using resampling statistics.														
0.0-0.2	15±7	11±6	8±3	12±5	8±5	14±6	4±2	8±3	39±11	22±9	15±7	26±9	28±11	14±8
0.2-0.4	5±7	0±0	0±0	0±0	15±15	0±0	1±1	1±1	4±3	1±1	10±9	4±5	4±5	1±8
0.4-0.6	0±0	2±2	0±0	3±2	3±2	2±2	0±0	0±0	5±4	6±6	5±7	8±8	1±0	6±1
0.6-0.8	1±2	1±1	0±0	3±2	5±7	0±0	2±3	0±0	4±4	1±2	1±2	3±4	1±1	2±2
0.8-1.0	79±9	87±7	92±3	83±6	69±16	84±6	93±4	91±3	48±15	70±10	69±11	59±11	66±12	77±11

An fw = Anorthosite footwall Nor fw = Norite footwall Peg fw = Pegmatoid footwal Pothole = Pothole edge RPeg fw = Replacement pegmatoid footwall Faulted = Faulted UG2

BMS = base-metal sulphide PGEM=platinum-group element mineral GB=grain boundary

PGEM/(PGEM+BMS)= %liberated PGEM/(%liberated PGEM+PGEM associated with liberated BMS)

Table 5.1 continued. *Chemical, mineralogical and flotation characteristics of fourteen samples of UG2 chromitite*

Sample locality	***An fw***	***Nor fw***	***Peg fw***		***Pothole***		***RPeg fw***	***Faulted***	***Faulted***	***Pothole***	***Nor fw***	***Faulted***	***Peg fw***	***An fw***
	A2	***B2***	***A1***	***B1***	***A3***	***B3***	***A4***	***B4***	***A5***	***C1***	***C2***	***C3***	***C4***	***C5***
W. Combined liberation index of PGE-bearing particles other than laurite in feed samples at 80%<75µm (area %).														
n	156	163	502	157	191	152	162	168	182	208	160	171	173	162
0.0-0.2	16	9	7	12	8	12	4	6	36	16	8	27	23	12
0.2-0.4	7	0	0	0	15	0	1	1	5	2	12	5	1	1
0.4-0.6	0	2	0	3	3	2	0	0	6	7	6	10	2	1
0.6-0.8	2	1	0	3	5	0	3	0	5	0	2	3	1	2
0.8-1.0	75	88	92	83	69	85	91	93	49	74	72	56	73	83
X. PGE mineral median equivalent circle diameter (µm) in feed samples at 80%<75µm														
By number	1.9	2.1	2.1	2.1	1.8	2.2	1.6	2.2	2.0	2.3	2.4	2.0	2.3	2.2
By area	3.9	5.5	3.8	3.9	5.9	5.0	3.9	4.2	4.8	3.9	5.4	4.1	4.9	6.9
Y. Time to reduce sample to 80%<75µm														
Time (minutes)	95	72	117	72	106	90	80	72	40	60	72	69	96	74
Z. Cu flotation characteristics														
R_f	61.6	57.3	66.2	76.6	60.0	74.5	54.5	70.4	55.4	34.0	37.3	32.2	34.4	39.0
R_s	24.0	25.7	20.6	15.7	25.7	17.0	30.7	22.2	28.5	24.7	28.2	25.3	29.3	34.6
100-U	14.4	16.9	13.2	7.7	14.3	8.5	14.8	7.4	16.0	41.3	34.5	42.5	36.3	26.4
k_f	2.02	2.06	2.24	3.08	2.01	2.07	1.73	2.05	2.04	1.76	1.74	1.57	1.49	1.92
k_s	0.18	0.20	0.16	0.15	0.17	0.16	0.21	0.14	0.14	0.14	0.13	0.12	0.15	0.17

An fw = Anorthosite footwall Nor fw = Norite footwall Peg fw = Pegmatoid footwal Pothole = Pothole edge RPeg fw = Replacement pegmatoid footwall Faulted = Faulted UG2

BMS=base-metal sulphide equivalent circle diameter BMS liberation index= area of BMS/total area of particle

R_f= recovery of fast-floating material R_s= recovery of slow-floating material 100-U=non-floating fraction

k_f= fast-floating rate constant k_s= slow-floating rate constant

Table 5.1 continued *Chemical, mineralogical, milling and flotation characteristics of fourteen samples of UG2 chromitite*

Sample locality	*An fw*	*Nor fw*	*Peg fw*		*Pothole*		*RPeg fw*	*Faulted*	*Faulted*	*Pothole*	*Nor fw*	*Faulted*	*Peg fw*	*An fw*
	A2	*B2*	*A1*	*B1*	*A3*	*B3*	*A4*	*B4*	*A5*	*C1*	*C2*	*C3*	*C4*	*C5*
AA. Ni flotation characteristics														
R_f	32.4	24.3	38.1	22.7	31.8	37.2	28.1	20.6	19.5	17.7	19.8	14.0	17.8	18.4
R_s	28.7	27.4	22.4	19.1	29.3	26.9	35.7	48.0	29.3	31.4	35.2	29.9	31.7	30.0
100-U	38.9	48.2	39.5	58.2	38.9	35.9	36.2	31.5	51.2	50.9	45.0	56.1	50.5	51.6
k_f	1.41	1.72	1.92	1.91	1.64	1.82	1.20	1.36	1.32	1.42	1.50	1.19	0.99	1.28
k_s	0.17	0.18	0.14	0.14	0.17	0.15	0.17	0.16	0.12	0.12	0.12	0.10	0.13	0.11
AB. PGE+Au flotation characteristics														
R_f	75.1	73.8	79.8	80.3	63.4	74.4	59.9	56.5	39.7	66.3	71.5	68.2	74.8	74.8
R_s	18.8	19.6	16.3	15.3	25.9	21.0	33.7	37.7	28.7	24.5	22.6	24.0	19.9	21.1
100-U	6.2	6.6	3.9	4.4	10.7	4.6	6.4	5.8	31.6	9.2	6.0	7.8	5.3	4.1
k_f	2.13	2.90	2.38	2.45	2.05	2.06	1.60	2.17	1.62	1.98	2.10	2.01	2.24	2.16
k_s	0.20	0.24	0.22	0.18	0.21	0.25	0.22	0.24	0.15	0.21	0.19	0.19	0.22	0.21
AC. Pt flotation characteristics														
R_f	77.3	83.1	81.6	72.4	68.5	79.5	71.5	70.4	32.9	69.2	72.3	71.7	76.7	78.6
R_s	17.4	13.4	14.4	19.6	22.9	15.7	22.7	24.3	34.9	22.5	21.8	21.2	18.3	17.6
100-U	5.2	3.4	4.0	8.0	8.6	4.7	5.8	5.3	32.2	8.3	5.9	7.1	4.9	3.8
k_f	1.91	2.44	2.13	2.27	1.74	1.74	1.41	1.68	1.31	1.68	1.81	1.78	1.97	1.88
k_s	0.06	0.07	0.07	0.05	0.05	0.06	0.07	0.08	0.02	0.05	0.07	0.06	0.07	0.08

An fw = Anorthosite footwall Nor fw = Norite footwall Peg fw = Pegmatoid footwal Pothole = Pothole edge RPeg fw = Replacement pegmatoid footwall Faulted = Faulted UG2

R_f= recovery of fast-floating material R_s= recovery of slow-floating material 100-U=non-floating fraction

k_f= fast-floating rate constant k_s= slow-floating rate constant

Table 5.1 continued *Chemical, mineralogical, milling and flotation characteristics of fourteen samples of UG2 chromitite*

Sample locality	***An fw***	***Nor fw***	***Peg fw***		***Pothole***		***RPeg fw***	***Faulted***	***Faulted***	***Pothole***	***Nor fw***	***Faulted***	***Peg fw***	***An fw***
	A2	***B2***	***A1***	***B1***	***A3***	***B3***	***A4***	***B4***	***A5***	***C1***	***C2***	***C3***	***C4***	***C5***
AD. Pd flotation characteristics														
R_f	73.0	79.3	79.1	68.8	61.4	77.2	59.8	56.5	31.9	66.1	73.2	67.1	74.1	76.0
R_s	20.5	15.8	15.9	22.3	27.4	17.6	31.8	36.6	34.6	23.3	19.9	22.7	18.7	18.4
100-U	6.5	4.9	5.1	8.9	11.2	5.2	8.5	6.8	33.6	10.6	6.9	10.2	7.3	5.5
k_f	1.71	2.44	2.11	1.98	1.65	1.80	1.19	1.54	1.38	1.87	2.07	1.78	2.01	2.02
k_s	0.06	0.06	0.06	0.05	0.05	0.06	0.07	0.09	0.02	0.04	0.06	0.05	0.05	0.06
AE. Rh flotation characteristics														
R_f	69.9	84.7	75.4	70.5	65.1	78.0	60.9	54.9	23.7	55.3	61.6	57.7	72.9	70.8
R_s	29.8	15.1	20.5	29.2	26.9	17.1	34.7	39.8	41.5	32.3	30.9	32.3	22.9	24.7
100-U	0.2	0.3	4.1	0.3	8.0	4.9	4.4	5.3	34.8	12.4	7.5	10.0	4.2	4.4
k_f	2.13	2.92	2.24	2.46	1.63	1.70	1.16	1.54	1.15	1.40	1.59	1.45	1.89	1.62
k_s	0.25	0.21	0.25	0.23	0.06	0.06	0.11	0.10	0.03	0.05	0.07	0.06	0.09	0.09

An fw = Anorthosite footwall Nor fw = Norite footwall Peg fw = Pegmatoid footwal Pothole = Pothole edge RPeg fw = Replacement pegmatoid footwall Faulted = Faulted UG2

R_f= recovery of fast-floating material R_s= recovery of slow-floating material 100-U=non-floating fraction

k_f= fast-floating rate constant k_s= slow-floating rate constant

5.2 Mineralogy of crushed feed samples

5.2.1 Bulk modal analysis

Image analysis results

Image analysis measurements indicated that the chromite content of the samples investigated range between 50.1 to 75.9 mass per cent (Table 5.1E). Base-metal sulphide minerals are present at concentration levels between 0.03 and 0.18 mass per cent, with the lowest values recorded in samples from area C, i.e. samples C1 to C5 (Table 5.1E).

Comparison with chemical assay values

Cr_2O_3 assay values were recalculated to mass per cent chromite, assuming an average Cr_2O_3 content in chromite of 42.86%.* Generally, there is good agreement between the chromite content measured by image analysis, and the chromite content calculated from Cr_2O_3 values, with differences smaller than 10 per cent for most samples (Table 5.1E). Most of the differences can be ascribed to plucking out of chromite grains during polishing, especially in samples containing sintered chromite on which it is difficult to obtain a good polish. Deviations of the actual Cr_2O_3 content from the average value would also lead to discrepancies.

5.2.2 Base-metal sulphide modal composition

Image analysis results

The relative amounts of the different base-metal sulphides in the samples examined are reported in Table 5.1F and graphically depicted in Figure 26. With the exception of sample B2, samples from areas A and B are characterised by the presence of pentlandite, chalcopyrite, pyrrhotite and, to a lesser extent, pyrite. Qualitative EDS analysis indicated that Fe>Ni in pentlandite. In sample B2, pyrrhotite has been replaced by pyrite and the pentlandite is nickeliferous (Ni>Fe). Sample B2 also

---

* Based on the average of electron-microprobe analyses of chromite in Appendix D.

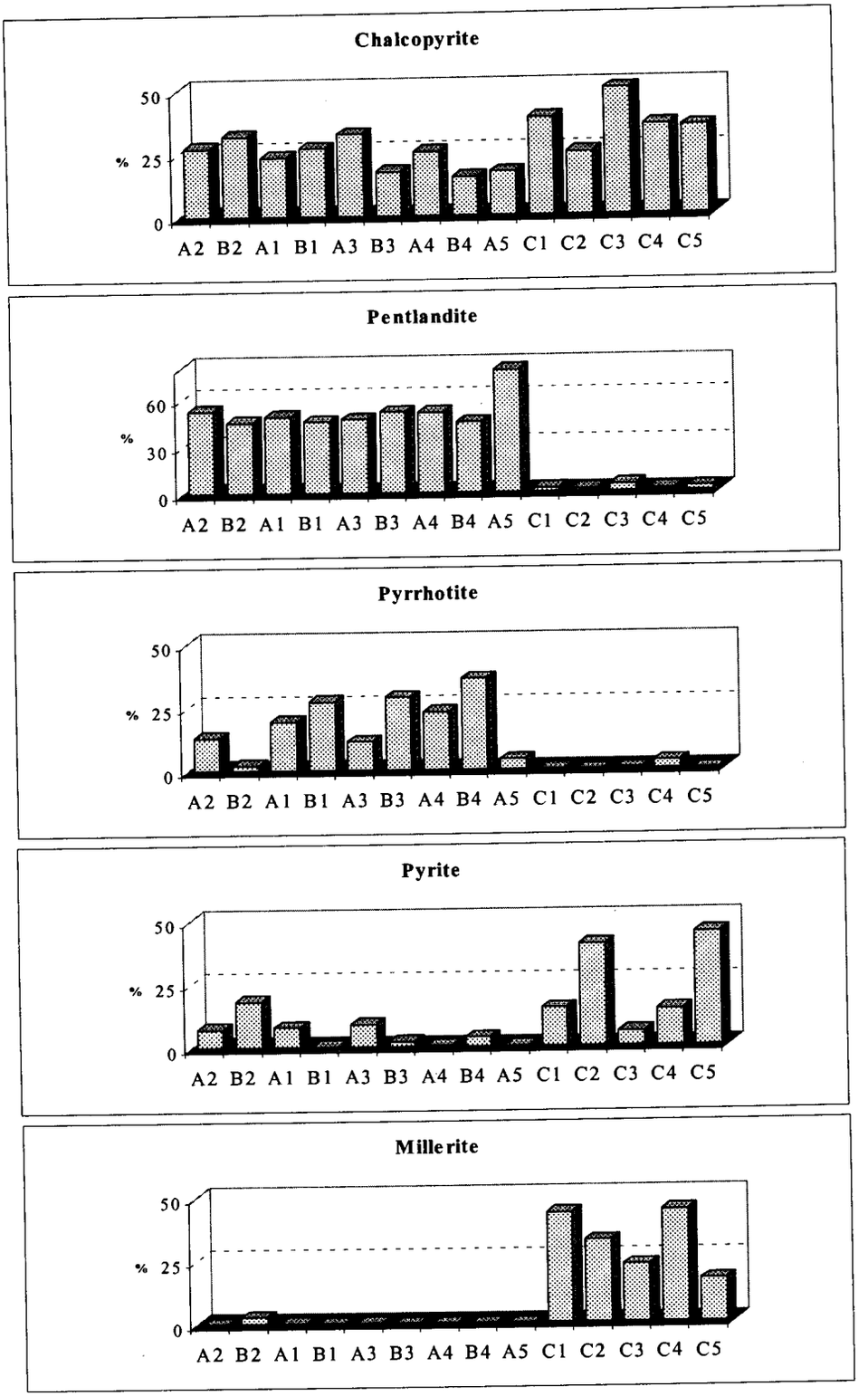

Figure 26 *Volumetric proportions of base-metal sulphide minerals in fourteen samples of UG2 chromitite.*

contains low but significant amounts of millerite, a mineral rarely encountered in samples from areas A and B.

Millerite, pyrite and chalcopyrite are the major base-metal sulphide phases in samples from area C, with pentlandite (Ni>Fe) and pyrrhotite representing minor components. Examination of polished sections of samples from area C by optical and scanning-electron microscopy also indicated the presence of occasional grains of siegenite.

Comparison with chemical assay values

From the modal amounts of pentlandite, chalcopyrite, millerite, pyrite and pyrrhotite (Table 5.1G), copper, nickel and sulphur contents were calculated for each sample. The following assumptions were made: copper content in chalcopyrite of 34.04%; nickel content in pentlandite and millerite of 31.75% and 62.24% respectively; iron content in chalcopyrite, pentlandite, pyrite, pyrrhotite and millerite of 30.44%, 33.81%, 44.69%, 61.41% and 1.27% respectively; and sulphur content in chalcopyrite, pentlandite, pyrite, pyrrhotite and millerite of 34.91%, 33.26%, 38.10%, 52.45% and 35.27% respectively.[+]

As a result of the low concentration levels of these elements, the associated measurement errors are considerable, and the chemical assay values for copper, nickel and sulphur do not always compare well with the calculated values (compare Table 5.1B with I). Nevertheless, the same general trends reported in section 5.1 could be discerned, in particular the low values of copper, nickel and sulphur in samples from area C. Note also the very low amounts of iron contained in sulphide minerals in samples from area C compared to samples from areas A and B – below 70 ppm compared to more than 240 ppm.

5.2.3 Chromite textures and grain-size distributions

Textural features of chromite in the samples investigated are similar to those described by Hiemstra (1985), Hulbert and Von Gruenewaldt (1985), and Eales and

---

[+] Based on the averages of electron-microprobe analyses of the sulphide minerals in Appendix F.

Reynolds (1986), ranging from scattered chromite subhedra in a silicate matrix (Figure 27), to patches where chromite grains appear to have been sintered together, resulting in large polygonal chromite grains with little or no interstitial silicate (Figure 28).

Chromite grain-size measurements (Figure 29 and Table 5.1J) indicate that the median measured chromite grain diameters for most samples (A1, A2, B1, B2, C2, C3, C4, C5) range between 164 and 177 μm. Due to the sintering of chromite grains, median chromite diameters in samples A3, B3, C1, and to a greater extent A4 and B4, are much larger, ranging between 184 and 221μm. All of the samples in the second group were associated with iron-rich replacement pegmatoid and/or potholes.

Minor fracturing of chromite grains was observed in most of the samples. Sample A5, collected from an intensely faulted area, is the only sample displaying extensive cataclasis (Figure 30). This is reflected in the small median measured chromite diameter of this sample (127 μm).

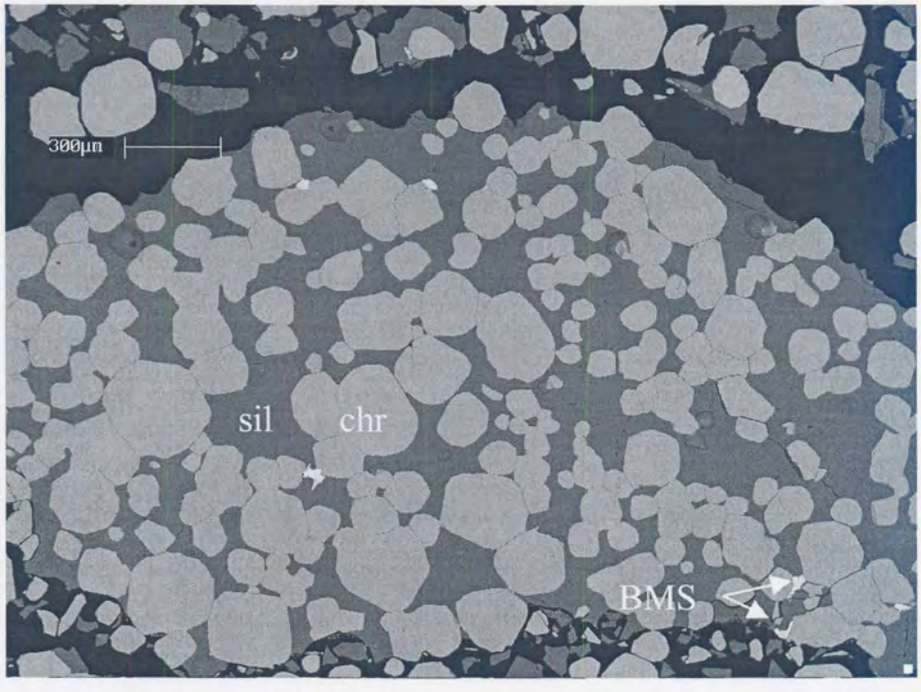

Figure 27 *Chromite textures (chr=chromite, sil=silicate, BMS=base-metal sulphide). Backscattered-electron image.*

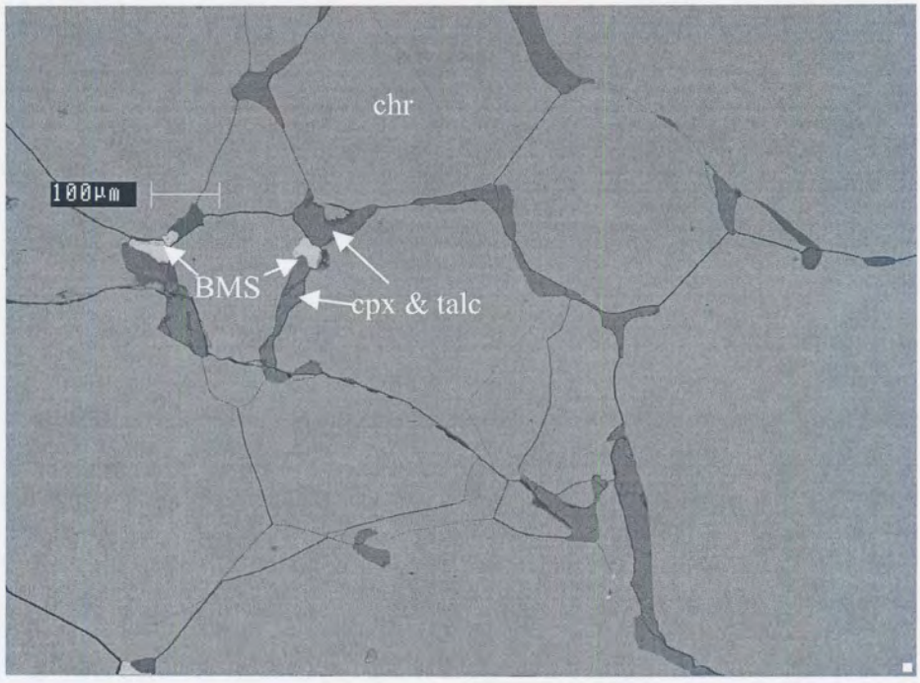

Figure 28 *Sintered chromite (chr) grains with interstitial clinopyroxene (cpx) and talc. Base-metal sulphides (BMS) are pentlandite and chalcopyrite. Backscattered-electron image.*

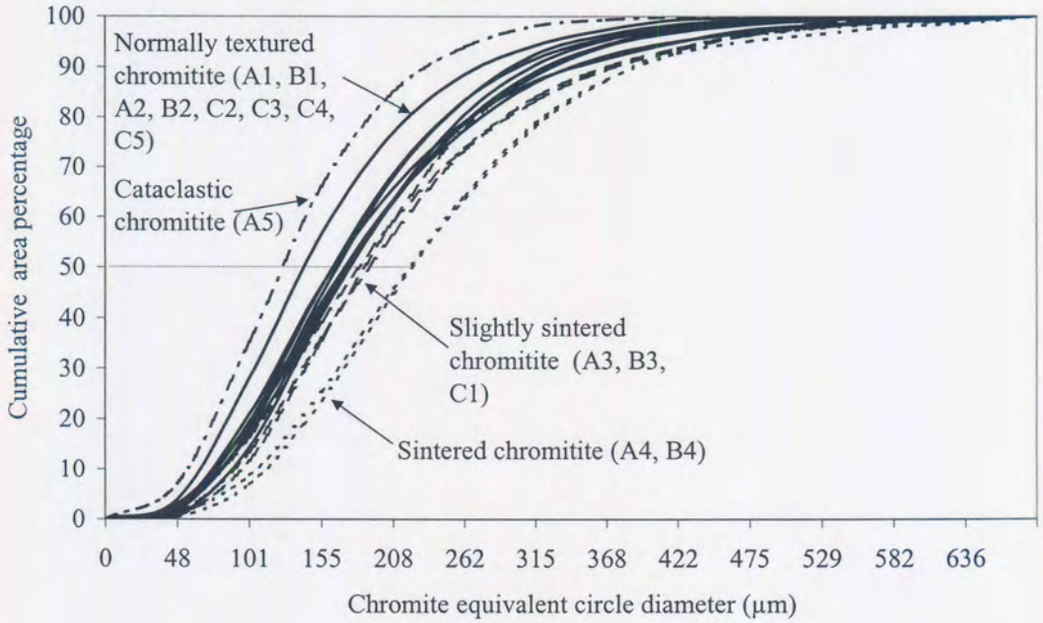

Figure 29 *Cumulative chromite grain-size distributions of 14 samples based on area measurements on polished sections. Median equivalent circle diameter values for each sample can be read off along the X-axis where the 50% line indicated on the graph intersects the size distribution curve for that sample. The slight bin size inequalities is an artefact of the measuring technique.*

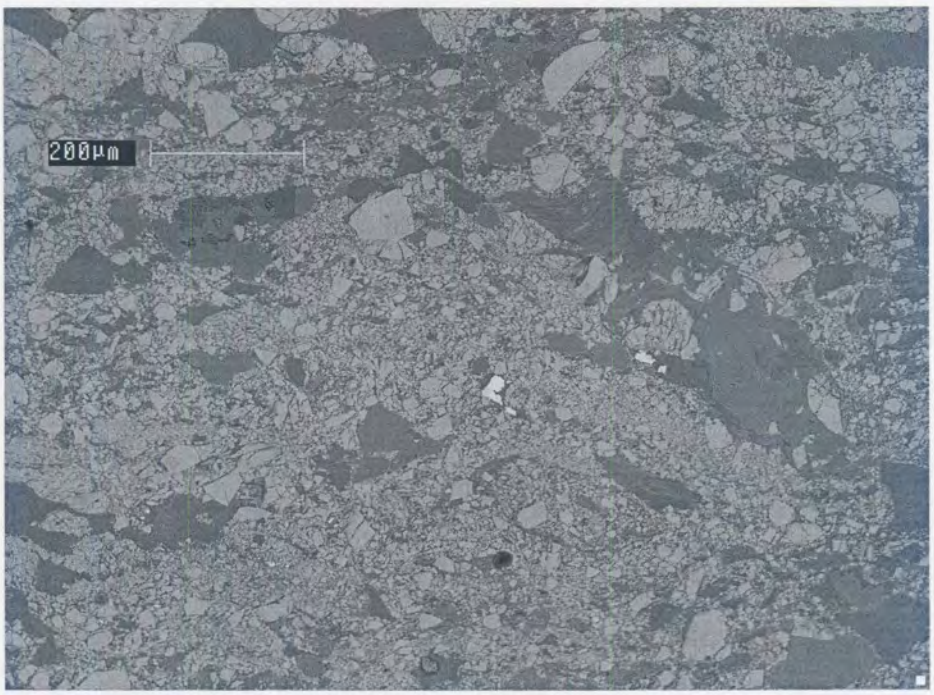

Figure 30 *Cataclastic chromite cemented by prehnite, quartz and chlorite (dark areas in image). Bright grains are pentlandite. Backscattered-electron image.*

5.2.4 Other oxide phases

Other oxide minerals occur in trace amounts. Tiny laths of rutile are often found in chromite grains. An increase in the rutile grain size was frequently observed in sintered chromite grains.

An interesting oxide assemblage, consisting of baddeleyite, an unidentified Zr-Ti oxide phase (possibly srilankite) and rutile, was observed in association with base-metal sulphides and other late- to post-magmatic phases a number of times (Figure 31), especially in samples from area C. Rare-earth element oxides are present but scarce. Magnetite occurs in trace amounts, mostly in hangingwall or footwall material from samples A4 and B1, usually at the centre of serpentine veinlets.

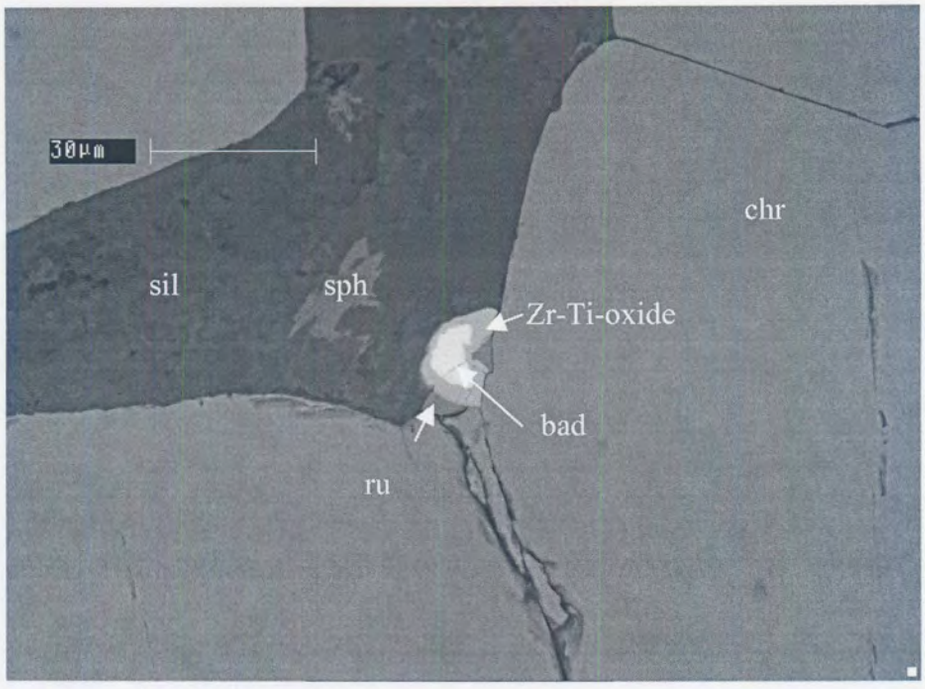

Figure 31 *Complex oxide assemblage consisting of baddeleyite (bad) (brightest grain) in the centre, rimmed by Zr-Ti-oxide (slightly darker), and rutile (ru) at the grain boundary of chromite (chr) and a fine-grained intergrowth of secondary hydrous silicates (sil) and sphene (sph). Backscattered-electron image.*

5.2.5 Silicate mineralogy

Great variabilility is displayed in the silicate mineralogy, both between and within samples. In general, plagioclase is the most commonly found silicate phase, followed by orthopyroxene (Tables 5.1 K and 5.2). Where plagioclase is the dominant silicate, chromite grains may be separated from plagioclase by a thin rind of orthopyroxene. Similarly, orthopyroxene grains are sometimes separated from chromite by a plagioclase rim. Such textures have been interpreted by Eales and Reynolds (1986) as the products of reactions involving oxide, orthopyroxene, feldspar and liquid.

With the possible exception of sample A1, most samples of UG2 chromitite display some degree of alteration of orthopyroxene to talc, usually along grain boundaries and cleavage planes (Figure 32). Chloritization of plagioclase occurs locally.

Minor amounts of diopsidic clinopyroxene are present in most samples. An increase in clinopyroxene was observed in sintered samples, especially A4 and B4 (Tables 5.1K and 5.2), often displaying a similar type of texture as that described for plagioclase and orthopyroxene. In this case though, embayed grains of clinopyroxene and plagioclase are separated from chromite by a thin layer of pargasitic hornblende (edenite) (Figure 33). Tremolite + talc and tremolite + chlorite assemblages, formed from clinopyroxene, were observed in a few areas.

Trace to minor amounts of a variety of phases including phlogopite (invariably chlorine-bearing), talc, chlorite (sometimes chlorine-bearing), rutile, baddeleyite, sphene, chlorapatite, rare-earth element oxides, Zr-Ti oxide, epidote, prehnite, tremolite, quartz, albite, pumpellyite and calcite, as well as base-metal sulphides and PGE minerals, occur interstitially between chromite and orthopyroxene or plagioclase grains. Sphene appears to have a particular affinity for phlogopite, often occurring along phlogopite cleavage planes and grain edges. A similar association of base-metal sulphide and PGE minerals with biotite, phlogopite and other hydrous silicates, quartz, rutile and zircon have been reported in samples from the Merensky Reef (Ballhaus & Stumpfl, 1986).

Olivine, partly serpentinised, occurs in small amounts in most samples. Since the olivine is usually not associated with chromite, it is assumed to have originated from the footwall and/or hangingwall.

Some samples, in particular those from area C (C1 to C5), are characterised by the replacement of the primary silicates by complex assemblages containing albite, quartz, pumpellyite, epidote, chlorite, talc, and less commonly sphene, tremolite, prehnite, K-feldspar, calcite and serpentine and sericite (Figures 34 and 35 and Tables 5.1K and 5.2). The extent of alteration ranges from isolated pockets to almost complete replacement of orthopyroxene and plagioclase in some samples (C1 and C3 in particular).

Table 5.2 *Relative amounts of silicate minerals based on qualitative observations using optical and scanning-electron microscopy, as well as XRD analysis. An=calcic plagioclase, opx=orthopyroxene, cpx=clinopyroxene, ed=edenite, tr=tremolite, phl=phlogopite, chl=chlorite, calc=calcite, qtz=quartz, ab=albite, epd=epidote, pre=prehnite, pu=pumpellyite, sph=sphene, apa=chlorapatite, kfsp=K-feldspar, serp=serpentine, schl=septechlorite, grap=graphite*

	An	**Opx**	**Cpx**	**Ed**	**Tr**	**Phl**	**Talc**	**Chl**	**Calc**	**Qtz**	**Ab**	**Epd**	**Pre**	**Pu**	**Sph**	**Apa**	**Other**
A2	●●●	●●●				●●	•	•			•			•			
B2	●●●	●●●	•			●●	●●	•	•								Kfsp
A1	●●●	●●●	●●			●●	•	•	•		•					•	
B1	●●●	●●●	●●	●●	•	●●	●●	●●	•						●●	•	
A3	●●●	●●●			•	●●	•	•			•		•	•	•		
B3	●●●	●●●	●●	●●		●●	•	•					•	•		•	
A4	●●●	●●●	●●	●●		●●	•	•						•			
B4	●●●	●●●	●●	●●	•	●●	•	•				•				•	Kfsp
A5	●●●	●●●			•	•	●●	●●		●●	●●		●●	•	•		serp schl grap
C1	●●●	●●●	•		•	●●	●●	●●		●●	●●	●●	•	●●	●●	•	
C2	●●●	●●●				●●	•	•		•	•	•		•	•		
C3	●●●	●●●			•	●●	●●	●●	•	●●	●●	●●	•	●●	●●	•	serp
C4	●●●	●●●			•	●●	●●	●●	•	●●	●●	●●		●●	●●		
C5	●●●	●●●			•	●●	•	•		•	•	•		•			

●●● *>~10%* ●● *1-10%* • *trace*

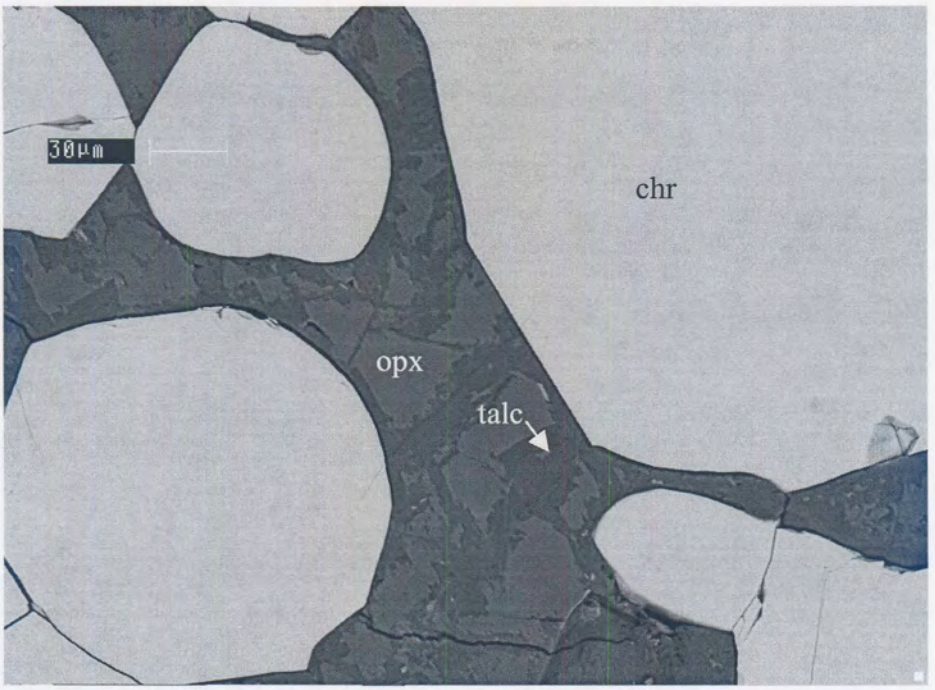

Figure 32 *Alteration of bronzite (opx) to talc along cleavage planes and grain boundaries. Backscattered-electron image*

Figure 33 *Resorbed grains of clinopyroxene (cpx) and plagioclase (an) (with dark chlorite veinlets (chl)) in amphibole (edenite)(ed). Backscattered-electron image.*

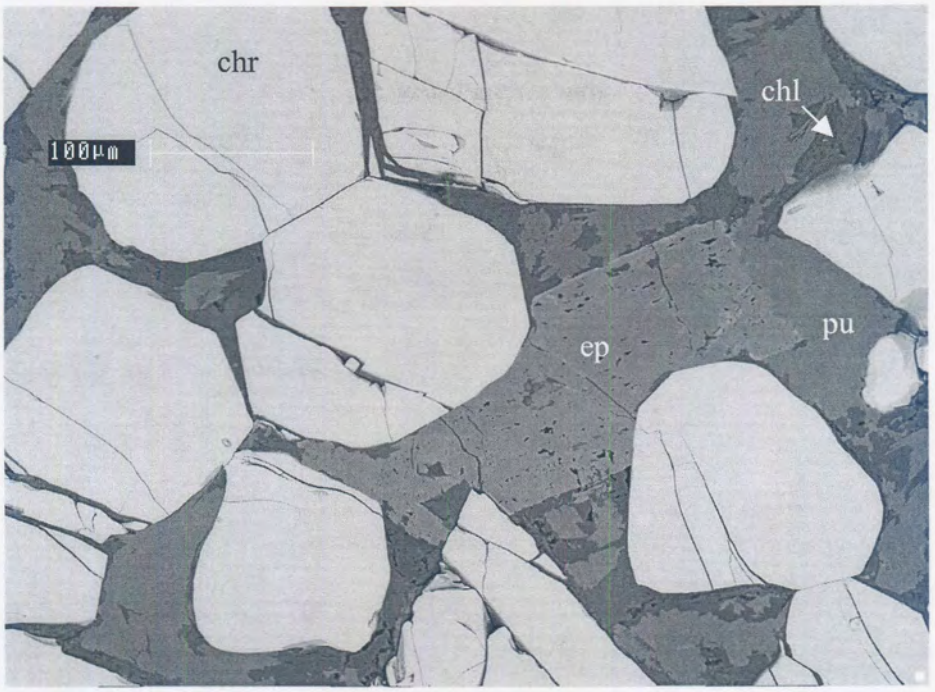

Figure 34 *Zoned epidote (ep) crystal crosscutting pumpellyite (pu) rimmed by chlorite (chl). Backscattered-electron image.*

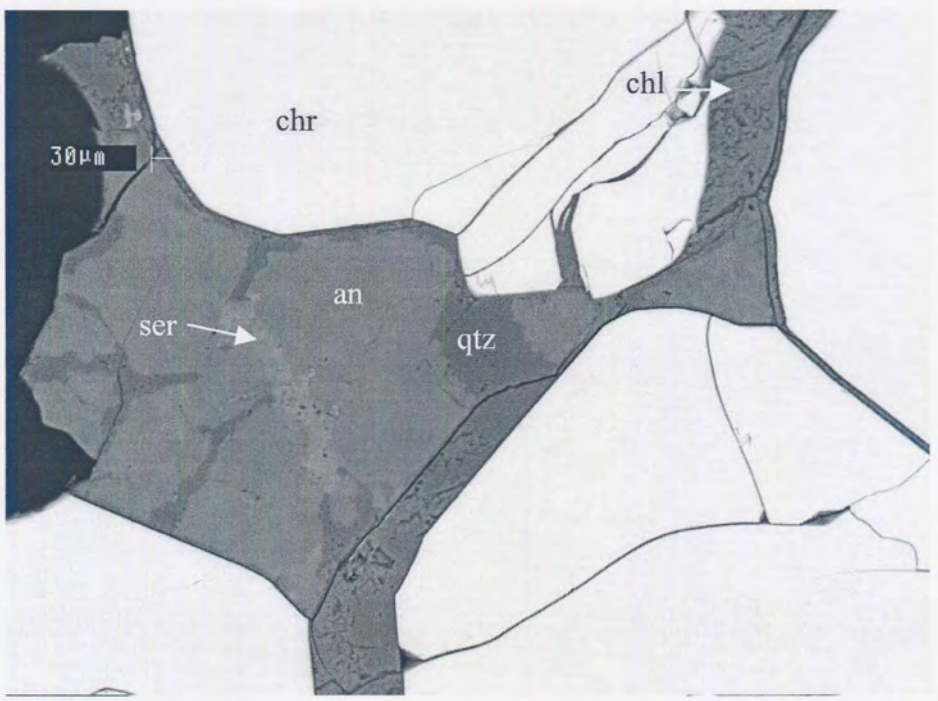

Figure 35 *Alteration of plagioclase (an) to quartz (qtz), chlorite (chl) and sericite (ser). Backscattered-electron image.*

In cataclastic chromitite (sample A5), fractured chromite grains are cemented by a number of secondary phases including septechlorites, serpentine, quartz, pumpellyite, prehnite, chlorite, calcite, tremolite, albite and graphite (Figure 30, Tables 5.1K and 5.2).

5.2.6 Base-metal sulphide mode of occurrence

Pentlandite - chalcopyrite - pyrrhotite ± pyrite assemblages

In the samples from areas A and B, chalcopyrite, pentlandite and pyrrhotite generally form composite grains at chromite-silicate grain boundaries (Table 5.1L and Figure 36), commonly in association with phlogopite and trace amounts of other late- and post-magmatic phases. In intensely sintered areas, sulphide grains may become locked between chromite grains.

Pentlandite rarely occurs as flames in pyrrhotite. Pyrrhotite is sometimes partially rimmed by pentlandite and occasionally also by chalcopyrite (Figure 37). Slight fraying of sulphide grain edges can sometimes be seen where in contact with secondary silicates. Sulphide minerals, especially pentlandite and chalcopyrite, can occasionally be seen together with secondary silicates along microfissures traversing primary silicates and chromite.

Pyrite usually occurs as chains of small grains along pentlandite cleavage planes and grain edges (Figure 38). In rare cases millerite appears to be replacing pentlandite. Trace amounts of galena were observed in most of the samples, usually occurring as small grains associated with secondary silicates, especially in samples B1, B3, C1 and C2. A few isolated grains of copper-rich sulphides (mostly bornite) were observed as inclusions in chromite.

In cataclastic UG2 chromite sulphide minerals generally occur in the silicate matrix that cements the chromite grains (Figure 30). Relatively coarse, euhedral pentlandite grains were observed in places in cataclastic UG2, suggesting recrystallization.

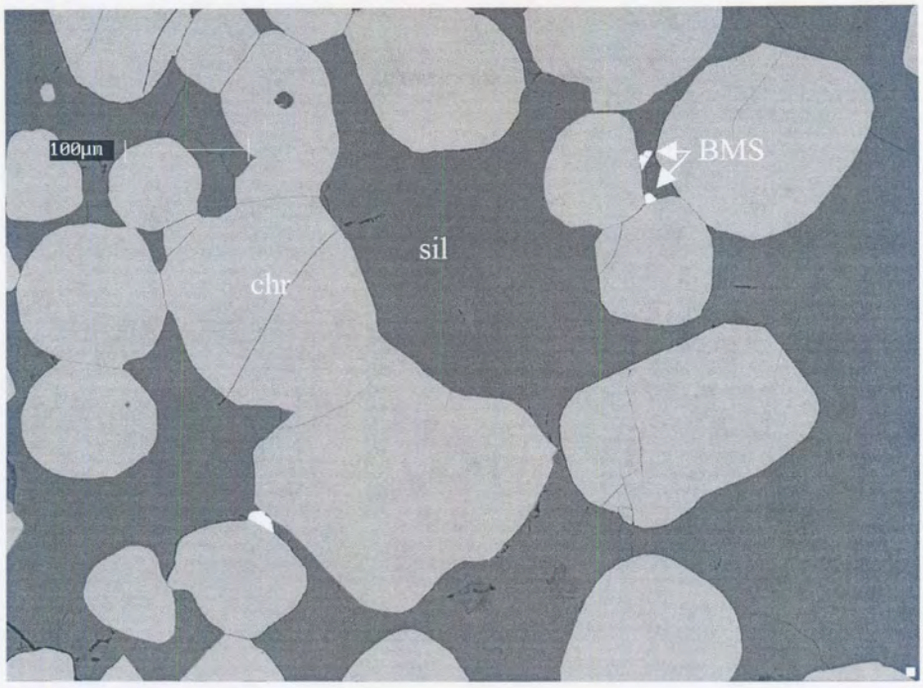

Figure 36 *UG2 chromitite consisting of rounded chromite grains in a matrix of plagioclase. Small base-metal sulphide (BMS) grains occur at chromite (chr) - silicate (sil) grain boundaries. Backscattered-electron image.*

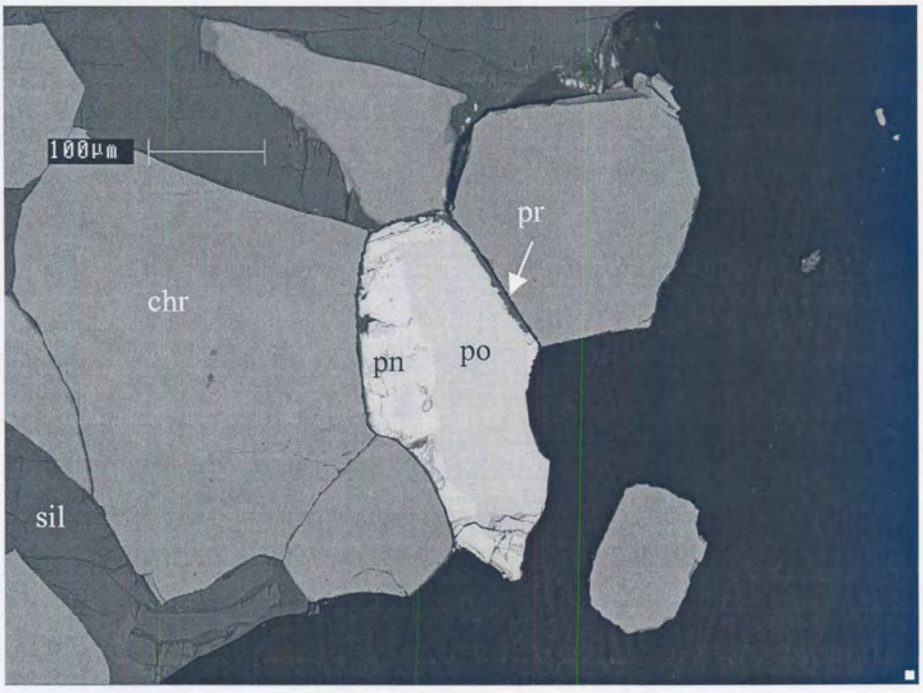

Figure 37 *Pyrhhotite (po) partially rimmed by pentlandite (pn) at a chromite(chr) – silicate (sil) grain boundary. A thin rim of prehnite (pr) separates sulphide from gangue. Backscattered-electron image.*

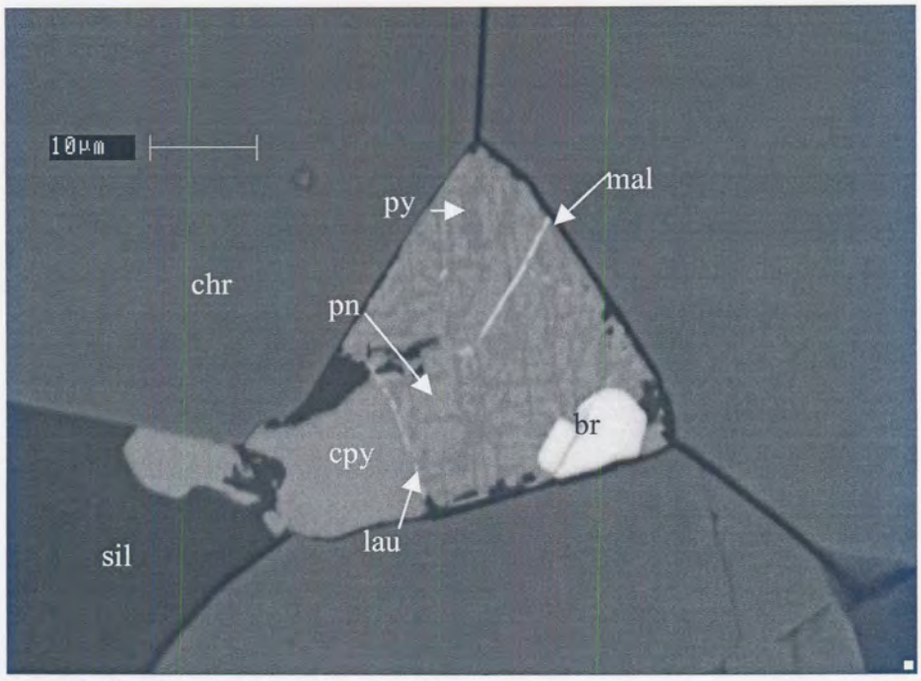

Figure 38 *Pentlandite (pn) being replaced by pyrite (py) along cleavage planes. Note the presence of a thin laurite (lau) parting at the grain boundary between chalcopyrite (cpy) and pentlandite. Other PGE minerals present are braggite (br) and malanite (mal). Silicates (sil) are quartz and plagioclase. Backscattered-electron image.*

Millerite - chalcopyrite - pyrite assemblages (samples C1 to C5)

In patches where primary silicate minerals persist, composite sulphide grains occur at chromite-silicate grain boundaries, usually associated with phlogopite and a host of secondary silicate minerals. Sulphide grains often display corroded outlines, appearing to have been partly replaced by secondary hydrous silicates (Figures 39 to 41). More extensive alteration of primary silicate assemblages leads to local redistribution (probably on a scale of tens or hundreds of microns) and recrystallization of sulphide minerals, resulting in euhedral to subhedral sulphide grains intergrown with secondary silicates (Figure 42, Table 5.1L).

The content of pentlandite in samples C1 to C5 is very low (<0.01%). Thus, pentlandite and millerite are rarely found in direct contact in these samples, making it difficult to establish the genetic relationship between these two phases. Pyrite, the major iron sulphide present, occurs both in composite grains with millerite and chalcopyrite, or, as relatively coarse-grained porous pyrite (especially in samples C1,

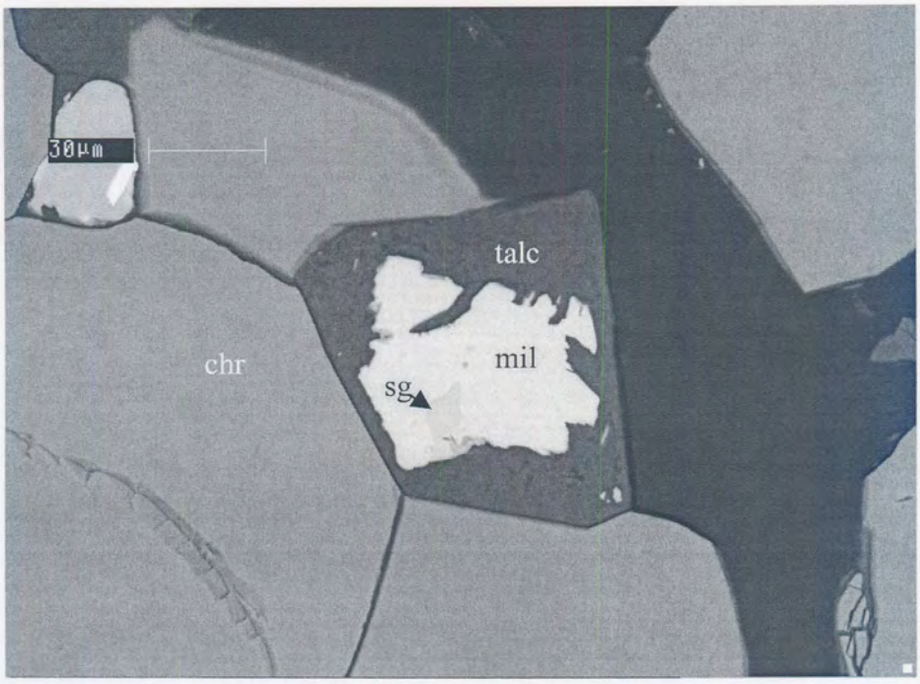

Figure 39 *Corroded base-metal sulphide grain consisting of millerite (mil) and siegenite (sg) in talc. Backscattered-electron image.*

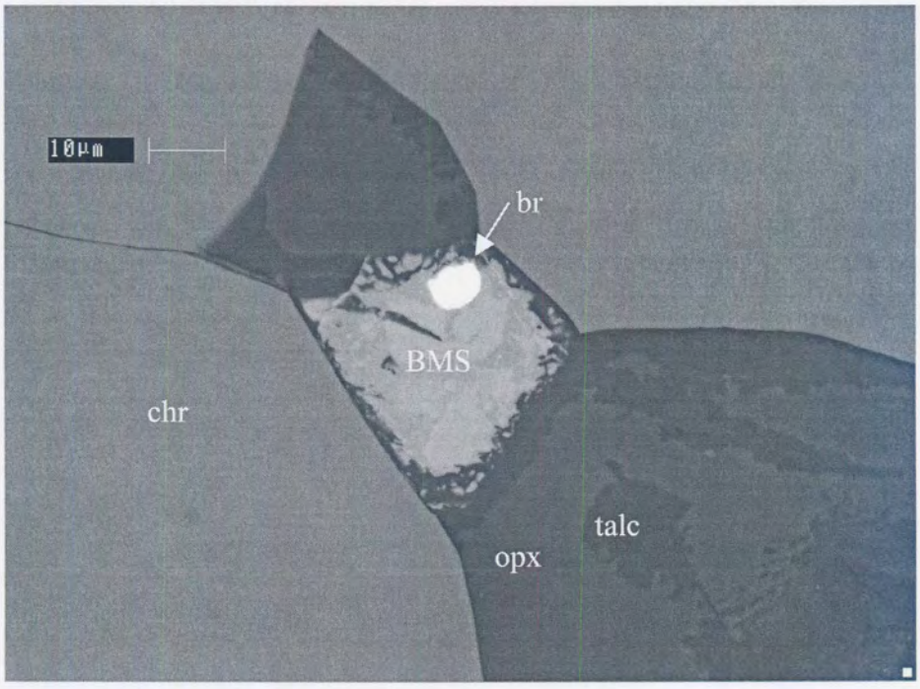

Figure 40 *Corroded base-metal sulphide grain (BMS) (chalcopyrite + millerite + pyrite) with zoned braggite (br). Silicates are orthopyroxene (opx) being altered to talc. Backscattered-electron image.*

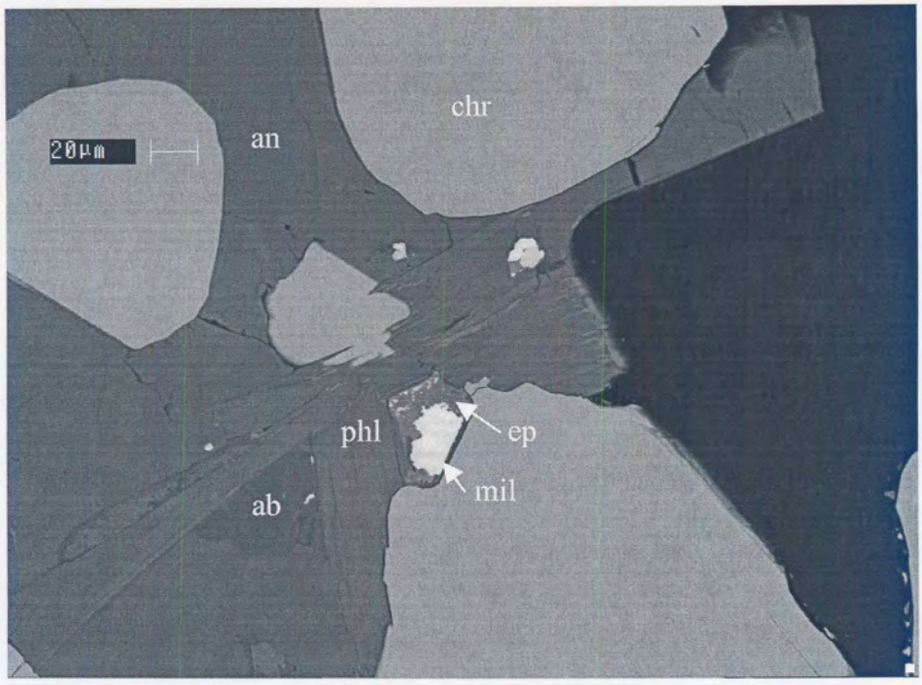

Figure 41 *Corroded millerite (mil) grain associated with epidote (ep). Other phases are phlogopite (phl), albite (ab) and Ca-plagioclase (an). Backscattered-electron image.*

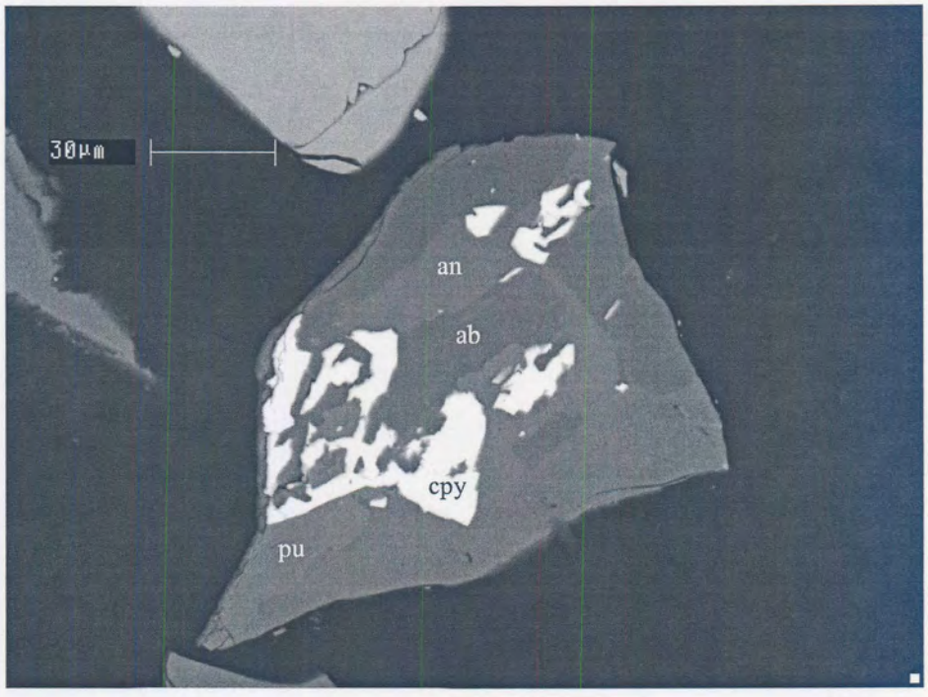

Figure 42 *"Skeletal chalcopyrite" (cpy) associated with Ca-plagioclase (an), albite (ab) and pumpellyite (pu). Backscattered-electron image.*

C3 and C5) at chromite-silicate grain boundaries or filling cracks in chromite. Siegenite is a ubiquitous but minor component, usually associated with millerite.

5.2.7 Base-metal sulphide grain-size distribution

Base-metal sulphide grain-size distributions are graphically illustrated in Figure 43. The median sulphide grain diameters in normally textured chromitite from areas A and B (samples A1, A2, B1 and B2) lies between 30 and 32 µm (Table 5.1L), with maximum diameters coarser than 100 µm. Samples from area C are characterised by much smaller median values - between 17 and 22 µm and grains coarser than 100 µm were rarely observed. The average of the median base-metal sulphide diameters for samples A1, A2, B1 and B2 is 31 µm, and for samples C1 to C6, 20 µm. Statistical analysis (Simon & Bruce, 1991) indicated that the chance of the 11µm difference between these two values being attributable to chance is only 1%. A small chromite diameter of 17 µm was also recorded for cataclastic UG2 (sample A5).

In samples characterised by a coarsening of chromite due to sintering (B3, A3, B4 & A4), the sulphide grains are also bigger with measured median diameters >33 µm (the average value for this group of samples is 39 µm). The exception in the last instance being sample C1, presumably as a result of corrosion of sulphide grains in area C. Statistical analysis (Simon & Bruce, 1991) indicated that the likelihood of the 8µm difference between the average for samples B3, A3, B4 and A4 and that for samples A1, A2, B1 and B2 is attributable to chance, is only 6%.

5.2.8 Modal distribution of PGE minerals

PGE minerals associated with pentlandite-chalcopyrite-pyrrhotite±pyrite assemblages (areas A and B)

The PGE mineral assemblages in samples A1, A2, B2 and A3 consist predominantly (more than 90 volume %) of sulphide minerals, mostly Pt-Pd-Ni sulphide, Pt-sulphide, Pt-Rh-Cu-Ni-sulphide and laurite (Table 5.1M, Figure 44). Samples B1 and B3 contain small amounts of Pt-Fe alloy and other non-sulphide PGE minerals.

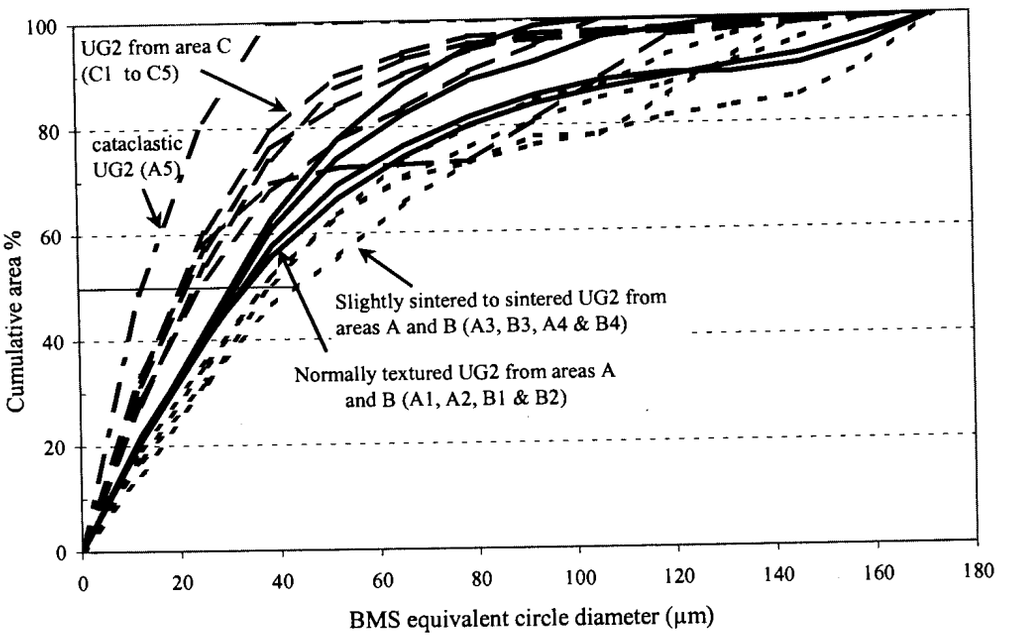

Figure 43 *Measured base-metal sulphide grain-size distributions in fourteen samples of crushed UG2 chromitite. Median equivalent circle diameter values for each sample can be read off along the X-axis where the 50% line indicated on the graph intersects the size distribution curve for that sample.*

Samples A4 and B4 are characterised by PGE mineral assemblages consisting predominantly of Pt-Fe alloys (often rhodium- or palladium-bearing), laurite, and to a lesser extent PGE-Bi-Te compounds, and other non-sulphide PGE minerals (Table 5.1M and Figure 44).

The PGE mineral assemblage of cataclastic UG2 chromitite (sample number A5) is dominated by laurite and non-sulphide PGE minerals such as Pt-Fe alloys (Table 5.1M and Figure 44). Although Pt-Rh-Cu-Ni-sulphide and Pt-Pd-Ni-sulphides represent a significant proportion of the PGE minerals, Pt-sulphide is relatively scarce.

<u>PGE minerals associated with millerite-pyrite-chalcopyrite assemblages (C1 to C5)</u>

One of the most striking aspects of the PGE mineral assemblages from the mining area represented by these samples, is the sharp drop in the modal proportions of Pt-sulphide and a concomitant increase in Pt-Rh-Cu-Ni -sulphide and Pt-Pd-Ni-sulphide compared to that found in most samples from areas A and B (A1, A2, B1, B2, A3 & B3) (Table 5.1M and Figure 44). Qualitative EDS analyses of Pt-Pd-Ni-sulphide also

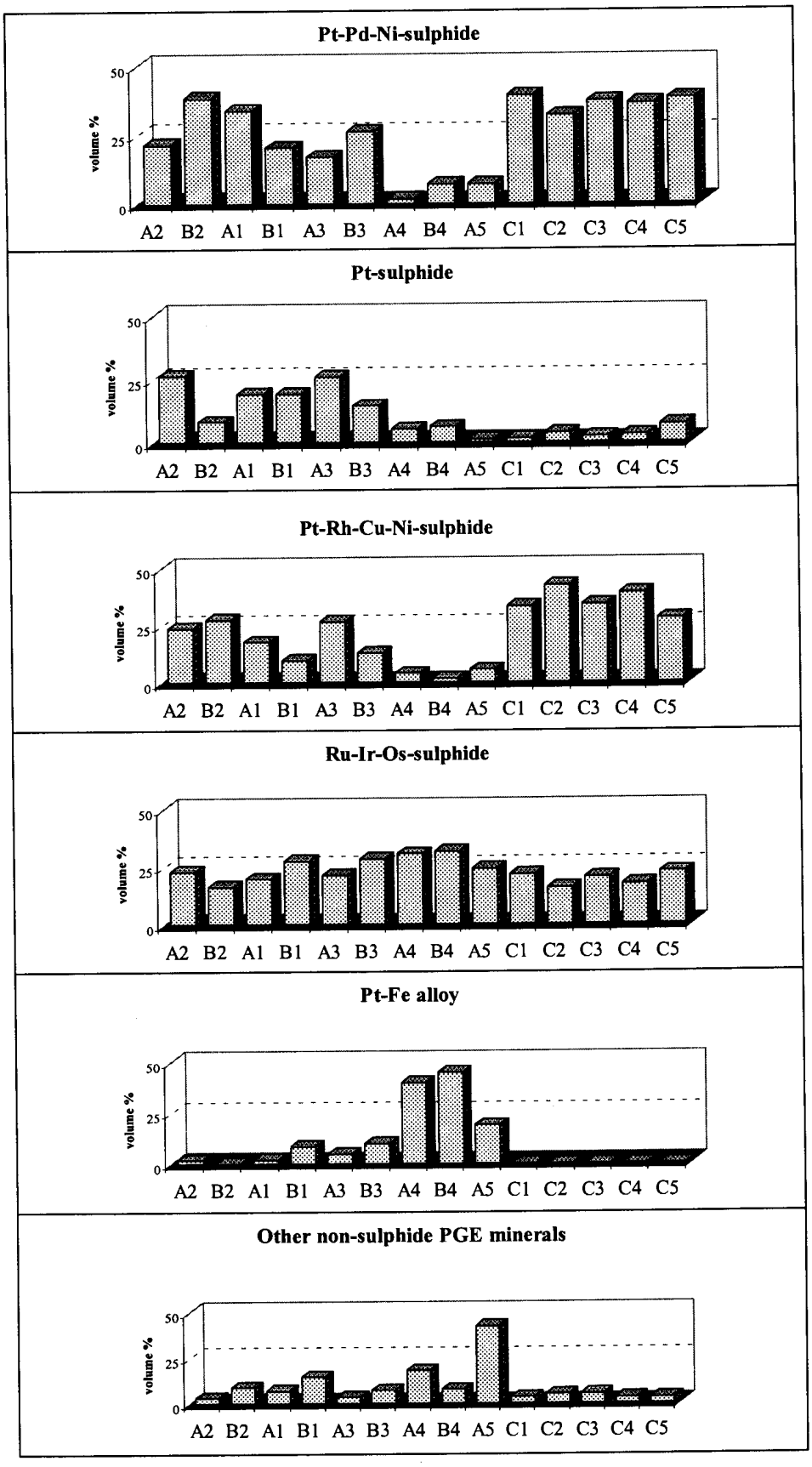

Figure 44 *PGE mineral distribution in fourteen samples of UG2 chromitite.*

suggest a change to more palladian compositions. Note also the evidently complete absence of Pt-Fe alloys from these samples.

5.2.9 PGE mineral grain-size distribution

Based on a composite of all fourteen samples, the median PGE mineral grain diameter in UG2 chromitite from the study area is ~6.5 µm (Figure 45), which agrees well with the average value of 5.1 µm reported by McLaren (1980). PGE mineral grain sizes, expressed as equivalent circle diameter, range from <1 µm to ~ 50 µm.

Median PGE mineral grain-diameter values for the samples examined vary between 3.0 and 10.2 µm, based on area per cent (Table 5.1O). Due to the large error associated with these measurements, the differences between these values are not statistically significant (Table 4.17). That there are significant differences in PGE mineral grain sizes between the samples is indicated by the median PGE mineral diameter calculated from the percentage number of grains, with values ranging from 1.8 to 2.9 (Table 5.1O). Although this value does not reflect the true grain diameter, it is statistically more reliable and does allow for comparisons between samples. Note the generally larger median percentage number of grains for samples from area C with an average value of 2.8 µm (ranging from 2.7 to 2.9 µm), compared to an average of 2.2 µm (between 1.8 and 2.8 µm) for samples from areas A and B.‡

5.2.10 PGE mineral mode of occurrence

The mode of occurrence of PGE minerals in the crushed feed samples have been summarised in Table 5.1P and Figure 46. In all samples, the largest proportion of the PGE minerals (40 to 70%) occurs at grain boundaries of base-metal sulphide and/or oxide and/or silicate, or have been liberated (up to 20%) during crushing of the ore.

With the exception of sample A5, the remainder of the PGE minerals in samples from areas A and B mostly form part of base-metal sulphide composite grains (20 to 40%).

---

‡ This is a small, but statistically significant difference. See Table 4.17.

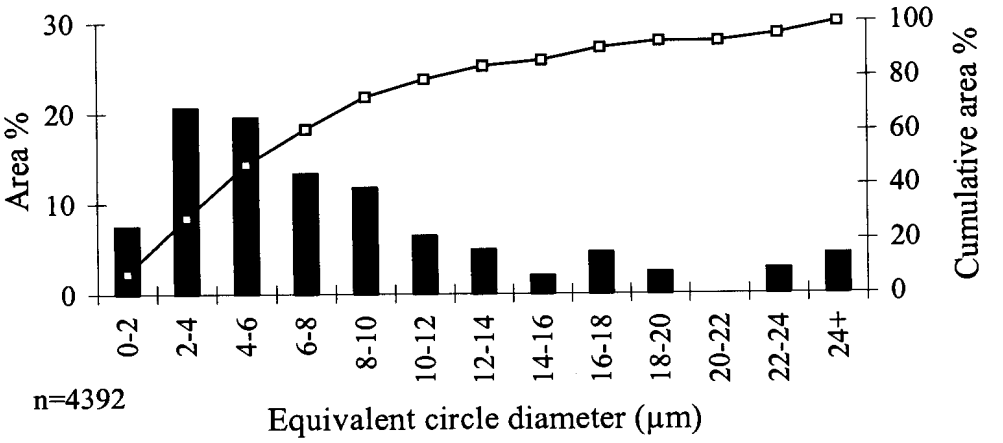

Figure 45 *PGE mineral grain-size distribution in fourteen crushed feed samples.*

The frequency of association of PGE mineral grains with different base metal sulphides is reported in Table 5.1Q. Caution is advised when interpreting these results. For instance, in sample A1, 49 per cent of the PGE minerals in contact with sulphide is associated with pentlandite. This does not necessarily mean that the PGE minerals are preferentially associated with pentlandite, rather, since pentlandite represent 49 per cent of the base-metal sulphide assemblage, it means that there is no preferential PGE mineral-pentlandite association. In addition, in samples where a smaller percentage of the PGE minerals are associated with base-metal sulphides (samples from area C and sample A5), the results are based on a relatively small number of grains and consequently not reliable.

Samples from area C and sample A5 are characterised by a relatively high percentage of PGE mineral grains enclosed in silicate gangue, or at silicate-silicate grain boundaries, generally between 30 and 50% compared to less than 15% in the other samples.

In all samples, less than 10% of PGE mineral grains occur as inclusions in chromite. More than 90% of these inclusions consist of laurite ($(Ru,Os,Ir)S_2$), representing ~25% of the total laurite. Apart from the laurite-chromite association, no evidence could be found that specific PGE minerals occur preferentially in association with either oxide or silicate.

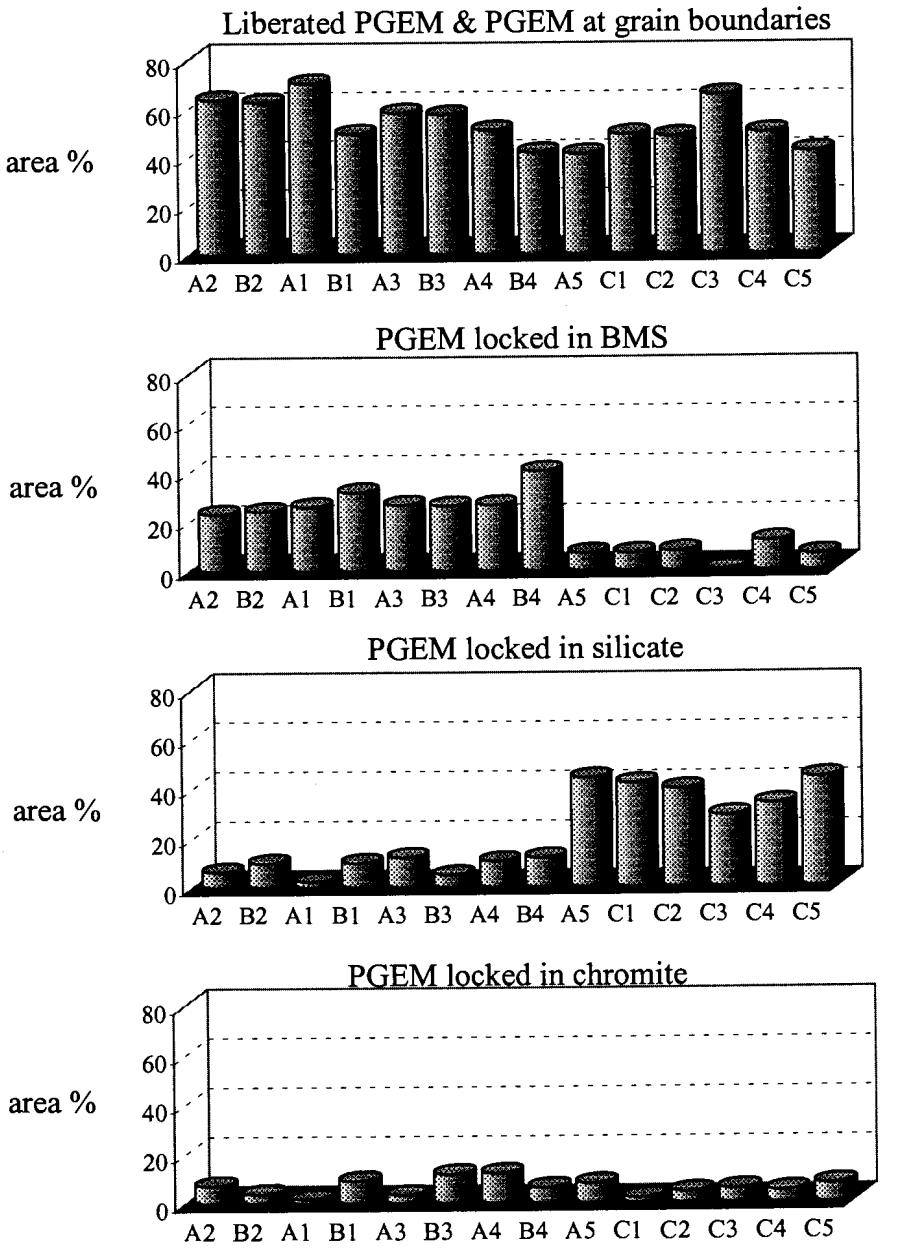

Figure 46 *Mode of occurrence of PGE minerals (PGEM) in fourteen samples of UG2 chromitite at <2mm.*

5.2.11 Chromite composition

Sintered chromite grains display higher optical reflectivity and backscattered-electron intensity compared to normal-textured chromite. Although an in-depth analysis of the variations in chromite compositions is beyond the scope of this investigation, a

number of selected chromite grains from different samples were analysed by electron microprobe to get an indication of the effect sintering of chromite grains has on composition (Table 5.3 and Tables 1 to 8 Appendix D).

Sporadic core-rim analyses indicated no systematic compositional variation within chromite grains. Silicon and calcium are generally not present at levels above the detection limits. Nickel, vanadium, cobalt, copper, manganese and zinc are present in concentrations above the detection limits, but show very little variation. The average chromite nickel content is about 0.15 per cent, which, for UG2 ore containing 50 to 75 per cent chromite is equivalent to 600 to 900 ppm nickel, accounting for most of the nickel not present in acid soluble form (Table 5.1B). Similarly, most of the cobalt that is not present in acid soluble form appears to be accommodated by chromite.

A comparison of the chemical composition of normal and sintered chromite grains in sample A1 shows an increase in titanium, chromium, and iron values, and a decrease in aluminium and possibly magnesium, in the sintered grains. Chromite grains from sample A4 showed an increase in titanium and iron, but a decrease in chromium, aluminium, and magnesium in sintered grains. Compositions of sintered grains in sample B4 are similar to those in sample A4. A comparison of compositions of chromite grains in sample C1 shows an increase in titanium in the sintered grains, no further systematic variations could be discerned from the data.

Some of the compositional variation can probably be ascribed to systematic changes in chromite composition with stratigraphic height (McLaren & De Villiers, 1982), an aspect not considered in this study. In general the sintered chromite grains appear to be significantly more titaniferous.

5.2.12 Silicate compositions

Feldspar

Feldspar EDS analyses are tabulated in Tables 1 to 8, Appendix E. Calcic plagioclase compositions are highly variable corresponding to that of labradorite-bytownite ($An_{55-85}Ab_{15-44}Or_{0-2}$). Zoning is common. Albite-oligoclase ($Ab_{87-95}An_{5-13}$) and K-feldspar ($Or_{74-86}Ab_{14-25}An_{0-1}$) occur less commonly.

Table 5.3 *Average chromite compositions of UG2 chromitite from samples A1, A4, C1 and B4. The 95% confidence interval was calculated using Student's t-distribution.*

Sample	A1 (pegmatoid fw)				C1 (pothole edge)						A4 (replacement pegmatoid fw)				B4 (replacement pegmatoid fw)	
Texture	<300µm normal		>300µm sintered		<200µm normal		>200µm sintered		>300µm sintered		<300µm normal		>500µm sintered		>200µm sintered	
TiO_2	0.85	±0.03	1.07	±0.08	0.91	±0.15	1.19	±0.01	1.29	±0.02	0.99	±0.02	2.31	±0.28	1.30	±0.03
V_2O_3	0.33	±0.02	0.35	±0.07	0.45	±0.05	0.44	±0.04	0.40	±0.03	0.27	±0.01	0.28	±0.02	0.40	±0.01
Al_2O_3	16.85	±0.36	15.05	±0.62	14.96	±0.44	15.16	±0.08	15.19	±0.07	17.44	±0.14	14.46	±0.75	15.01	±0.09
Cr_2O_3	42.79	±0.34	43.96	±0.42	43.92	±0.63	43.49	±0.11	42.94	±0.06	44.18	±0.21	40.72	±0.19	41.81	±0.08
Fe_2O_3	8.95	±0.16	9.42	±0.16	9.44	±0.34	9.87	±0.07	10.16	±0.10	6.08	±0.09	10.05	±0.47	9.88	±0.35
FeO	19.20	±0.17	19.60	±0.43	20.58	±0.55	19.52	±0.06	20.14	±0.06	21.88	±0.09	25.29	±0.45	22.06	±0.28
MnO	0.26	±0.00	0.27	±0.00	0.28	±0.01	0.28	±0.01	0.26	±0.01	0.26	±0.00	0.30	±0.01	0.27	±0.00
NiO	0.14	±0.01	0.13	±0.02	0.13	±0.02	0.16	±0.01	0.16	±0.01	0.17	±0.00	0.15	±0.01	0.17	±0.00
CoO	0.02	±0.01	0.01	±0.01	0.02	±0.01	0.02	±0.01	0.02	±0.01	0.02	±0.01	0.02	±0.01	0.02	±0.00
CuO	0.02	±0.01	0.03	±0.03	0.03	±0.01	0.04	±0.02	0.04	±0.02	0.03	±0.01	0.03	±0.01	0.02	±0.01
ZnO	0.08	±0.01	0.07	±0.03	0.11	±0.01	0.10	±0.02	0.11	±0.02	0.10	±0.01	0.14	±0.01	0.05	±0.01
MgO	9.65	±0.14	9.23	±0.33	8.59	±0.42	9.32	±0.05	8.93	±0.03	8.01	±0.07	5.43	±0.37	8.21	±0.05
Total	99.01		99.02		99.25		99.39		99.45		99.28		98.86		99.12	

For individual analyses and calculated ion proportions, see Appendix D, Tables 1 to 8.

Pyroxene

Pyroxene compositions are relatively constant, corresponding to that of the orthopyroxene bronzite ($En_{83-88}Fs_{11-16}Wo_{1-2}$). The composition of clinopyroxene compositions is that of diopside ($Wo_{44-48}En_{47-48}Fs_{5-8}$). EDS analyses of pyroxene are listed in Tables 9 to 13, Appendix E.

Phlogopite

Selected phlogopite analyses are summarised in Table 14, Appendix E. The chemical composition of phlogopite is variable. Zoning is sometimes visible on backscattered electron images, especially in samples from area C. Of interest is the presence of Cl at concentration levels of up to 0.5 weight %.

Other silicate phases

Analyses of selected grains of edenitic hornblende and tremolite, and the hydrous Ca-Al silicates, pumpellyite, epidote and prehnite have been recorded in Tables 15, 16 and 17, Appendix E. Due to the fine-grained and intergrown nature of talc, chlorite, septechlorite and serpentine, it was difficult to obtain good analyses. Nevertheless, the analyses in Table 18, Appendix E, give some indication of the compositions of these phases.

5.2.13 Base-metal sulphide compositions

Electron-microprobe analysis was performed on selected grains of base-metal sulphide from samples A1, B4, C1 and C2.

Chalcopyrite

The composition of chalcopyrite is essentially stoichiometric $CuFeS_2$ (Table 5.4 and Appendix F, Tables 1 to 3). Platinum, rhodium and ruthenium contents of chalcopyrite are consistently below the detection limits of the analysis technique. Palladium was found to be present at a concentration level above the detection limit in only one grain out of fifty-four analysed.

Table 5.4 *Average compositions of chalcopyrite in samples A1, B1 and C1 determined by electron-microprobe analysis. The 90% confidence interval was calculated using the Student t-distribution.*

Sample no.	**A1** *(n=20)*		**B4** *(n=13)*		**C1** *(n=21)*	
S	34.93	±0.09	35.04	±0.12	34.74	±0.18
Fe	30.44	±0.11	30.54	±0.20	30.13	±0.17
Ni	0.06	±0.05	0.07	±0.04	0.02	±0.01
Co	0.04	±0.01	0.04	±0.01	0.04	±0.01
Cu	34.02	±0.15	33.92	±0.25	33.77	±0.24
Rh	b.d.l.		b.d.l.		b.d.l.	
Pd	b.d.l.		b.d.l.		b.d.l.	
Pt	b.d.l.		b.d.l.		b.d.l.	
Ru	b.d.l.		b.d.l.		b.d.l.	
Atomic proportions						
S	2.01	±0.00	2.01	±0.01	2.01	±0.00
Fe	1.00	±0.00	1.01	±0.00	1.00	±0.00
Ni	0.00	±0.00	0.00	±0.00	0.00	±0.00
Co	0.00	±0.00	0.00	±0.00	0.00	±0.00
Cu	0.99	±0.00	0.98	±0.00	0.99	±0.00
Rh	b.d.l.		b.d.l.		b.d.l.	
Pd	b.d.l.		b.d.l.		b.d.l.	
Pt	b.d.l.		b.d.l.		b.d.l.	
Ru	b.d.l.		b.d.l.		b.d.l.	

b.d.l. = below detection limits n = number of grains analysed

Pyrrhotite

Pyrrhotite analyses were obtained from two samples, A1 and B4 (Table 5.5, and Appendix F, Tables 4 and 5). These analyses indicate that the average composition of pyrrhotite from samples A1 and B4 is $Fe_{0.99}S_{1.00}$ (close to that of troilite) and $Fe_{0.90}S_{1.00}$ respectively. *

---

* These findings appear to be at odds with those of McLaren (1980) and McLaren and de Villiers (1982). These authors reported troilite in a sample of UG2 taken in the vicinity of a discordant ultramafic pegmatoid. This sample was characterised by a PGEM assemblage consisting of laurite and non-sulphide PGE minerals. Pyrrhotite (Fe_{1-x} with $x \geq 0.01$) dominated at other localities investigated by these authors. Clearly pyrrhotite compositions from more samples need to be compared to determine the relationship between pyrrhotite composition, PGE mineral assemblage and effect of postmagmatic alteration.

Platinum, palladium, rhodium and ruthenium contents of pyrrhotite in both samples are generally below the detection limits of the electron microprobe technique. Out of forty-five grains analysed, the presence of palladium at concentration levels above the detection limit was indicated in two grains. Platinum was found to be present in one grain.

Table 5.5 *Average compositions of pyrrhotite from samples A1 and B4 determined by electron-microprobe analysis. The 90% confidence interval was calculated using the Student t-distribution.*

Sample no.	**A1** *(n=18)*		**B4** *(n=27)*	
S	36.53	±0.16	38.80	±0.15
Fe	62.87	±0.17	60.57	±0.16
Ni	0.05	±0.03	0.13	±0.06
Co	0.07	±0.01	0.06	±0.01
Cu	0.02	±0.01	0.03	±0.01
Rh	b.d.l.		b.d.l.	
Pd	b.d.l.		b.d.l.	
Pt	b.d.l.		b.d.l.	
Ru	b.d.l.		b.d.l.	
Atomic proportions				
S	1.00	±0.00	1.00	±0.00
Fe	0.99	±0.00	0.90	±0.00
Ni	0.00	±0.00	0.00	±0.00
Co	0.00	±0.00	0.00	±0.00
Cu	0.00	±0.00	0.00	±0.00
Rh	b.d.l.		b.d.l.	
Pd	b.d.l.		b.d.l.	
Pt	b.d.l.		b.d.l.	
Ru	b.d.l.		b.d.l.	

b.d.l. = below detection limit n = number of grains analysed

Pyrite

Pyrite compositions in the four samples analysed are variable – $Fe_{0.92\text{-}1.04}Ni_{0.00\text{-}0.04}Co_{0.00\text{-}0.04}S_{2.00}$ (Table 5.6, analyses of individual grains in Appendix F, Tables 6 to 9). Platinum, palladium and ruthenium were not detected above the detection limits in any of the grains analysed. Rhodium however was detected in three grains out of a total of forty-six analysed, in one case at a concentration level of ~0.1 mass per cent (see also Figure 47).

Table 5.6 *Average compositions of pyrite in samples A1, B4, C1, C2 determined by electron-microprobe analysis. The 90% confidence interval was calculated using the Student t-distribution.*

Sample no.	A1 (n=10)		B4 (n=6)		C1 (n=18)		C2 (n=12)	
S	53.60	±0.32	53.65	±0.68	53.10	±0.23	53.49	±0.18
Fe	45.70	±0.26	47.17	±0.42	46.28	±0.38	45.68	±0.38
Ni	0.21	±0.14	0.02	±0.01	0.39	±0.19	0.34	±0.14
Co	1.18	±0.28	0.06	±0.02	0.43	±0.19	1.04	±0.24
Cu	0.02	±0.02	0.09	±0.10	0.03	±0.01	0.27	±0.12
Rh	b.d.l.		b.d.l.		b.d.l.		b.d.l.	
Pd	b.d.l.		b.d.l.		b.d.l.		b.d.l.	
Pt	b.d.l.		b.d.l.		b.d.l.		b.d.l.	
Ru	b.d.l.		b.d.l.		b.d.l.		b.d.l.	
Atomic proportions								
S	2.00	±0.00	2.00	±0.00	2.00	±0.00	2.00	±0.00
Fe	0.97	±0.01	1.01	±0.01	1.00	±0.01	0.98	±0.01
Ni	0.00	±0.00	0.00	±0.00	0.01	±0.00	0.01	±0.00
Co	0.03	±0.01	0.00	±0.00	0.01	±0.00	0.02	±0.00
Cu	0.00	±0.00	0.00	±0.00	0.00	±0.00	0.01	±0.00
Rh	b.d.l.		b.d.l.		b.d.l.		b.d.l.	
Pd	b.d.l.		b.d.l.		b.d.l.		b.d.l.	
Pt	b.d.l.		b.d.l.		b.d.l.		b.d.l.	
Ru	b.d.l.		b.d.l.		b.d.l.		b.d.l.	

b.d.l. = below detection limit n = number of grains analysed

Millerite

Electron microprobe analyses from two samples (C1 and C2) indicate millerite compositions of $Ni_{0.93\text{-}0.98}Fe_{0.01\text{-}0.05}Co_{0.00\text{-}0.02}S_{1.00}$ (Table 5.7 and Appendix F, Tables 10 and 11). Platinum, palladium, and ruthenium concentrations in millerite are consistently below the detection limit of the electron microprobe. Out of thirty grains analysed, one grain was found to contain rhodium above the detection limit.

Pentlandite

Pentlandite compositions vary considerably both between and within samples with average compositions of $Fe_{4.58}Ni_{4.32}Co_{0.06}S_{8.00}$, $Fe_{4.67}Ni_{4.15}Co_{0.10}S_{8.00}$, and $Fe_{4.29}Ni_{4.58}Co_{0.06}S_{8.00}$ for samples A1, B4 and C1 respectively (Table 5.8 and Appendix F, Tables 12 to 14). Note the comparatively high nickel content of the

Table 5.7 *Average millerite compositions in samples C1 and C2 determined by electron-microprobe analysis. The 90% confidence interval was calculated using the Student t-distribution.*

Sample no.	**C1** *(n=20)*		**C2** *(n=10)*	
S	35.22	±0.18	35.35	±0.11
Fe	1.25	±0.23	1.33	±0.42
Ni	62.15	±0.34	62.14	±0.41
Co	0.92	±0.09	0.68	±0.28
Cu	0.05	±0.01	0.05	±0.02
Rh	b.d.l.		b.d.l.	
Pd	b.d.l.		b.d.l.	
Pt	b.d.l.		b.d.l.	
Ru	b.d.l.		b.d.l.	
Atomic proportions				
S	1.00	±0.00	1.00	±0.00
Fe	0.02	±0.00	0.02	±0.01
Ni	0.96	±0.01	0.96	±0.01
Co	0.01	±0.00	0.01	±0.00
Cu	0.001	±0.000	0.001	±0.000
Rh	b.d.l.		b.d.l.	
Pd	b.d.l.		b.d.l.	
Pt	b.d.l.		b.d.l.	
Ru	b.d.l.		b.d.l.	

b.d.l. = below detection limit n = number of grains analysed

pentlandite grains from sample C1, a typical feature of pentlandite from millerite-bearing assemblages (Misra & Fleet, 1973). Cobalt-contents of all grains analysed are relatively low, generally <1 mass per cent. Most pentlandite grains contain significant amounts of palladium and rhodium. Of the fifty-six pentlandite grains analysed, fifty grains contain palladium above the detection limit (at concentration levels up to10 914 ppm), and thirty-one grains rhodium (up to 7 879 ppm). The concentration levels of palladium and rhodium in pentlandite are highly variable, and consequently a much larger number of grains will have to be analysed to obtain reliable average values. Platinum and ruthenium contents are generally below the detection limits.

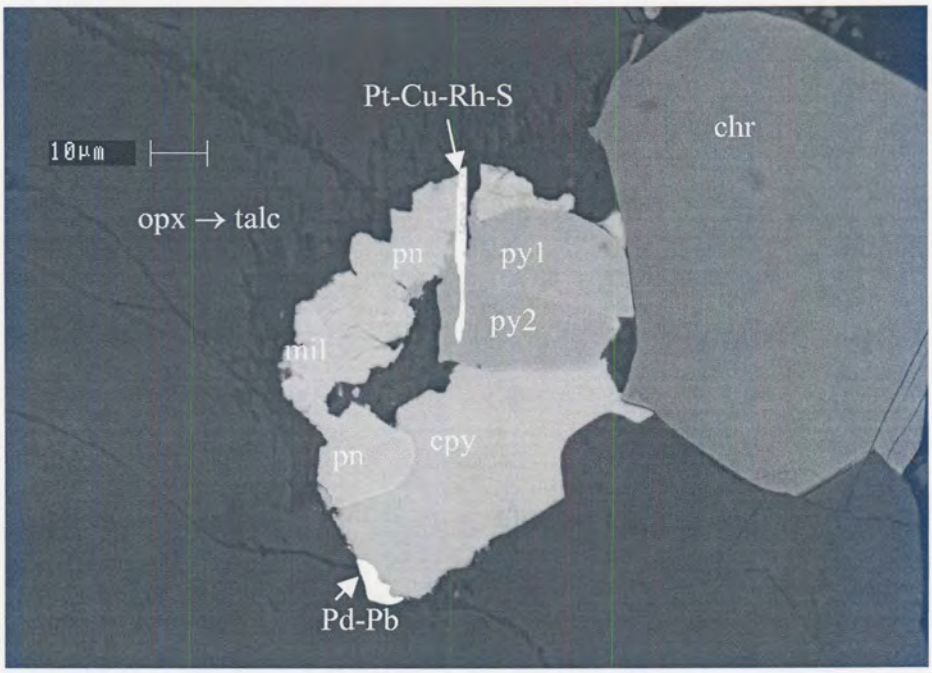

Figure 47 *Composite sulphide grain consisting of pentlandite (pn), chalcopyrite (cpy), millerite (mil) and pyrite (py) with malanite (Pt-Rh-Cu-Ni -S) and Pd-Pb occurring at the grain boundary of chromite (chr) and bronzite being altered to talc (opx → talc). Of special interest is the two grains of pyrite (py1 & py2) with different backscattered electron intensity due to the presence of submicroscopic PGE, probably rhodium or ruthenium.* [§]

Siegenite

A mineral with the average composition $Ni_{1.73}Co_{1.13}Fe_{0.08}S_4$, corresponding to that of siegenite, the intermediate member of the linnaeite-polydymite solid solution series, was commonly observed in trace amounts in the samples from area C. What makes these grains interesting is the fact that of the six grains analysed, three contained platinum (up to ~2 mass per cent) and/or rhodium (up to ~3.5 mass per cent) at concentration levels above the detection limits (Appendix F, Table 15). No palladium was observed in any of these grains.

[§] Concentration levels too low to determine positively whether the PGE is Rh or Ru by EDS analysis using a scanning-electron microscope.

Table 5.8 *Average pentlandite compositions in samples A1, B4 and C1 determined by electron-microprobe analysis. The 90% confidence interval was calculated using the Student t-distribution.*

Sample no.	**A1** *(n=25)*		**B4** *(n=27)*		**C1** *(n=4)*	
S	32.99	±0.08	33.39	±0.09	32.79	±0.25
Fe	32.92	±0.16	33.88	±0.21	30.62	±0.39
Ni	32.63	±0.23	31.80	±0.21	34.34	±0.67
Co	0.45	±0.06	0.73	±0.05	0.46	±0.43
Cu	0.04	±0.01	0.05	±0.01	0.05	±0.03
Rh	b.d.l.-0.7879		b.d.l.-0.5864		b.d.l.-0.0226	
Pd	b.d.l.-1.0914		b.d.l.-0.3499		b.d.l.-0.4059	
Pt	b.d.l.		b.d.l.		b.d.l.	
Ru	b.d.l.		b.d.l.		b.d.l.	
Atomic proportions						
S	8.00	±0.00	8.00	±0.00	8.00	±0.00
Fe	4.58	±0.00	4.67	±0.03	4.29	±0.05
Ni	4.32	±0.03	4.15	±0.03	4.58	±0.08
Co	0.06	±0.01	0.10	±0.01	0.06	±0.06
Cu	0.00	±0.00	0.01	±0.00	0.01	±0.00
Rh	b.d.l.-0.06		b.d.l.-0.04		b.d.l.	
Pd	b.d.l.-0.08		b.d.l.-0.03		b.d.l.-0.03	
Pt	b.d.l.		b.d.l.		b.d.l.	
Ru	b.d.l.-0.01		b.d.l.		b.d.l.	

b.d.l. = below detection limit n = number of grains analysed

5.2.14 PGE mineral characteristics

No attempt was made to determine compositional differences in PGE minerals between samples. Electron microprobe analyses of the major PGE minerals are reported in Appendix G, Tables 1 to 5.

Sulphides of platinum and palladium include cooperite (~average composition $Pt_{0.9}Pd_{0.1}Ni_{0.1}S_{1.0}$) (Appendix G, Table 1), braggite (~average composition $Pt_{0.4}Pd_{0.5}Ni_{0.1}S_{1.0}$) and vysotskite ($Pd_{0.7}Ni_{0.2}S_{1.0}$) (Appendix G, Table 2). These minerals tend to form euhedral to subhedral crystals occurring singly or in composite grains with other PGE minerals as inclusions in, or at grain-boundaries of, base-metal

sulphides and gangue. Complex zoning, which in its simplest form consists of a platinum-rich rim and palladian core, was frequently observed especially in samples from area C and sample B2 (Figures 48 and 49).

*Pt-Rh-Cu-Ni-sulphide (*average composition $Cu_{1.0}Pt_{1.1}Rh_{0.4}Co_{0.3}Ni_{0.2}Fe_{0.1}S_{4.0}$) (Appendix G, Table 3) appears to belong to the malanite-cuprorhodsite-cuproiridsite solid solution series (ideal composition $Cu(Pt,Rh,Ir)_2S_4$). The compositions of the analysed grains are very similar to that of nickeloan malanite reported from the Imandra Layered Complex in northwestern Russia (Barkov *et al.*, 1997). This mineral commonly forms laths (Figure 49), often skeletal (Figures 48 and 50), especially when it occurs in pentlandite with which it seems to have a special affinity. In some grains this mineral (or one similar to it) seems to have exsolved along pentlandite cleavage planes (see Figure 71 for an example).

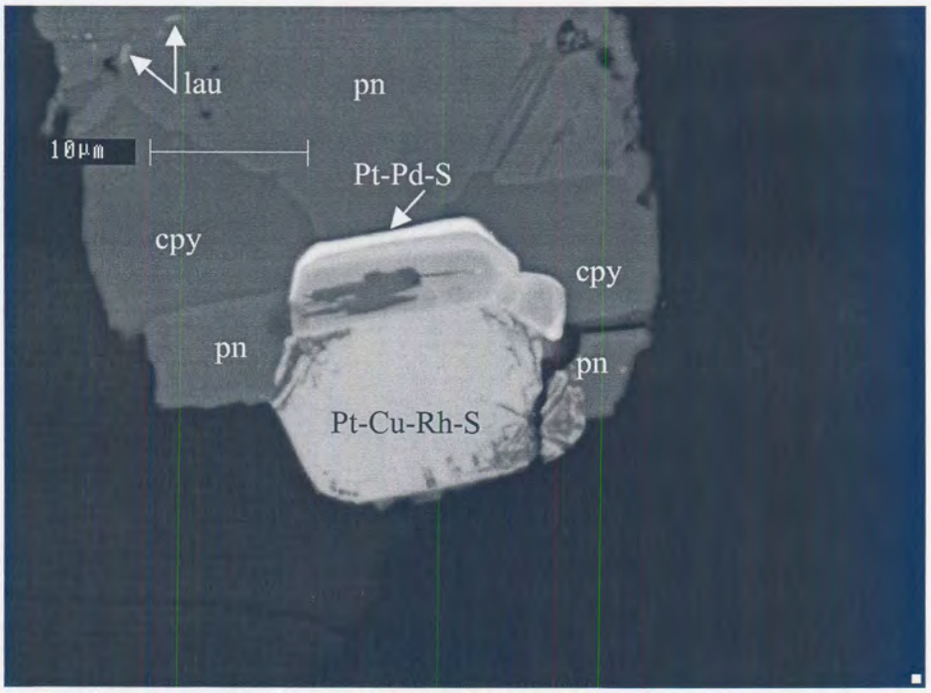

Figure 48 *Zoned Pt-Pd-S (more Pt-rich towards the rim) attached to Pt-Rh-Cu-Ni-S. Note the skeletal appearance of Pt-Rh-Cu-Ni-S at the grain edge. Associated sulphides are pentlandite (pn) and chalcopyrite (cpy). Some laurite (lau) inclusions are also visible. Backscattered-electron image.*

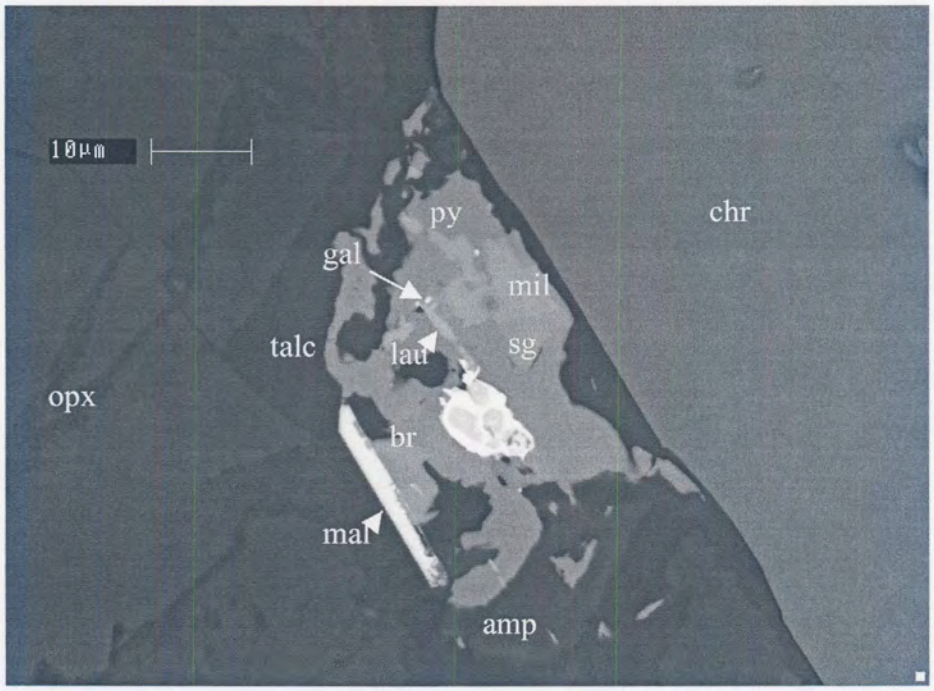

Figure 49 *Zoned Pt-Pd-sulphide (br) (more Pt-rich towards the rim), laurite (lau) and malanite (mal) associated with a composite sulphide grain consisting of siegenite (sg), millerite (mil), pyrite (py) and galena (gal) at the grain boundary of chromite (chr) and orthopyroxene (opx) being altered to talc. Small amounts of amphibole (amp) and pumpellyite (not visible in image) are also present. Backscattered-electron image.*

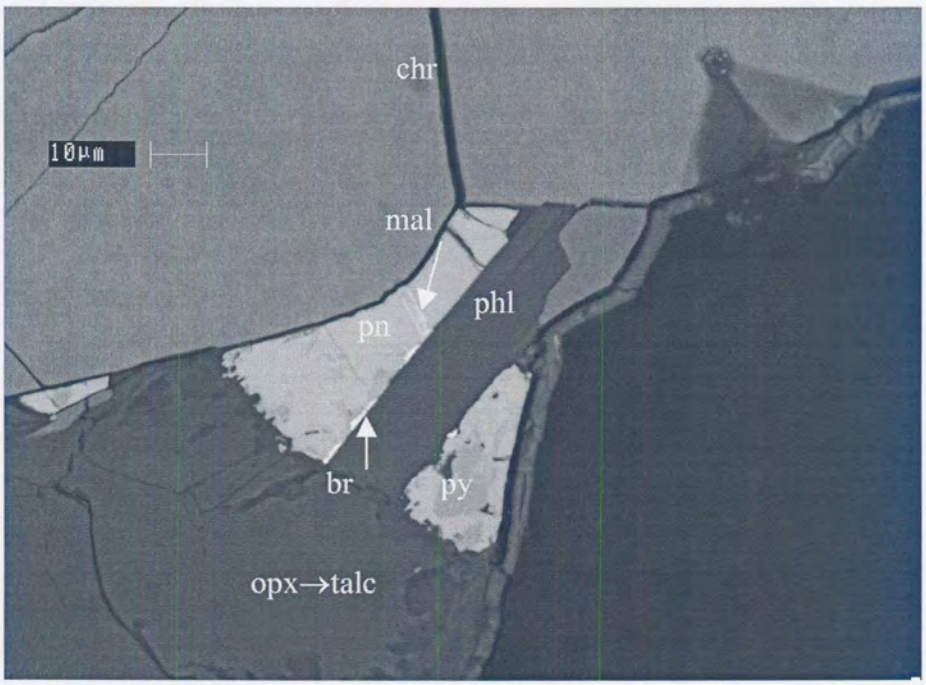

Figure 50 *Skeletal Pt-Rh-Cu-Ni-sulphide (mal) in pentlandite (pn) with pyrite (py) at chromite (chr)-orthopyroxene (opx)→talc. Note the presence of braggite (br) along the grain boundary of sulphide and crosscutting phlogopite (phl). Backscattered-electron image.*

Laurite (ideal composition (Ru,Os,Ir)S_2) commonly occurs as idiomorphic to hypidiomorphic grains in chromite (~20 volume per cent), silicate and base-metal sulphides, or at the grain-boundaries of these minerals. Laurite is sometimes zoned (Figure 51). Less commonly, laurite forms trails of small anhedral inclusions in composite base-metal sulphide grains, often appearing to have exsolved from pentlandite.

Pt-Fe alloys

The average composition of this phase is $Pt_{2.8}Fe_{1.1}$ (Appendix G, Table 4). It occurs as anhedral to euhedral grains in base-metal sulphides and silicate. Note the presence of small amounts of rhodium and palladium. Merkle (1988) also observed the presence of rhodium and palladium in Pt-Fe alloys from the UG1 layer. Pt-Fe alloys often display emulsion intergrowth textures with base-metal sulphides, similar to those described by other researchers (McLaren & de Villiers, 1982; Peyerl, 1982; Kinloch & Peyerl, 1990; Grimbeek, 1995) (Figure 51).

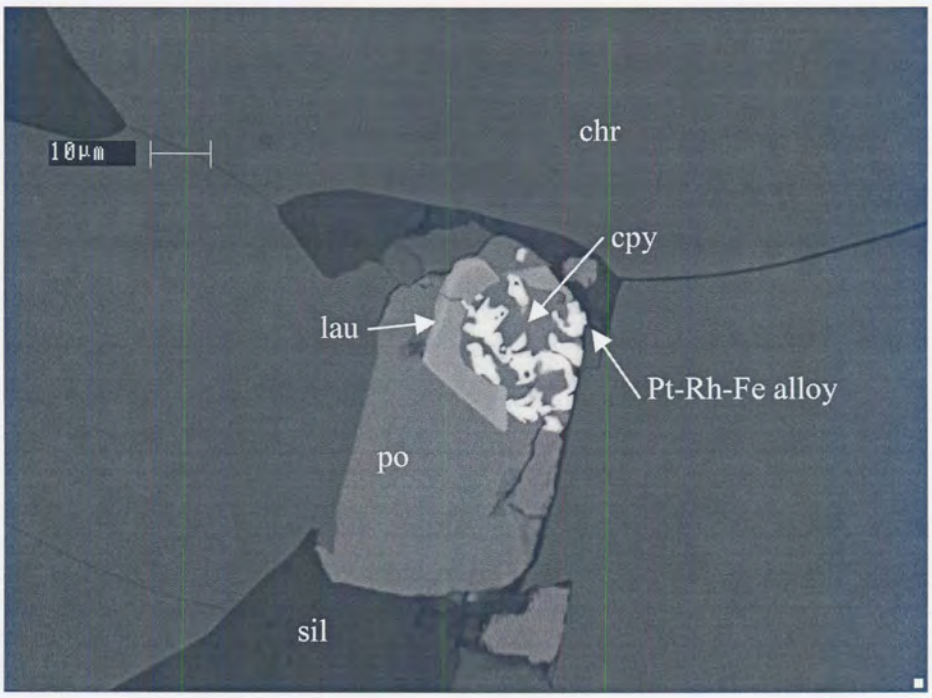

Figure 51 *Pt-Rh-Fe alloy (brightest grains) associated with zoned laurite (lau)(the higher backscattered-electron intensity is the result of a higher Os concentration in the rim) included in a composite chalcopyrite (cpy) and pyrrhotite (po) grain at the grain-boundary of silicate (sil) and chromite (chr). Backscattered-electron image.*

Analyses of *other non-sulphide PGE minerals* such as kotulskite, moncheite, and atheneite can be found in Appendix G, Table 5). Palladium-bearing phases, especially Pd-Pb, are occasionally present as tiny veinlets, of the order of 1 μm across, usually forming part of base-metal sulphide composite grains.

5.3 Characterisation of milled feed samples

5.3.1 General

In all samples except for sample A5, chromite grains were liberated from the silicate matrix during size reduction (Figure 52). Cataclastic textures, as found in sample A5, result in incomplete liberation of chromite, as fractured grains of chromite often remain cemented together by secondary silicates (Figure 53).

Trace amounts of nickel-bearing stainless steel particles were noted in all the samples. These particles originate from the milling rods and cause the introduction of unacceptably high levels of nickel to the samples. The effect can be demonstrated by comparing the nickel contents in two samples before and after rod milling (Table 5.9). The nickel values for both samples were considerably higher after rod milling.

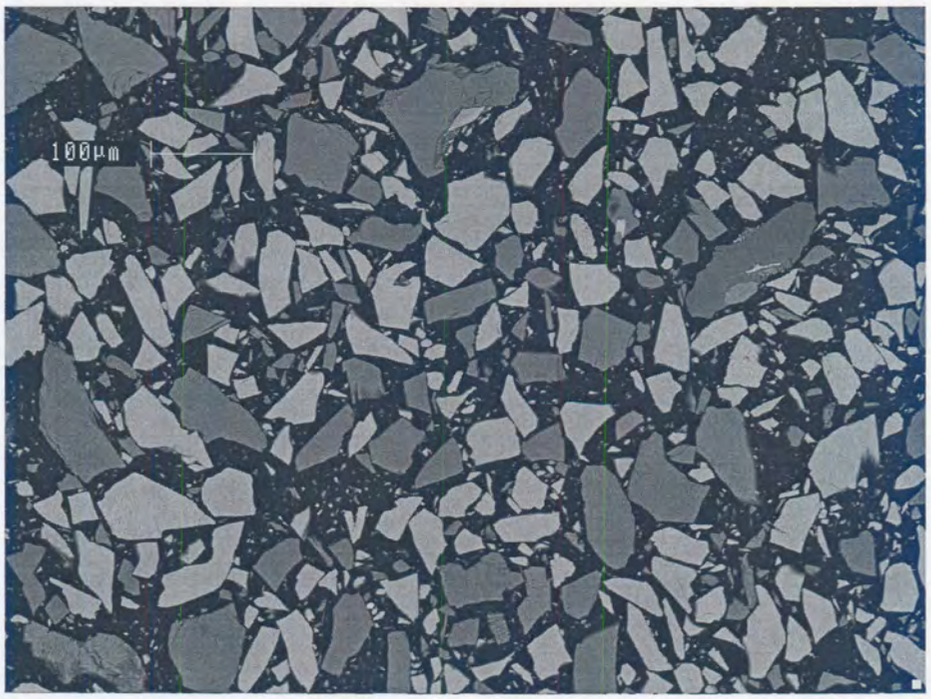

Figure 52 *Milled UG2 chromitite. Silicate = dark grey. Chromite = light grey. Backscattered-electron image.*

Table 5.9 *A comparison of acid soluble and total nickel values in two samples before and after rod milling.*

Sample no.	Total nickel (ppm)		Acid soluble nickel (ppm)	
	Before	After	Before	After
A1	942	1220	271	411
C1	637	993	82	219

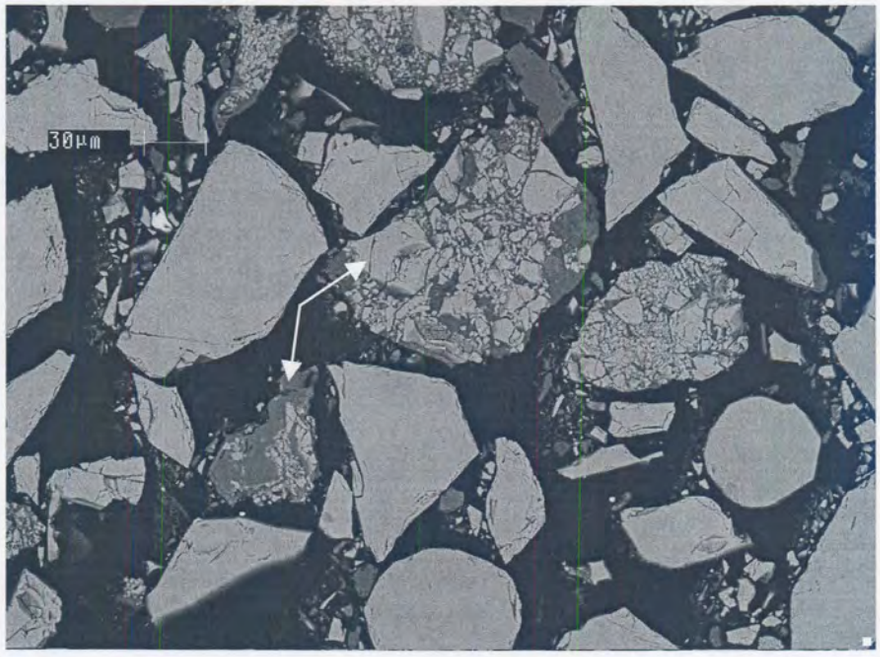

Figure 53 *Cataclastic UG2 milled to 80% <75µm. Arrows indicate fractured chromite grains cemented by hydrous sheet silicates. Backscattered-electron image.*

5.3.2 Chromite and silicate grain-size distributions

At 80% <75µm, chromite grain-sizes in all of the samples range from <10 µm to ~150 µm (Appendix H, Table 1). Differences between samples are small, with measured median equivalent circle diameters ranging from 32 µm to 44 µm (Table 5.1R).

Silicate grain-size distributions in all of the samples are also very similar, ranging from <10 µm to ~130 µm (Appendix H, Table 2), with measured median equivalent circle diameter values varying between 30 and 39 µm (Table 5.1S). More silicate fines are created, with an average of 39 per cent silicate reporting to the <17µm

fraction compared to only 15 per cent of the chromite. This can probably be ascribed to the natural tendency of sheet silicates such as talc, chlorite and phlogopite to form fines during size reduction.

5.3.3 Base-metal sulphide

Base-metal sulphide grain diameters in the milled feed samples range from <5 µm up to ~50 µm with median values between ~2 and 13 µm (Table 5.1T). Base-metal sulphide liberation is generally good (estimated >90 per cent) in most samples from areas A and B. The exceptions being samples A3 at 87%, A4 at 70%, and A5 at 69%. The degree of liberation is generally lower but extremely variable in the samples from area C (33 to 91 per cent).

5.3.4 PGE minerals

PGE mineral mode of occurrence & liberation in fourteen UG2 chromitite samples milled to 80% <75µm

The mode of occurrence of PGE minerals observed in all fourteen milled feed samples is tabulated in Table 3 of Appendix H. A simplified classification scheme is presented in Table 5.1U and Figure 54.

In all of the samples, between 48 and 79 per cent of the PGE minerals were liberated during milling. Except for sample A5, the remainder of the PGE minerals in the milled samples from areas A and B are mostly associated with liberated base-metal sulphide grains (9 to 38 per cent). By contrast, less than 7 per cent of the PGE minerals in the milled feed samples from area C and sample A5 are associated with liberated base-metal sulphides. In these samples, a significant proportion of the PGE minerals (24 to 41 per cent for samples from area C and 52 per cent for sample A5) is associated with gangue, mostly silicate.

The preferred association of PGE minerals with base-metal sulphides, coupled with the higher degree of liberation of these sulphides in samples from area A (except for sample A5) and B, results in a higher proportion of PGE mineral-bearing particles with a high combined liberation index in these samples compared to those from area C

and sample A5 (Table 5.1V). Exclusion of laurite from the combined liberation index calculations does not yield statistically different values (Table 5.1W).

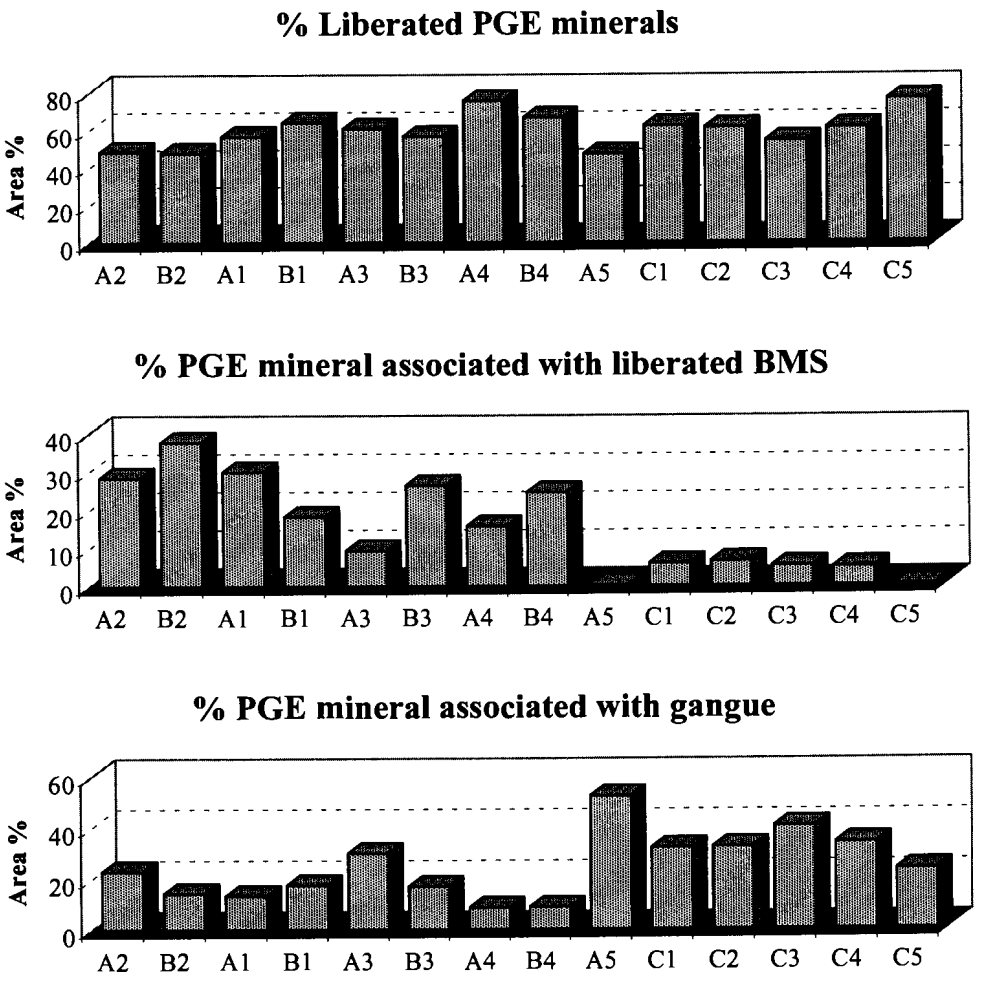

Figure 54 *Mode of occurrence of PGE minerals in fourteen samples of UG2 chromitite milled to 80% <75μm.*

PGE mineral grain-size distribution

Measured median PGE mineral grain diameters range between 3.8 and 6.9 μm based on area per cent, and between 1.6 and 2.4 μm based on number per cent (Table 5.1X).

The measured grain-size distributions of a composite of the PGE minerals found in all fourteen samples, before and after milling to 80% <75μm, are compared in Figure 55

and Table 5.10, and indicates that milling of the ore caused an even further reduction in the grain size of the PGE minerals.

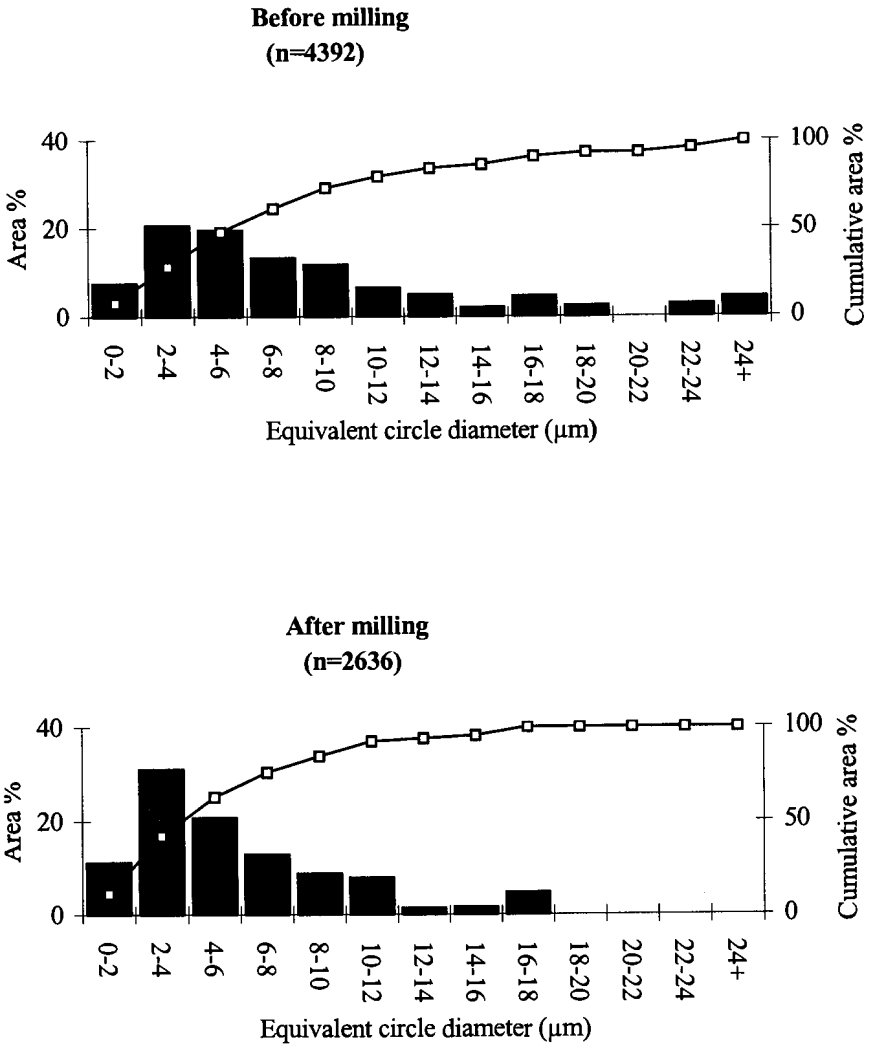

Figure 55 *PGE mineral grain-size distribution of UG2 chromitite at <2mm and at 80% <75µm.*

5.4 Characterisation of flotation product samples

5.4.1 Chromite in flotation products

Comparison of the chromite grain-size distributions in the different flotation products, shows that the chromite in the concentrates is fine-grained compared to that in the tailings (Figure 56 and Table 4, Appendix H). About 90 per cent of the chromite in the fast-floating concentrates occurs as grains smaller than 10 µm. Most of the chromite in the flotation concentrates is present as liberated grains.

Table 5.10 *A comparison of the grain-size distributions of PGE minerals in a composite of fourteen samples of UG2 feed crushed to <2mm and at 80% <75µm. n=number of PGE mineral grains measured.*

Particle size	***< 2mm***		***80% <75µm***	
n	4392		2636	
	area	*number*	*area*	*number*
Median 50th percentile (µm)	6.3	2.6	4.8	2.0
20th percentile (µm)	3.2	1.0	2.6	0.4
80th percentile (µm)	12.4	4.5	9.0	3.7

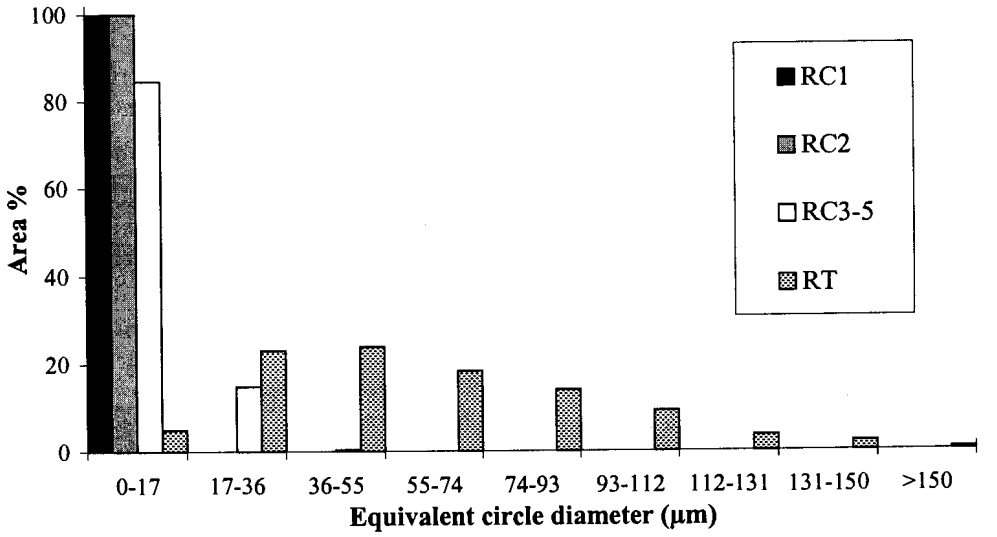

Figure 56 *Chromite grain size-distribution in flotation products of sample C1. RC1 = Rougher concentrate 1 (0-1 minutes), RC2 = Rougher concentrate 2 (1-3 minutes), RC3-5 = Combined rougher concentrates 3, 4 and 5 (3-20 minutes), RT = Rougher Tailings*

5.4.2 Silicate in flotation products

Silicate minerals are present in the flotation concentrates in two forms:

- as part of composite grains together with base-metal sulphide and/or PGE minerals (Figure 57)
- as fine-grained liberated silicates (Figure 57).

The silicate minerals in the flotation concentrates are generally very fine-grained with the coarser-grained silicates reporting to the flotation tailings (Figures 57, 58 and 59, and Table 5, Appendix H).

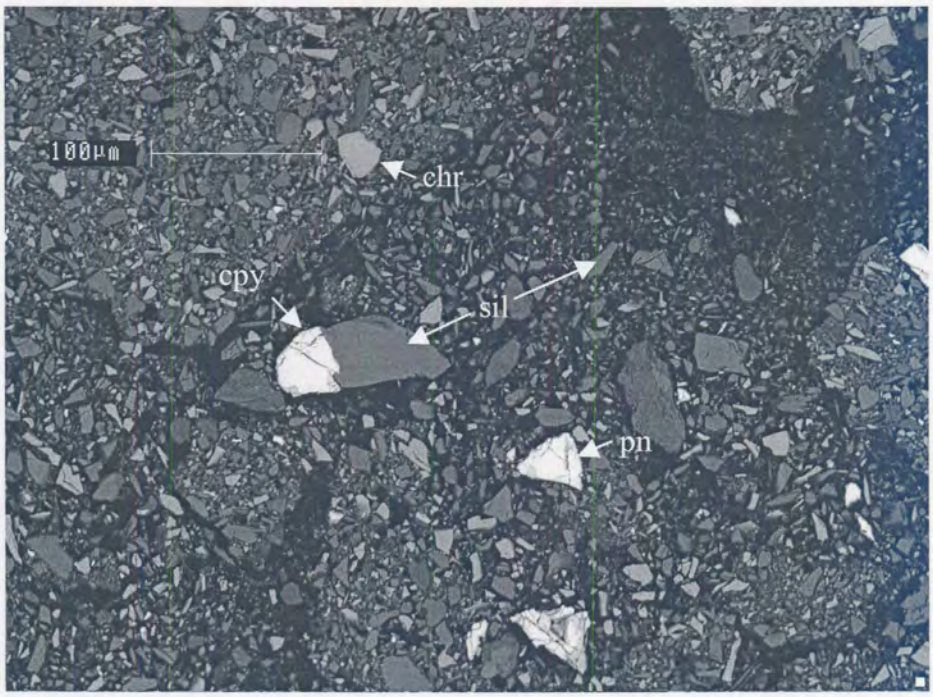

Figure 57 *Backscattered-electron image of a flotation concentrate sample. The sample consists predominantly of fine-grained liberated chromite (chr) and silicate (sil). Note the coarser silicate grain forming part of a composite particle with chalcopyrite (cpy). A liberated pentlandite (pn) grain can also be seen.*

The silicate mineralogy of the flotation products of six samples (A1, A3, B3, B4, C1 and C4) was quantified in terms of the relative proportions of Ca-Al-silicate, Mg-Fe-silicate, phlogopite, clinopyroxene, quartz, albite and K-Al silicate by EDS point counting (Appendix H, Table 6). These results, combined with the silicate gangue

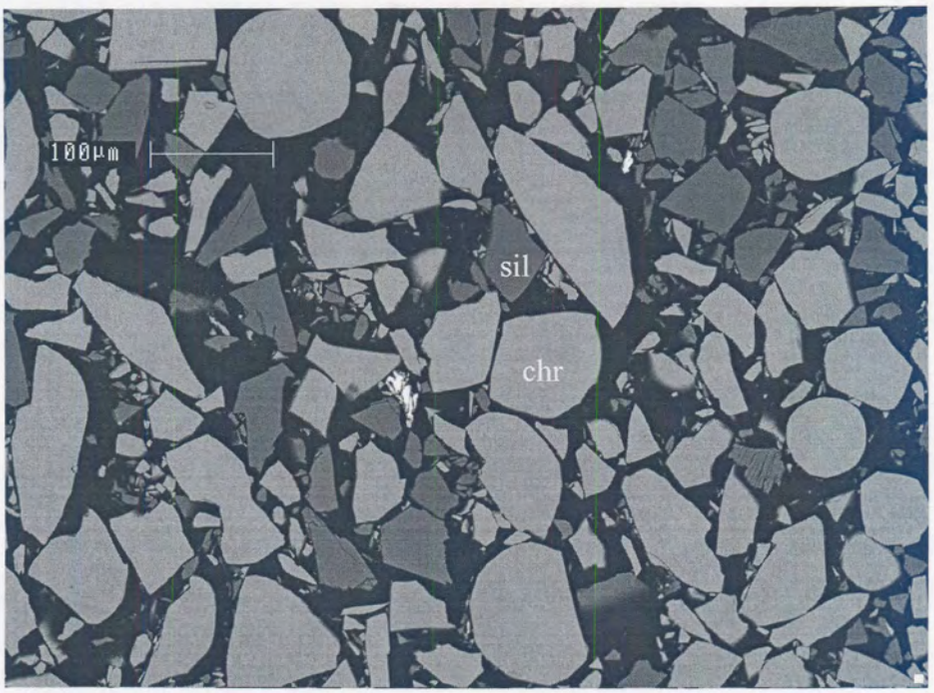

Figure 58 *Coarse liberated chromite (chr) and silicate (sil) grains in flotation tailings. Backscattered-electron image.*

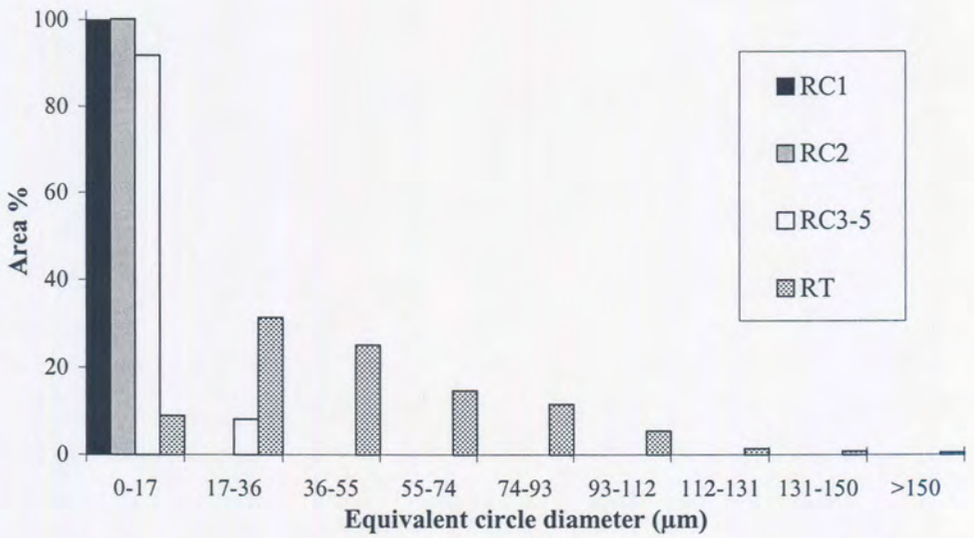

Figure 59 *Silicate grain size-distribution in flotation products of sample C1. RC1 = Rougher concentrate 1 (0-1 minutes), RC2 = Rougher concentrate 2 (1-3 minutes), RC3-5 = Combined rougher concentrates 3, 4 and 5 (3-20 minutes), RT = Rougher Tailings*

flotation results (Appendix J, Table 3), were used to calculate time-recovery profiles for Ca-Al-silicate (predominantly plagioclase) and Mg-Fe silicate (orthopyroxene and talc) (Figure 60).

Recoveries of Ca-Al-silicate after 20 minutes flotation range between seven and eighteen per cent (indicated in red). For sample A1, Fe-Mg-silicate recovery (in blue) after 20 minutes is very similar to that of Ca-Al-silicate, 13 per cent compared to 17 per cent respectively. For the other samples Fe-Mg-silicate recovery is higher than that of Ca-Al-silicate, especially in the samples from area C. In sample C1, Fe-Mg-silicate recovery after 20 minutes is 64 per cent compared to 7 per cent for Ca-Al-silicate.

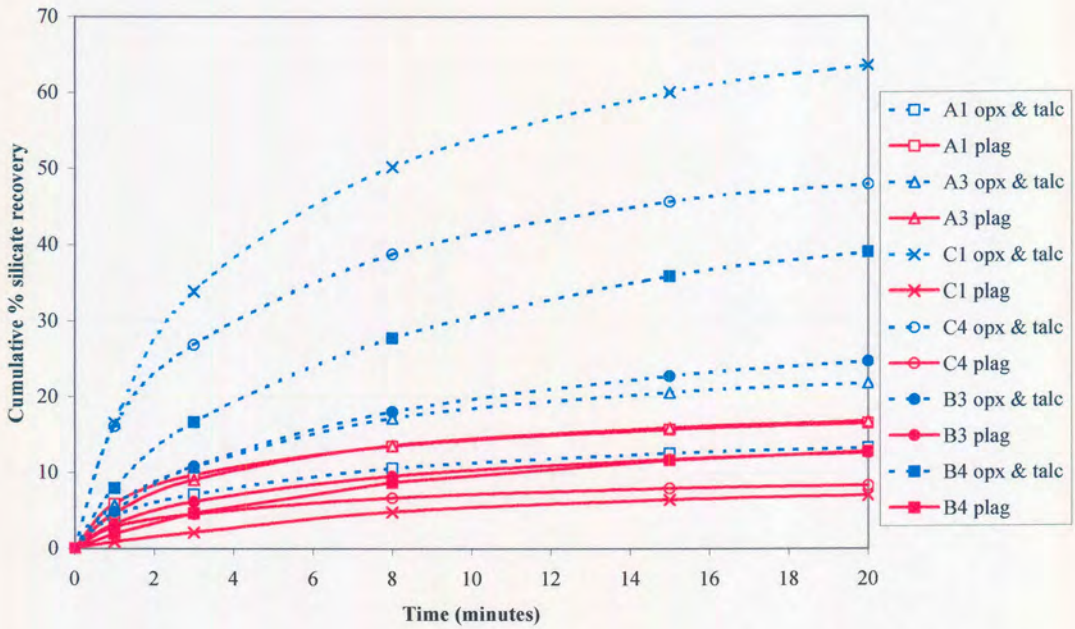

Figure 60 *A comparison of time-recovery profiles for Fe-Mg-silicate, orthopyroxene (opx) and talc, (blue) and Ca-Al-silicate, predominantly plagioclase (plag), (red) in six samples.*

Although the EDS point-counting technique cannot reliably distinguish between minerals with similar compositions, such as talc and orthopyroxene occurring in fine-grained intergrowths (see section 4.6.3), X-ray diffraction indicates that talc is concentrated in the flotation concentrates relative to the other silicate minerals (Figure 61).

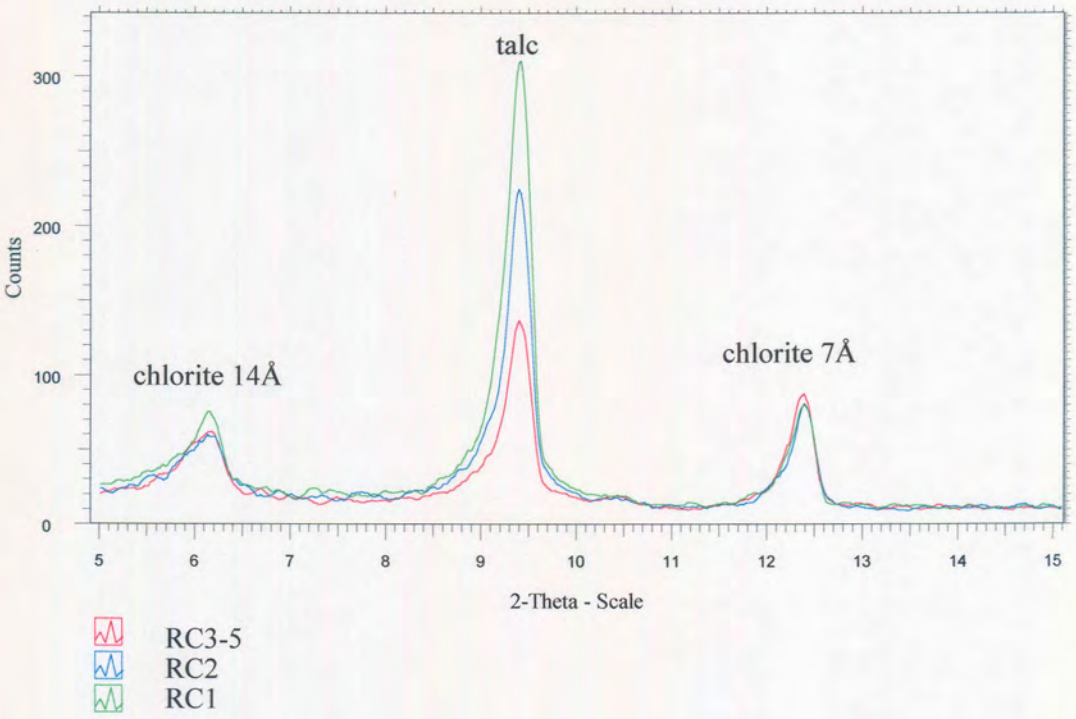

Figure 61 *X-ray diffractogram from 5°2θ to 15°2θ for RC1 (rougher concentrate 1, 0-1 minutes), RC2 (rougher concentrate 2, 1-3 minutes) and RC3-5 (combined rougher concentrate 3, 4 and 5, 3-20 minutes) of sample C1.*

5.4.3 Base-metal sulphides in flotation products

Grain-size distribution

The coarsest base-metal sulphide grains are recovered to the fastest floating concentrates, with progressively finer grains being recovered with time (Figure 62). Equivalent circle diameters of base-metal sulphide grains in the flotation concentrates are generally below 80 µm, with median values between 10 and 15 µm in the fast-floating concentrate (RC1), between 5 and 10 µm in the medium-floating concentrate (RC2), and smaller than 5 µm in the slow-floating (RC3-5) concentrate. Base-metal sulphide grains in flotation tailings samples are generally below 10 µm in size.

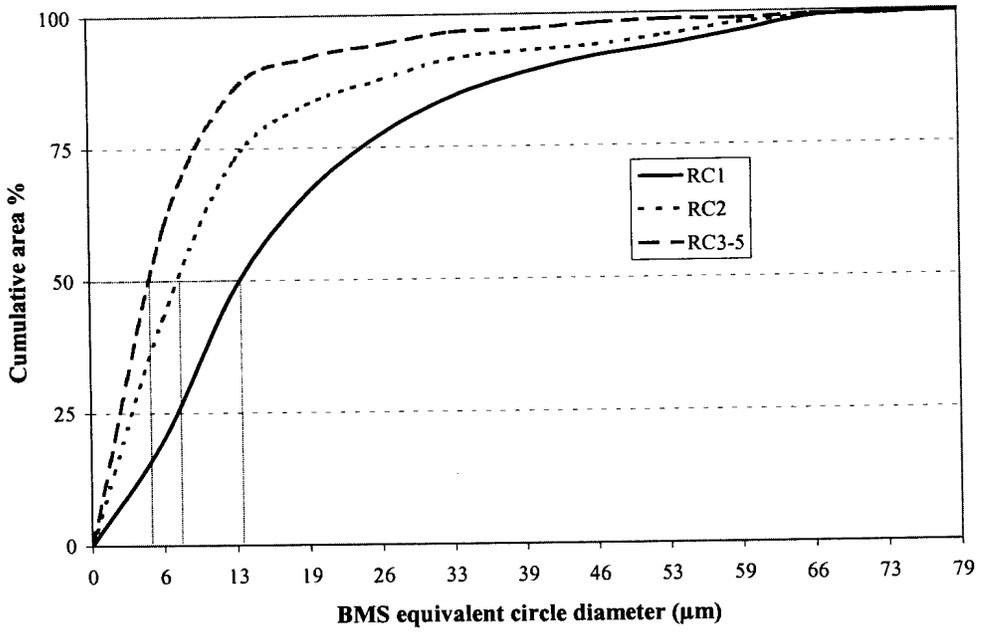

Figure 62 *Base-metal sulphide (BMS) size distributions in composite flotation concentrates of samples A1, A3, A5, and B4. RC1 = (rougher concentrate 1, 0-1 minutes), RC2 = (rougher concentrate 2, 1-3 minutes) and RC3-5 = (combined rougher concentrate 3, 4 and 5, 3-20 minutes).*

Liberation characteristics

In all of the samples, most of the base-metal sulphides in the concentrate samples appear to be liberated from gangue, with a decrease in the degree of liberation of base-metal sulphides from the fast-floating concentrate through to the slower floating concentrates (Table 7, Appendix H and Figure 63). Note the high degree of liberation measured in the concentrates of samples A1, A4 and B5 (more than 90 per cent in all concentrates). The degree of liberation of the base-metal sulphides recovered in the concentrates of samples A3, C1, C2 and A5 is lower (70 to 90 per cent).

Base-metal sulphides in the tailings samples occur almost exclusively as <10 µm grains at silicate-silicate grain boundaries, or as inclusions in silicate grains (Figure 64).

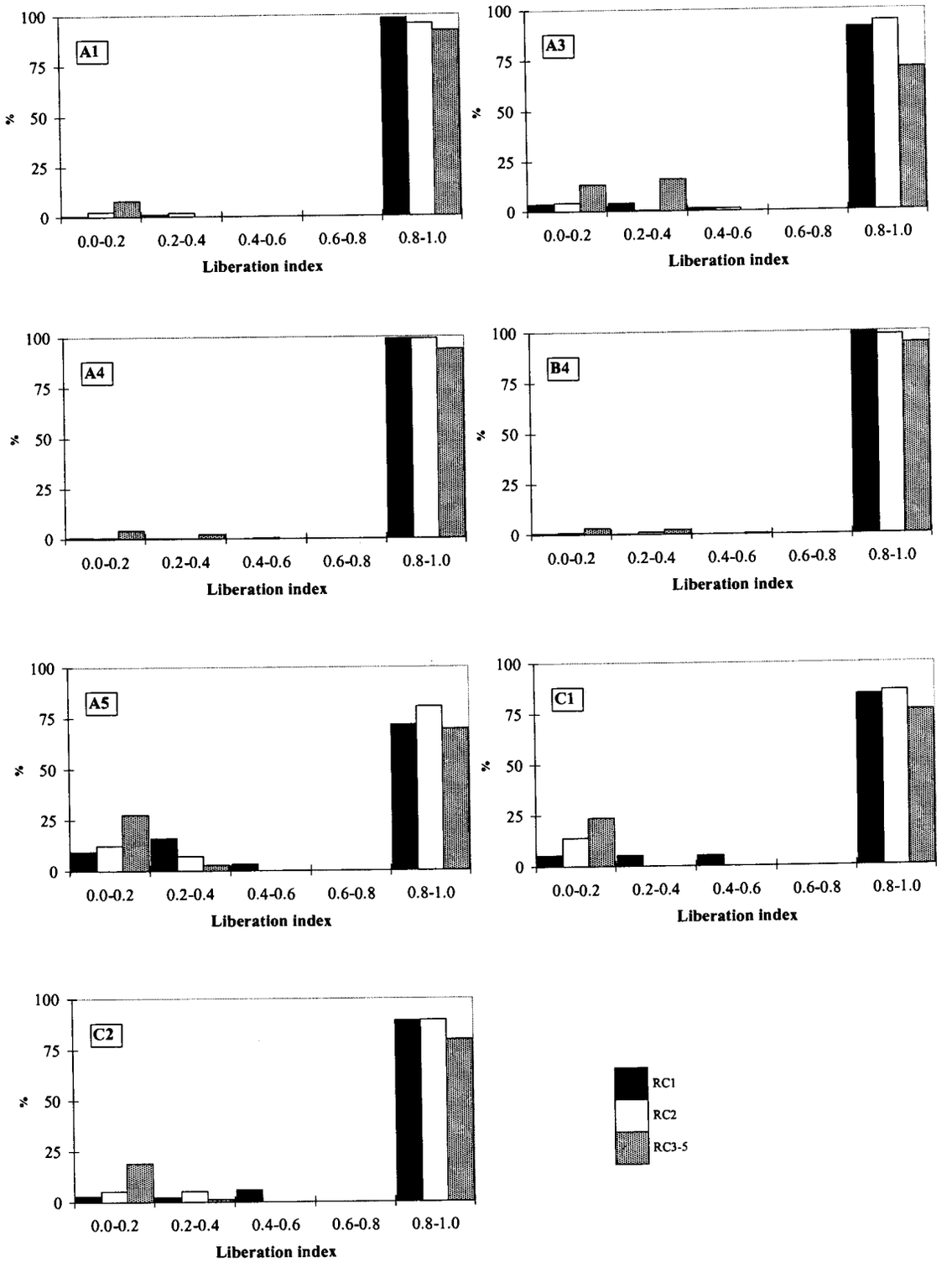

Figure 63 *Base-metal sulphide liberation index in flotation concentrates of samples A1, A3, C1, C2, A4, A5 and B4. RC1 = rougher concentrate 1 (0-1 minutes), RC2 = rougher concentrate 2 (1-3 minutes) and RC3-5 = combined rougher concentrates 3, 4 and 5 (3-20 minutes).*

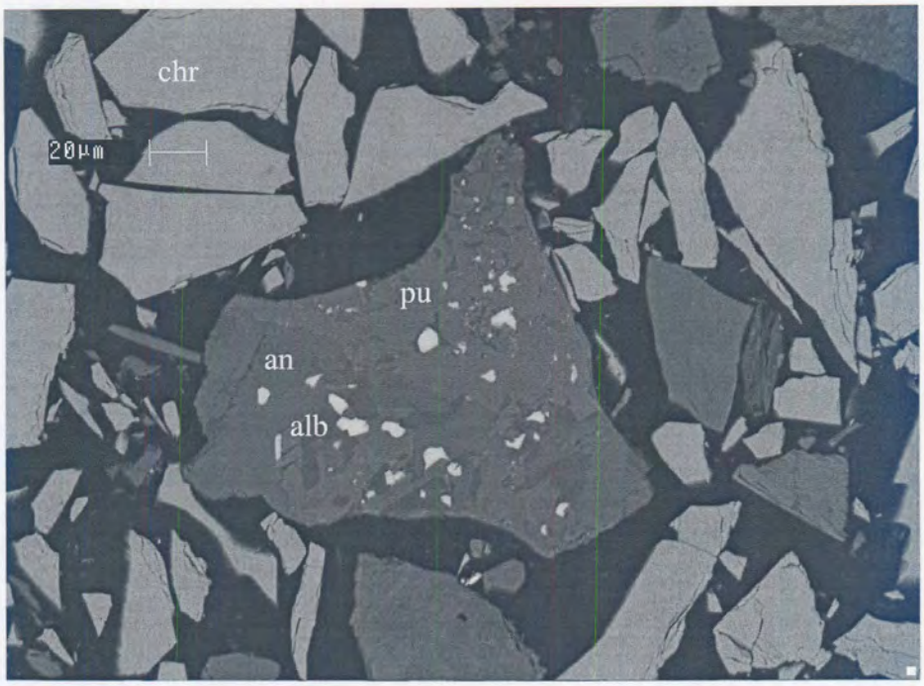

Figure 64 *Millerite and chalcopyrite (bright grains) associated with anorthite (an), pumpellyite (pu) and albite (alb) in flotation tailings. Backscattered-electron image.*

Type of base-metal sulphide

The relative proportions of the base-metal sulphides in the flotation feeds from areas A and B are graphically compared to that in the rougher concentrate 1, rougher concentrate 2, and a combined rougher concentrate 3, 4 and 5 in Figure 65. In most of the samples pyrrhotite appears to be relatively slow-floating compared to chalcopyrite, pentlandite and pyrite. Microscopic investigation of flotation concentrates indicated the presence of relatively coarse (up to 100 µm) liberated pyrrhotite particles reporting to slow-floating concentrates of samples B2 and A4.

The modal proportions of the base-metal sulphides in the flotation feeds and concentrates of samples from area C are compared in Figure 66. Where pyrrhotite is present, it is once again relatively slow-floating. Pyrite generally appears to be recovered at a faster rate than chalcopyrite.

A time-recovery profile was calculated for pentlandite, chalcopyrite, pyrrhotite, pyrite and millerite in each of the samples, and also for a composite of all the samples

(Tables 8 to 12, Appendix H).[§] The results for the composite sample are graphically illustrated by Figure 67. Overall, the rate of recovery for the individual sulphides appears to be pyrite>chalcopyrite≅millerite≅pentlandite>>pyrrhotite.[+]

Electron-microprobe analyses indicated that the compositions of pyrrhotite from different samples differ. This will affect the surface chemistry, and therefore flotation behaviour of pyrrhotite, and could potentially affect the recovery of PGEs. However, as pyrrhotite does not appear to host significant amounts of PGEs in solid solution (Table 5.4) or as discrete grains (Table 5.1Q), this line of investigation was not pursued any further.

5.4.4 Behaviour of PGE minerals during recovery

The flotation products of seven samples, A1, A3, A5, A4, B4, C1 and C2, were selected for the investigation of PGE mineral behaviour during flotation. To be able to reliably detect small differences between particle types reporting to different flotation products, the results for the seven samples were composited to improve the statistics.

PGE mineral mode of occurrence and liberation

The combined liberation index distributions of the PGE mineral-bearing particles in the different flotation products are compared in Figure 68 and Table 5.11. Most of the PGE minerals recovered to the fast-floating concentrate (rougher concentrate 1) occur

---

[§] As sulphide concentration levels in the flotation tailings were too low to obtain meaningful modal analysis results, a total recovery of 100 per cent was assumed. The amount of chalcopyrite in each of the sulphide concentrates was calculated from the copper content. This value, combined with the modal proportions of the other sulphides, was used to calculate the pentlandite, millerite, pyrite and pyrrhotite contents of each concentrate.

[+] Millerite is widely believed to be of a slow-floating nature. No indication could be found that this is true of millerite found in these samples of UG2 chromitite. At the same time the slow-floating nature of pyrrhotite is clearly borne out by the data.

Figure 65 *Relative proportions of chalcopyrite, pentlandite, pyrrhotite, pyrite and millerite in three flotation concentrates of samples from Areas A and B. RC1 = (rougher concentrate 1, 0-1 minutes), RC2 = (rougher concentrate 2, 1-3 minutes) and RC3-5 = (combined rougher concentrate 3, 4 and 5, 3-20 minutes)*

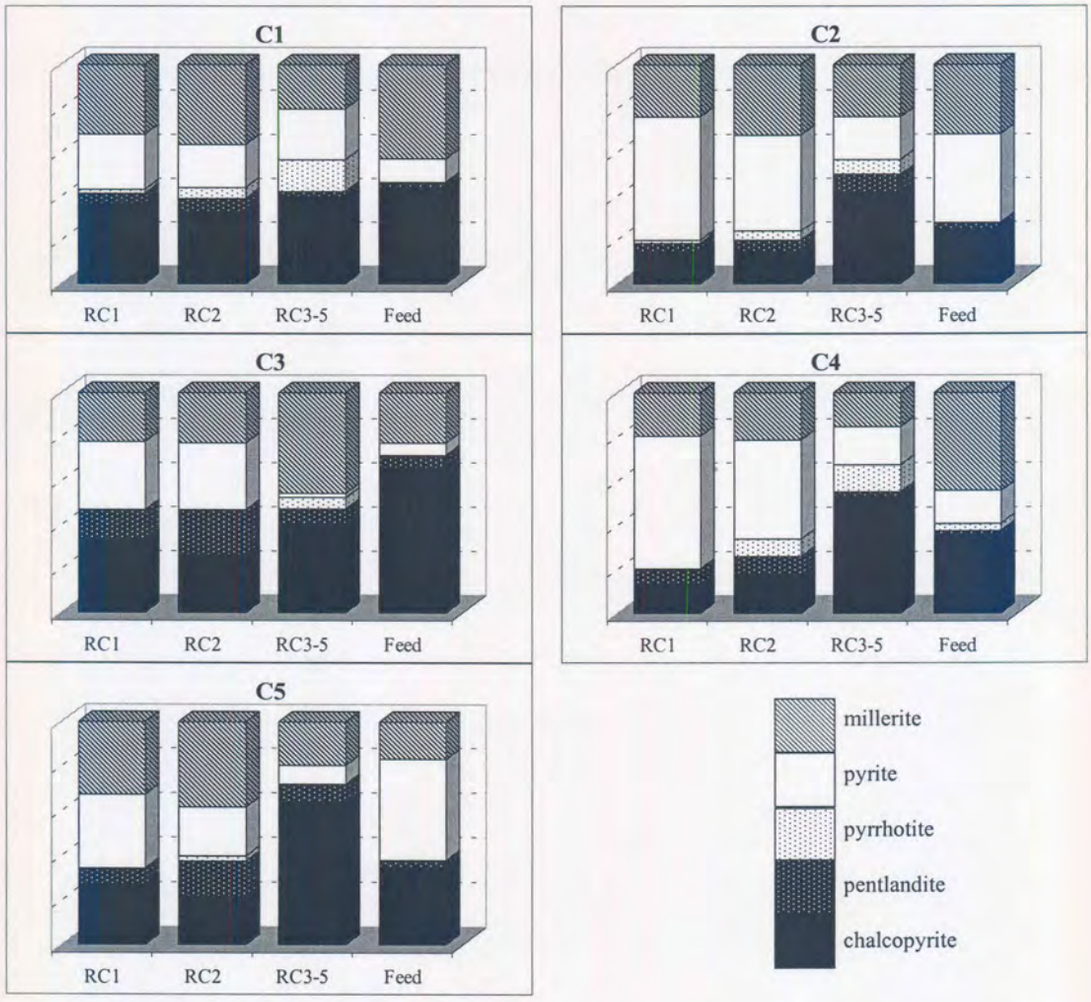

Figure 66 *Relative proportions of chalcopyrite, pentlandite, pyrrhotite, pyrite and millerite in three flotation concentrates of samples from Area C. RC1 = rougher concentrate 1 (0-1 minutes), RC2 = rougher concentrate 2 (1-3 minutes) and RC3-5 = combined rougher concentrates 3, 4 and 5 (3-20 minutes).*

in particles with a high combined liberation index, i.e. >0.8. These PGE minerals are predominantly liberated PGE minerals (Figure 69 and 70, Table 5.12) and PGE minerals associated with liberated base-metal sulphide grains (Figure 69, 71 and 72).

With time, an increased proportion of PGE minerals associated with gangue, mostly silicate, is recovered. During flotation of samples A3, C1, C2 and A5, a significant proportion of PGE minerals associated with gangue was recovered even to the faster-floating concentrates. The rougher tailings contain predominantly PGE mineral grains associated with gangue. This is reflected by the low combined liberation indices of PGE mineral-bearing particles in tailings samples (Table 5.11 and Figure 68).

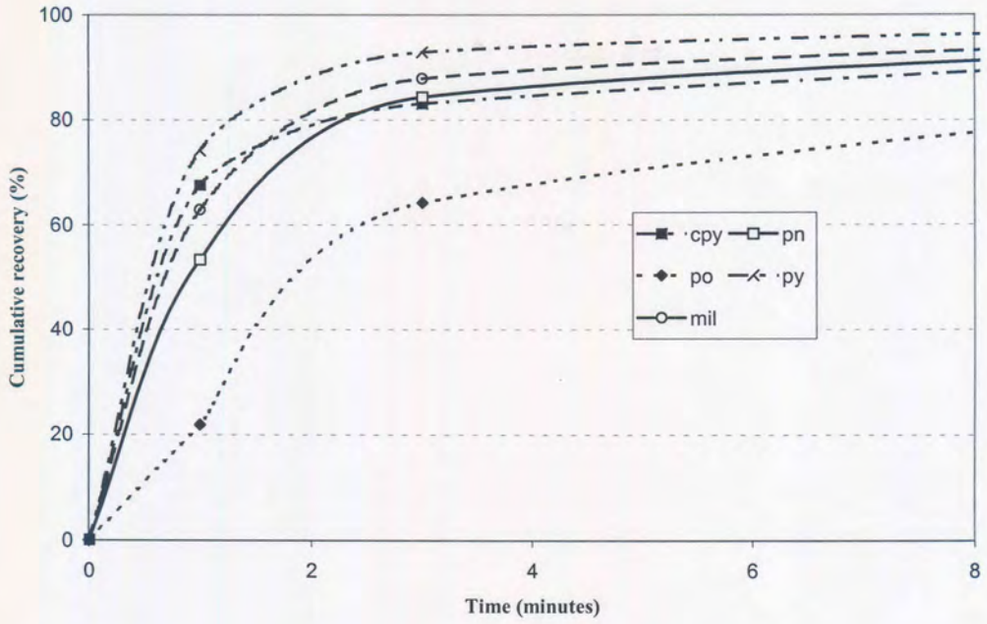

Figure 67 *Time-recovery profile for chalcopyrite (cpy), pyrite (py), pentlandite (pn), pyrrhotite (po) and millerite (mil) calculated from a composite of all the samples and assuming an ultimate sulphide recovery of 100%.*

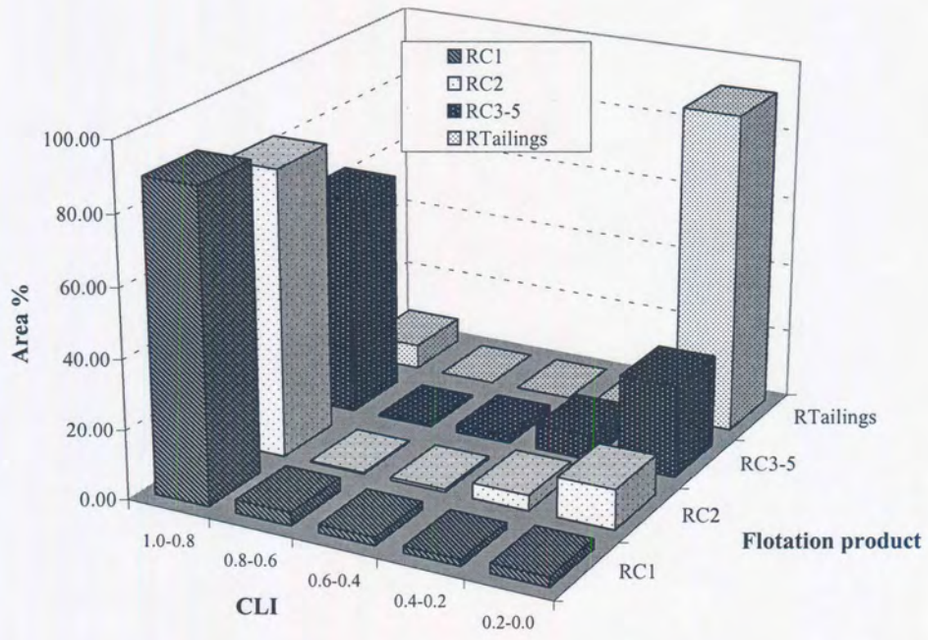

Figure 68 *Combined liberation index (CLI) of PGE minerals (excluding laurite) in the composite flotation products of samples A1, A3, A4, A5, B4, C1 and C2.*

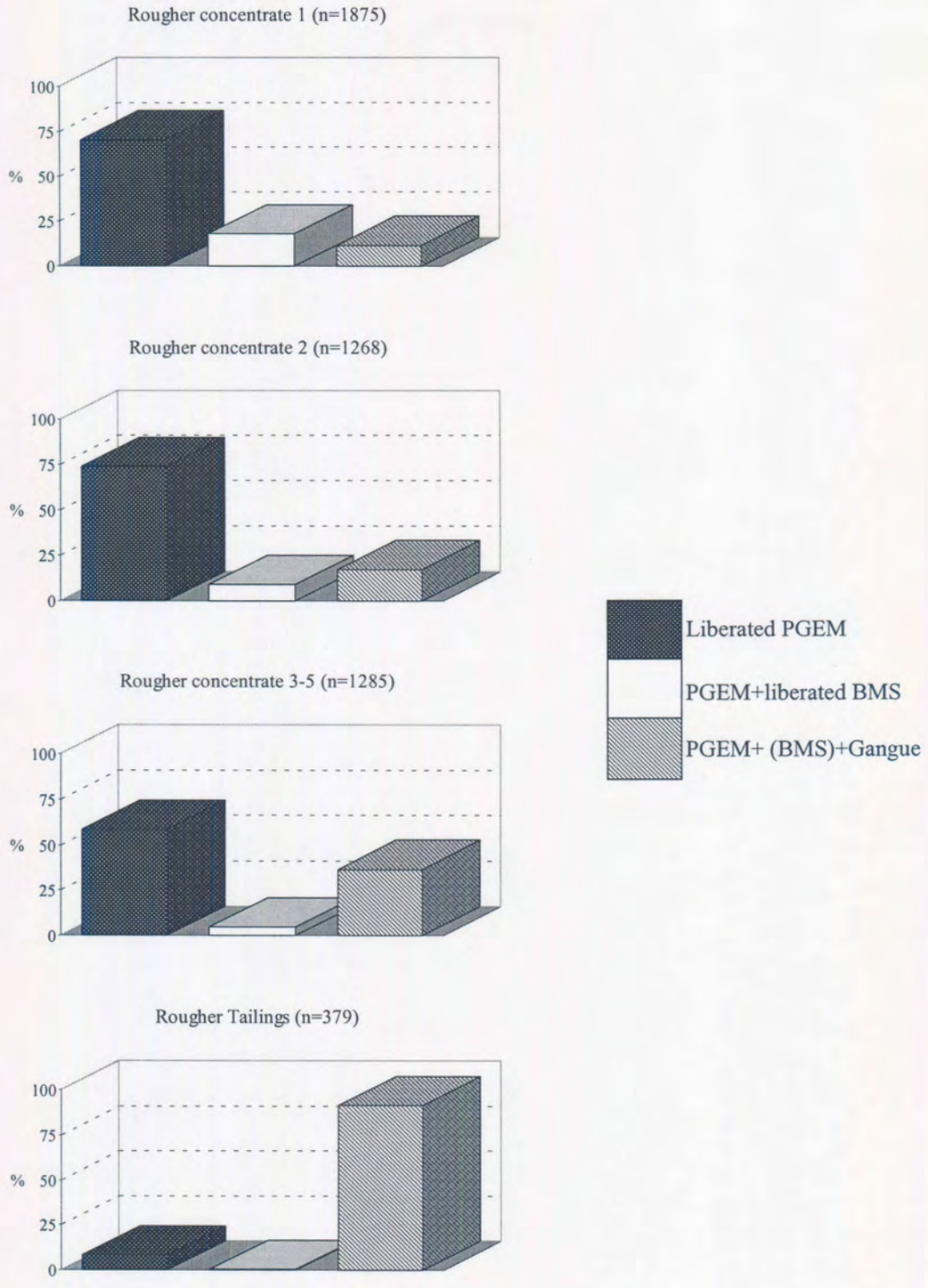

Figure 69 *Mode of occurrence of PGE minerals (PGEM) in different flotation products based on combined data of seven samples. (BMS = base-metal sulphide, n = number of PGE mineral grains measured).*

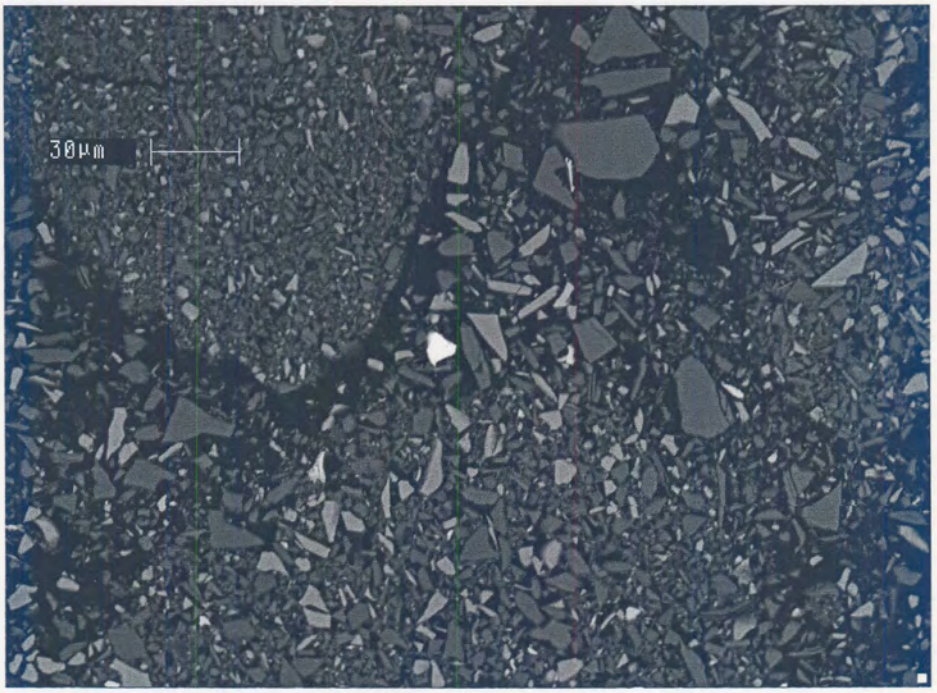

Figure 70 *Liberated PGE mineral (bright grain in the centre of the image) in flotation concentrate. Backscattered-electron image.*

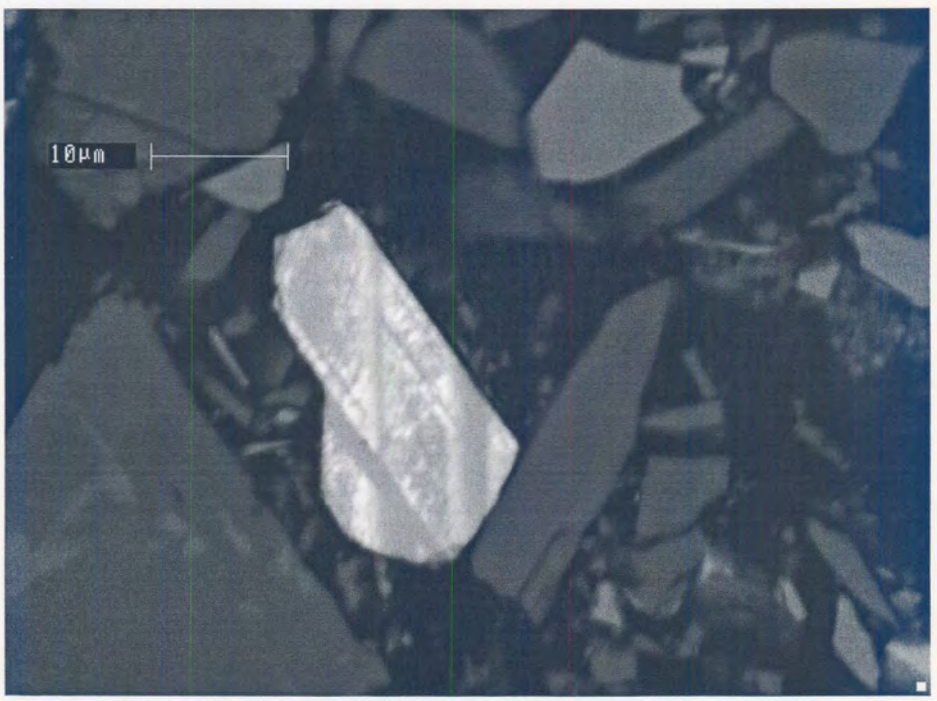

Figure 71 *Liberated pentlandite grain with exsolved Pt-Rh-Cu-Ni-sulphide in flotation concentrate. Backscattered-electron image.*

Figure 72 *Braggite (br) grain attached to pentlandite (pn) with pyrite inclusions (slightly darker). Backscattered-electron image.*

Flotation behaviour of liberated PGE mineral grains

Effect of grain size

In all of the samples, the coarsest PGE mineral grains were recovered in the fastest-floating concentrates, with progressively smaller grains reporting to the slower-floating concentrates and the tailings (Table 5.13 and Figure 73).

Type of PGE mineral

The relative proportions of the different PGE minerals present as liberated grains in the different flotation products of the seven samples are listed in Table 13 of Appendix H. The rates of flotation of the individual PGE mineral species were calculated based on a composite of the data for the seven samples. The results (Table 5.14 and Figure 74) indicate that there are differences in the rate of flotation of the different PGE mineral phases, with the rate of flotation being (Pt,Pd)-sulphide > Pt-sulphide > (Pt,Rh,Cu,Ni)-sulphide ≅ Pt-Fe alloy and the other non-sulphide PGE mineral phases ≅ (Ru,Os,Ir)-sulphide. To determine whether these differences may be

ascribed to differences in grain size, the grain-size distributions of (Pt,Pd)-sulphide (including cooperite), (Pt,Rh,Cu,Ni)-sulphide, (Ru,Os,Ir)-sulphide and non-sulphide PGEM (including Pt-Fe alloy) in the feed material were compared both in terms of area per cent and per cent number of grains (Figure 75A and B). The grain-size distributions for the four mineral groups are very similar, with median diameter values of 4 to 5µm, 5 to 6µm, ~7µm, ~7µm respectively. This does indicate that the slow-floating non-sulphide PGE minerals are also finer grained. On the other hand, the relatively slow-floating malanite appear to be coarser-grained compared to the faster-floating Pt-Pd–sulphide minerals.

Table 5.11 *Combined liberation index distribution in the flotation concentrates (RC1, 0 to 1 minutes, RC2, 1 to 3 minutes and RC3-5, 3 to 20 minutes) and tailings of selected samples.*

RC1	*A1*	*A3*	*A4*	*B4*	*A5*	*C1*	*C2*
0.0-0.2	1	2	0	3	9	2	2
0.2-0.4	0	6	2	0	1	2	1
0.4-0.6	0	1	0	0	5	2	8
0.6-0.8	0	1	0	0	1	1	23
0.8-1.0	98	90	97	96	84	93	66
RC2	*A1*	*A3*	*A4*	*B4*	*A5*	*C1*	*C2*
0.0-0.2	6	18	1	11	15	8	20
0.2-0.4	0	5	0	1	15	1	8
0.4-0.6	0	2	1	0	2	1	0
0.6-0.8	0	0	0	2	1	0	0
0.8-1.0	94	75	98	86	68	90	71
RC3	*A1*	*A3*	*A4*	*B4*	*A5*	*C1*	*C2*
0.0-0.2	13	17	9	12	33	51	52
0.2-0.4	1	22	0	4	18	3	2
0.4-0.6	0	3	0	2	7	2	3
0.6-0.8	1	0	0	1	2	0	0
0.8-1.0	85	58	90	82	40	45	43
RTailings	*A1*	*A3*	*A4*	*B4*	*A5*	*C1*	*C2*
0.0-0.2	97	90	74	94	92	98	98
0.2-0.4	0	0	0	3	3	0	0
0.4-0.6	0	0	0	0	1	0	0
0.6-0.8	0	0	0	0	0	0	0
0.8-1.0	3	10	26	3	4	2	2

Table 5.12 *PGE mineral (excluding laurite) mode of occurrence in flotation products of sample A1, A3, C2, A5, C1, B4 and A4. Bracketed values are the number of PGE mineral grains detected.*

	A1 (372)		***A3*** (276)		***A4*** (201)		***B4*** (253)		***A5*** (182)		***C1*** (306)		***C2*** (284)	
RC1	*No. %*	*Area %*	*No. %*	*Area %*	*No. %*	*Area %*	*No. %*	*Area %*	*No. %*	*Area %*	*No. %*	*Area %*	*No. %*	*Area %*
Liberated PGM	62	68	63	64	59	60	67	67	66	85	77	86	81	64
PGM + Liberated BMS	34	29	22	19	34	38	26	28	10	3	9	4	6	4
PGM+(BMS)+Gangue	3	3	15	17	7	2	8	5	23	12	14	10	13	33
	A1 (335)		***A3*** (163)		***A4*** (106)		***B4*** (202)		***A5*** (164)		***C1*** (145)		***C2*** (154)	
RC2	*No. %*	*Area %*	*No. %*	*Area %*	*No. %*	*Area %*	*No. %*	*Area %*	*No. %*	*Area %*	*No. %*	*Area %*	*No. %*	*Area %*
Liberated PGM	81	77	69	59	66	79	80	82	69	64	82	81	85	73
PGM+BMS	13	15	14	14	30	19	13	8	5	5	4	3	0	0
PGM+(BMS)+Gangue	6	8	17	27	4	2	7	10	26	31	14	16	15	27
	A1 (182)		***A3*** (248)		***A4*** (137)		***B4*** (184)		***A5*** (157)		***C1*** (208)		***C2*** (169)	
RC3-5	*No. %*	*Area %*	*No. %*	*Area %*	*No. %*	*Area %*	*No. %*	*Area %*	*No. %*	*Area %*	*No. %*	*Area %*	*No. %*	*Area %*
Liberated PGM	79	78	67	45	75	80	76	78	47	29	64	49	72	50
PGM+BMS	5	6	8	10	15	11	7	5	6	1	0	0	2	0
PGM+(BMS)+Gangue	16	16	26	46	10	9	18	17	46	69	36	51	26	49
	A1 (16)		***A3*** (25)		***A4*** (60)		***B4*** (26)		***A5*** (171)		***C1*** (52)		***C2*** (25)	
RTailings	*No. %*	*Area %*	*No. %*	*Area %*	*No. %*	*Area %*	*No. %*	*Area %*	*No. %*	*Area %*	*No. %*	*Area %*	*No. %*	*Area %*
Liberated PGM	13	1	20	7	20	22	4	2	5	3	8	3	7	20
PGM+BMS	6	1	0	0	3	2	0	0	1	0	0	0	0	0
PGM+(BMS)+Gangue	81	98	80	93	77	76	96	98	95	97	92	97	93	80

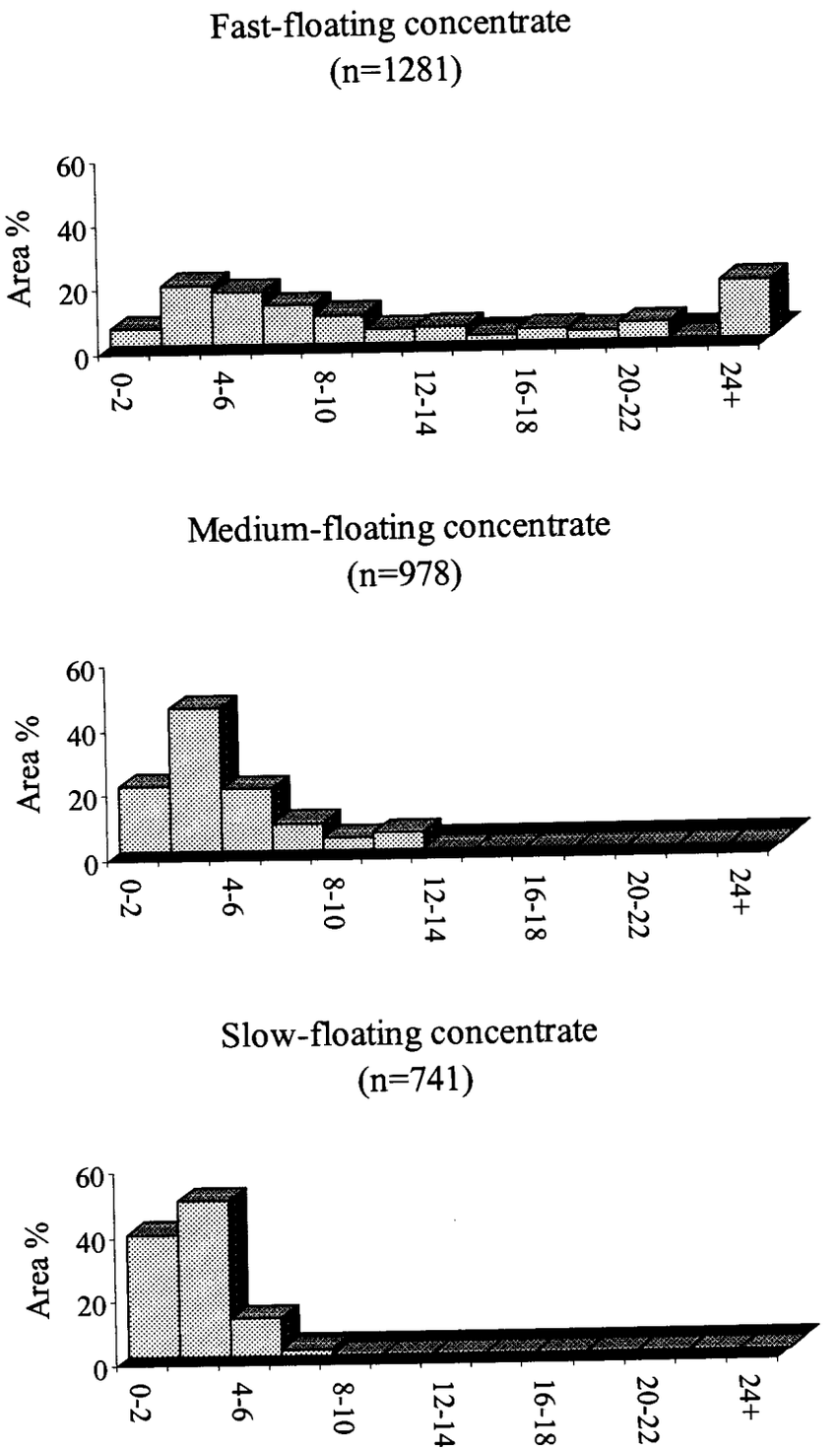

Figure 73 *Grain-size distribution of liberated PGE mineral grains in the combined slow-, medium-, and fast-floating concentrate of samples A1, A3, C1, C2, A5 and B4. (n = number of PGE mineral grains measured)*

Table 5.13 *Median grain diameter based on area percentage results of* ***liberated*** *PGE mineral grains in the flotation products of seven samples. All grain sizes values are reported as equivalent circle diameter in μm. Bracketed value is the number of liberated grains (excluding laurite) analysed in each sample.*

Sample	***RC1***	***RC2***	***RC3-5***	***RT***
A1	7.2 *(168)*	2.9 *(237)*	2.3 *(125)*	1.0 *(2)*
A3	6.6 *(157)*	3.0 *(105)*	1.9 *(146)*	1.9 *(5)*
A4	2.9 *(98)*	2.9 *(58)*	2.1 *(83)*	1.0 *(4)*
B4	4.6 *(131)*	3.0 *(122)*	1.9 *(108)*	1.0 *(1)*
A5	6.0 *(95)*	2.9 *(95)*	3.2 *(29)*	1.8 *(7)*
C1	11.4 *(204)*	3.4 *(112)*	2.5 *(111)*	2.5 *(3)*
C2	5.7 *(214)*	3.6 *(116)*	2.1 *(34)*	1.0 *(1)*

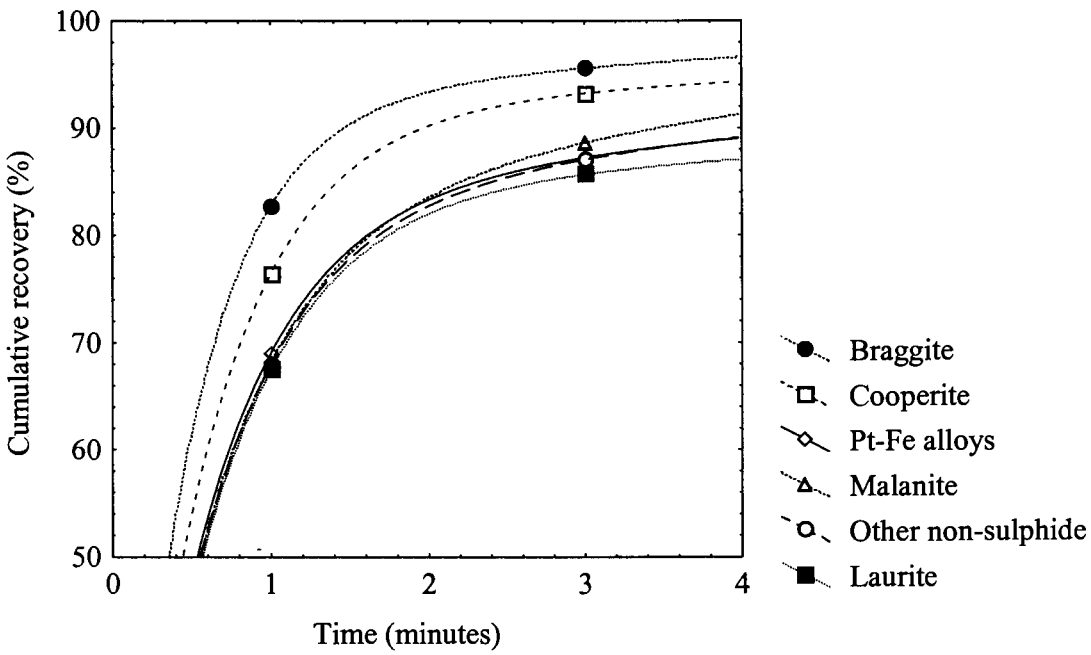

Figure 74 *Time-recovery curves for different PGE mineral phases. 'Other non-sulphide' refers to non-sulphide PGE minerals other than Pt-Fe alloys. A modified Kelsall model (Kelsall, 1961; Marais, 1989) was used to fit the data.*

Table 5.14 *Flotation behaviour of different PGE minerals. An ultimate recovery of 100% was assumed as not enough data points were available for the estimation of four parameters.*

	% Recovery				Cumulative % Recovery			Model parameters			
	RC1	**RC2**	**RC3-5**	**RT**	**RC1**	**RC2**	**RC3-5**	**ϕ**	**k_s**	**k_f**	**Final loss**
Time (mins.)	0-1	1-3	3-20		0-1	1-3	3-20		(min^{-1})	(min^{-1})	
Pt-Pd-S	83	13	4	0	83	96	100	0.09	0.24	2.17	0.00
Pt-S	76	17	6	1	83	93	99	0.09	0.12	1.76	0.00
Pt-Rh-Cu-Ni-S	68	21	11	0	83	89	100	0.22	0.23	1.67	0.00
Ru-S	68	18	10	4	83	86	96	0.17	0.07	1.60	0.00
Pt-Fe alloy	69	18	11	2	83	87	98	0.17	0.12	1.67	0.00
Other non-sulphide	68	19	12	1	83	87	99	0.19	0.14	1.65	0.00

ϕ = *slow-floating fraction*
k_s = *rate of flotation of slow-floating fraction*
k_f = *rate of flotation of fast-floating fraction*
Final loss = Σ*(observed value-predicted value)*^{2}

PGE minerals associated with liberated base-metal sulphide

The ratio $$\frac{\%\ \text{liberated PGEM}}{\%\ (\text{PGEM associated with liberated BMS}) + \%\ (\text{liberated PGEM})}$$

(where PGEM= PGE mineral, BMS=base-metal sulphide) in the slow-, medium- and fast-floating concentrates indicates that liberated PGE minerals are slower to respond to the flotation process than PGE minerals associated with liberated base-metal sulphides (Table 5.15).

Table 5.15 *% liberated PGE minerals as a fraction of (% liberated PGE mineral + PGE mineral associated with liberated base-metal sulphide) in the flotation concentrates of selected samples.*

	A1	*A3*	*A4*	*B4*	*A5*	*C1*	*C2*
RC1	0.70	0.77	0.61	0.71	0.96	0.95	0.94
RC2	0.84	0.81	0.80	0.91	0.93	0.97	1.00
RC3-5	0.93	0.82	0.88	0.93	0.95	1.00	0.99

Flotation behaviour of composite grains

PGE mineral-bearing particles with low combined liberation indices, i.e. those associated with silicate (Figure 76), or rarely chromite, tend to report to the slow-floating concentrates and tailings (Figures 68 and 69) (Tables 5.11 and 5.12).

Degree of exposed surface area

Comparing the amount of PGE mineral that is fully locked, or occur at grain boundaries between two phases, and those located at particle edges, gives a measure of the exposed surface area of PGE mineral in a particle. A composite of the flotation products of the seven samples indicated that of the particles with a combined

liberation index of less than 0.2, 33 per cent in rougher concentrate 1, 35 per cent in rougher concentrate 2, and 35 per cent in combined rougher concentrates 3, 4 and 5 appear to be completely enclosed by gangue, compared to 56 per cent in the tailings (Table 5.16).

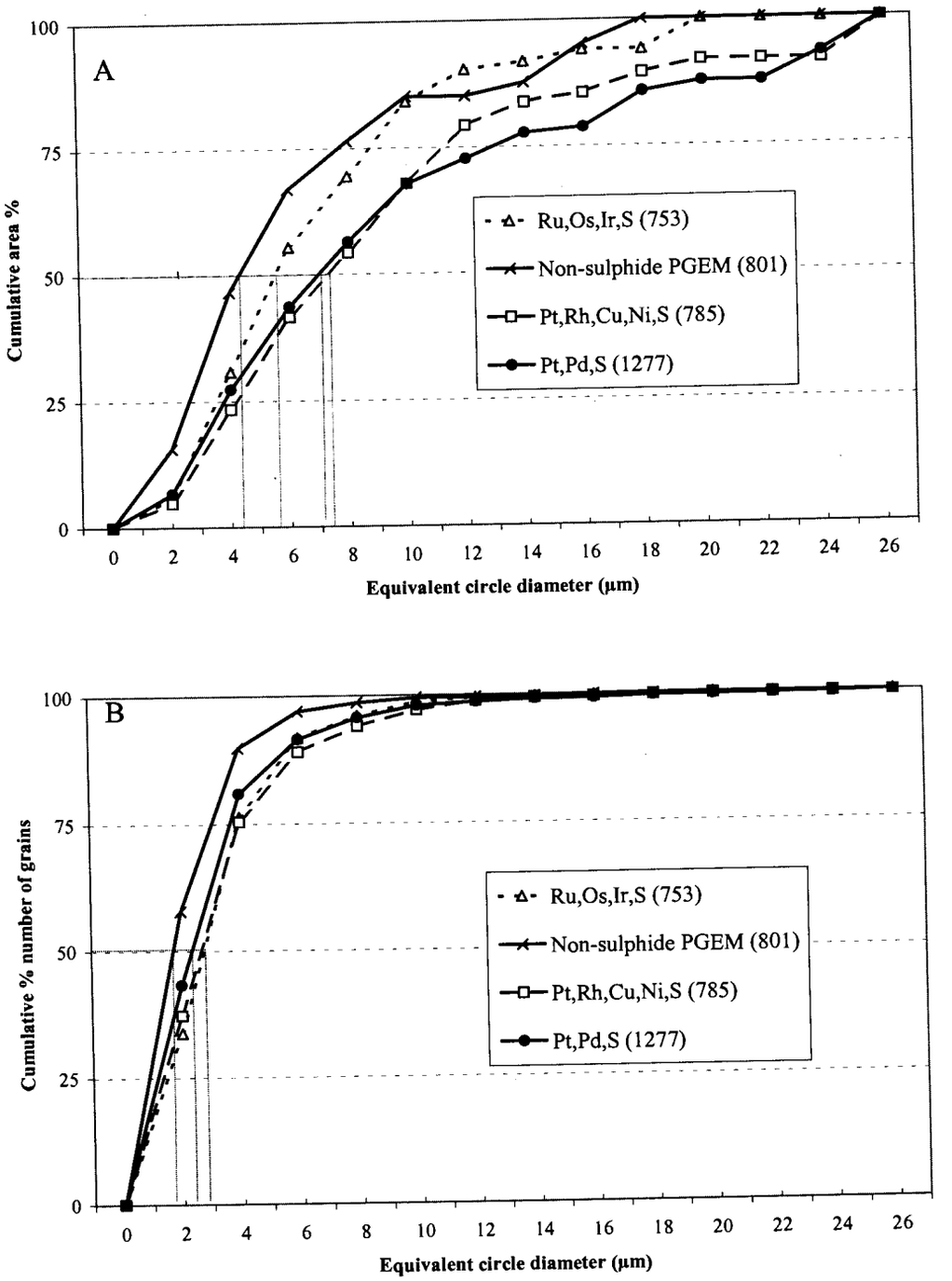

Figure 75 *Grain-size distributions of (Pt,Pd)-sulphide, (Pt,Rh,Cu,Ni)-sulphide, (Ru,Os,Ir)-sulphide and non-sulphide PGE minerals in UG2 chromitite expressed as area % (A) and % number of grains (B). Bracketed values indicate the number of grains on which the distribution is based.*

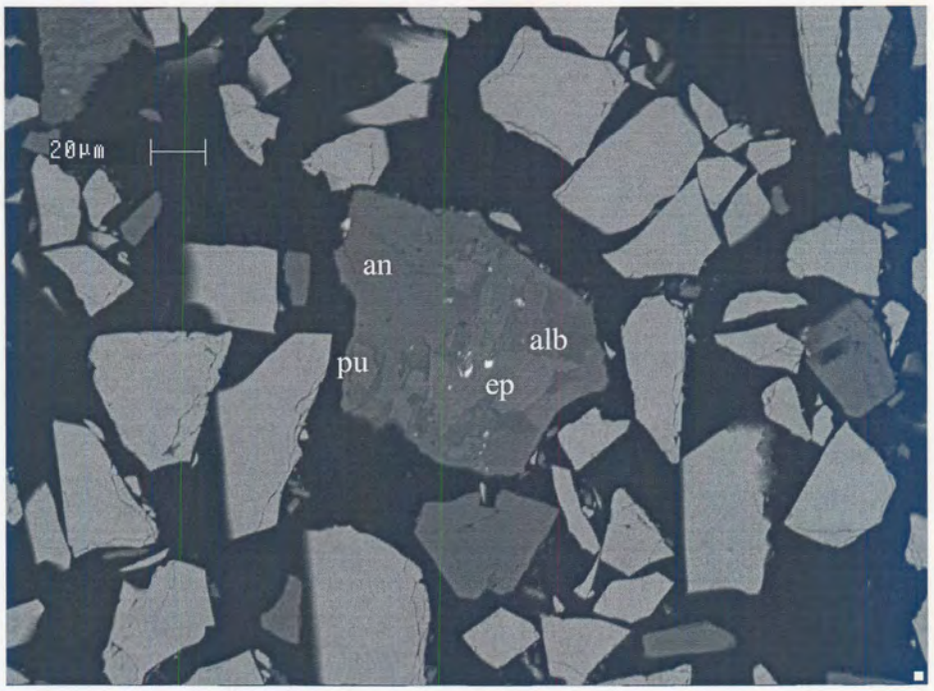

Figure 76 *Pt-Rh-sulpharsenide (bright grains) intergrown with epidote (ep), plagioclase (an) and pumpellyite (pu) in flotation tailings. Backscattered-electron image.*

Table 5.16 *Mode of occurrence of PGE minerals in particles with a combined liberation index of <0.2 in a composite of the flotation products of seven samples.*

PGEM association	*RC1*	*RC2*	*RC3-5*	*RTailings*
Associated with locked BMS	27	26	41	30
At grain edge of gangue	39	39	24	14
Enclosed in gangue	33	35	35	56

Particle size

The effect of particle size on the flotation behaviour of particles with a low combined liberation index (<0.2) is demonstrated by Figure 77. The median equivalent circle diameter of such particles in a composite of the flotation tailings is >40µm, compared to ~30 µm in combined rougher concentrate 3, 4 and 5, and between 10 and 20 µm in rougher concentrates 1 and 2.

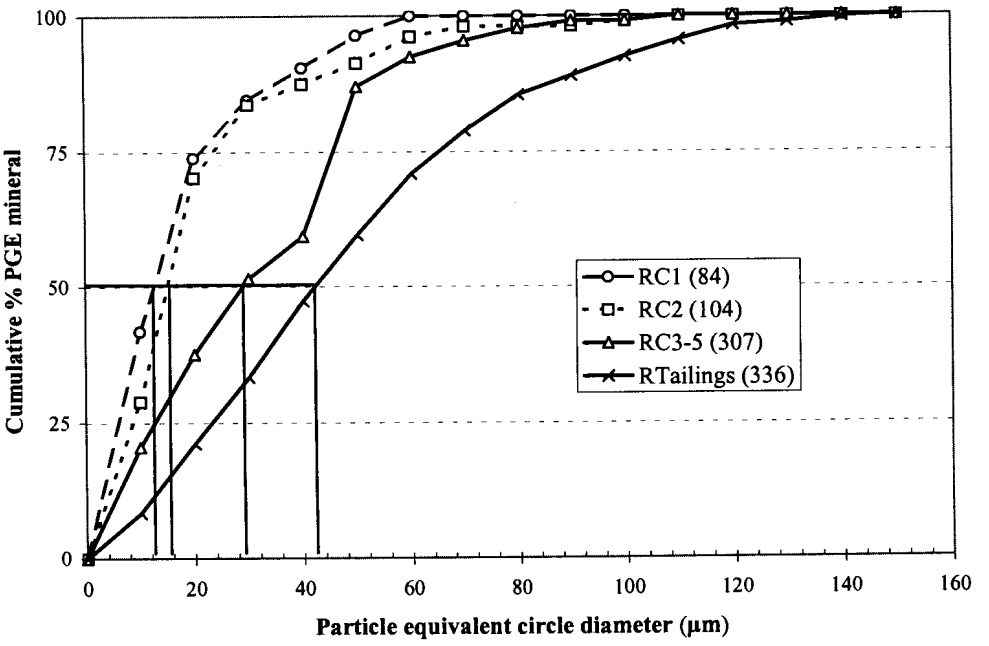

Figure 77 *A comparison of the size distributions of PGE mineral-bearing particles with combined liberation index of <0.2 in the fast-, medium- and slow-floating concentrates and rougher tailings. Bracketed values indicate the number of particles on which the distribution is based.*

5.5 Milling behaviour

5.5.1 Milling curves

The response of the fourteen samples to milling differs considerably, with sample A1 requiring about 120 minutes to achieve 80% <75µm, compared to just 40 minutes for sample A5 (Table 5.1Y and Figure 78, detailed results in Appendix I, Table 1).

5.5.2 Screen analysis

The screen analyses of the fourteen samples under investigation, milled to 80% <75µm, can be seen in Table 2, Appendix I. In all of the samples between 40 and 50 per cent of the sample mass is finer than 38 µm, and less than 2 per cent coarser than 106 µm. Differences between the samples are small.

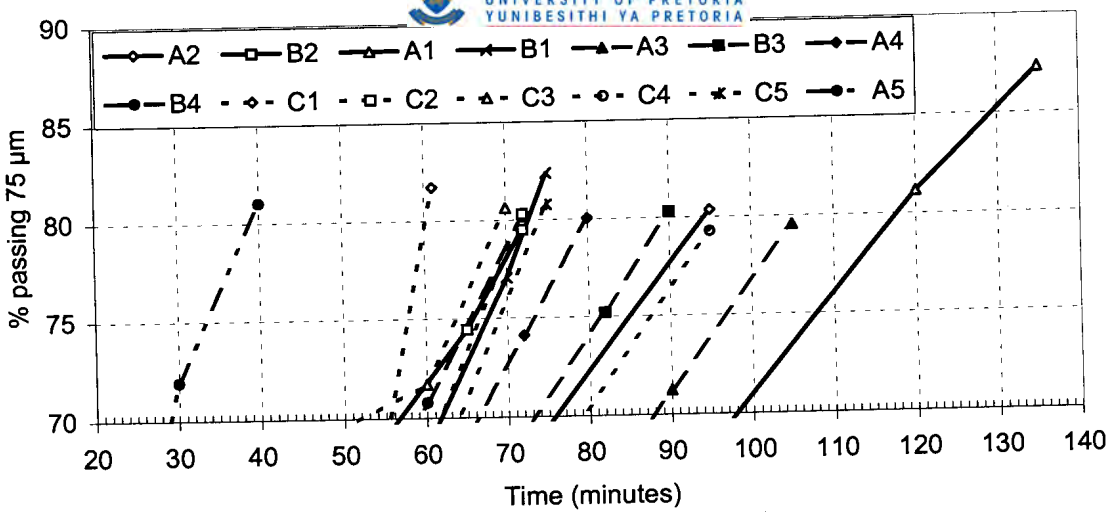

Figure 78 *Milling curves for fourteen samples of UG2 chromitite.*

——— *Normal UG2 (A1, A2, B1, B2)* - - - -*Sintered UG2 (A3, B3, B4, A4)*

..... *UG 2 from area C (C1, C2, C3, C4, C5)* — · · — *Cataclastic UG2 (A5)*

5.6 Flotation behaviour

5.6.1 Mass recoveries

Mass recoveries from the fourteen test samples at 80% <75µm range from 2.3 to 3.7 per cent after 1 minute flotation, and 10.3 to 14.7 per cent after 20 minutes (Table 1, Appendix J).

5.6.2 Cr_2O_3 recoveries

Cr_2O_3 values for the feed material determined from mass balance calculations, compare well with the assay values, with relative differences below 3 per cent in all of the samples, indicating a high level of precision during analytical and flotation procedures (Table 2, Appendix J). Cr_2O_3 recoveries after 1 minute flotation were below 3 per cent for all fourteen samples (Figure 79), with Cr_2O_3 contents of the combined concentrate ranging between 13 and 25 per cent (Table 2, Appendix J). After 20 minutes flotation recoveries had increased to between 6 and 9 per cent, with a Cr_2O_3 grade for the combined concentrate similar to that after 1 minute.

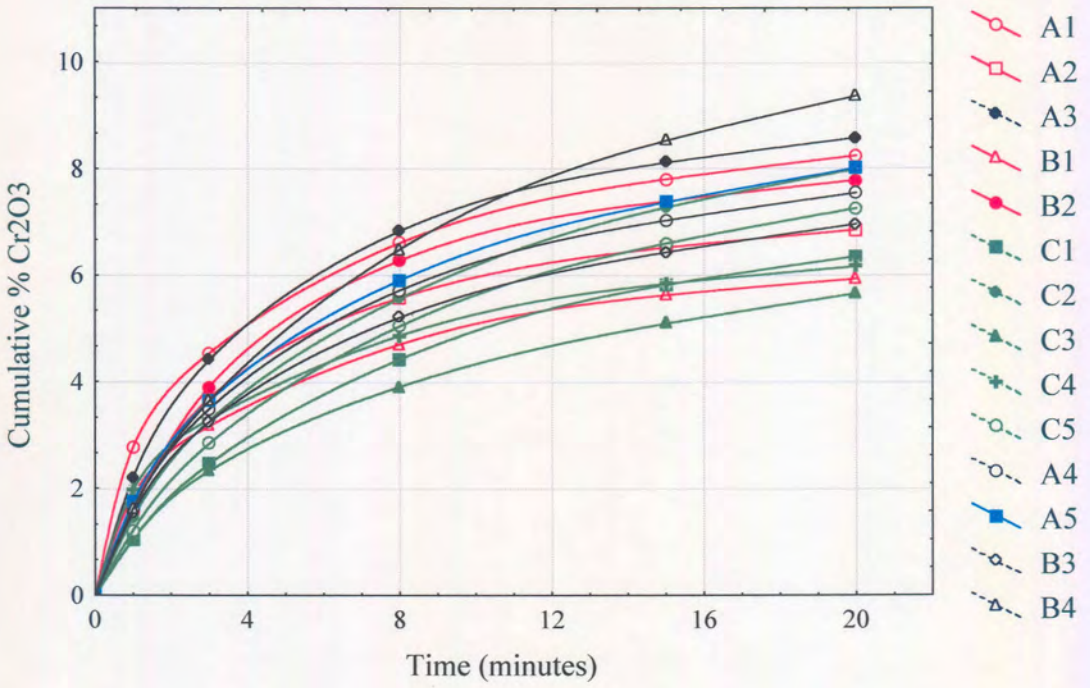

Figure 79 *Cr_2O_3 recoveries from fourteen UG2 chromitite samples milled to 80% <75 μm.*

5.6.3 Silicate gangue recoveries

By subtracting the amount of chromite and sulphide in each flotation product from the total dry mass, the behaviour of the silicate gangue component can be evaluated. Total silicate gangue recoveries after 20 minutes flotation ranged from 15 to 27 per cent (Figure 80 and Table 3, Appendix J). In general, silicate gangue recoveries are the lowest from samples A1, A2, B1 and B2 (indicated in red) with an increase in samples A3, B3, A4 and B4 (indicated in black) and A5 (blue). The highest silicate gangue recoveries were observed in samples from area C (indicated in green).

5.6.4 Copper recoveries

The Kelsall model fits the data well with loss values for all samples of less than 0.2 (Table 5, Appendix J). The differences between the calculated and assayed copper values are unacceptably large in some cases (Table 4, Appendix J). Nevertheless,

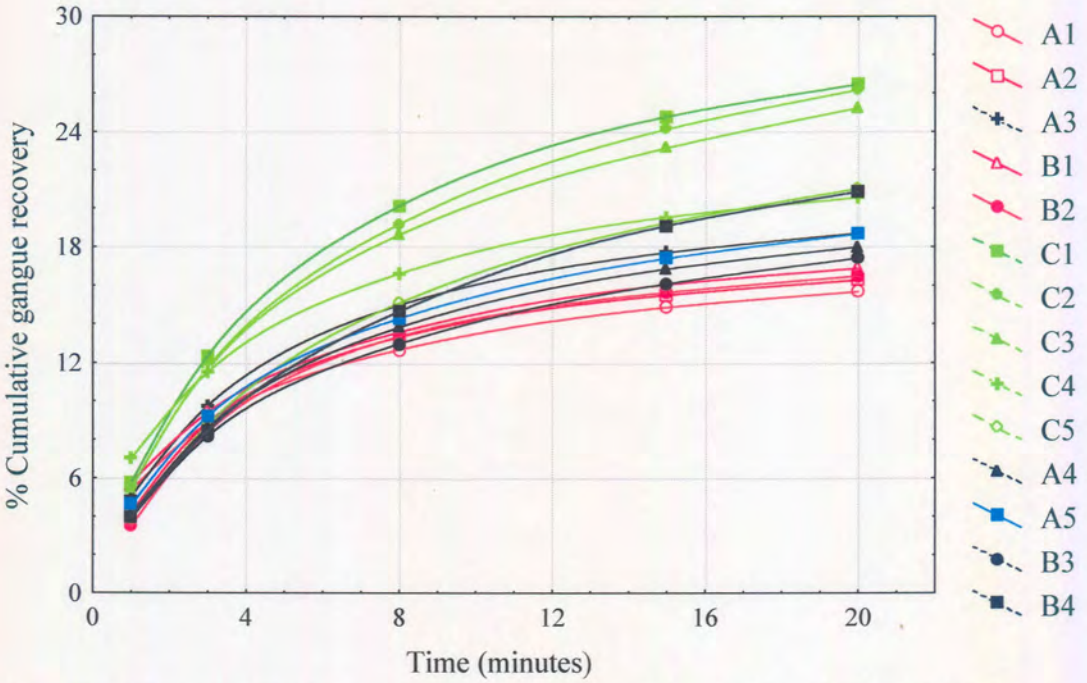

Figure 80 *Silicate recoveries from fourteen UG2 chromitite samples milled to 80% <75 µm.*

significant differences were observed between different groups of samples, with low ultimate recoveries for samples from Area C (Table 5.1Z and Figure 81). These samples are also characterised by relatively low fast-floating rate constants. Note the lower concentrate grades of the samples from Area C at all recoveries (Figure 82 and Table 4, Appendix J).

5.6.5 Nickel recoveries

Acid soluble nickel concentrations for the milled feed material, determined from mass balance calculations, compare well with the assay values, indicating a high level of precision during analytical and flotation procedures (Table 6, Appendix J). Loss values were below 0.3 for all samples (Table 7, Appendix J). However, due to the presence of nickel-bearing stainless steel particles in the flotation products, acid soluble nickel values for these samples are of little use. As the stainless steel particles reported mostly to the flotation tailings, acid soluble nickel recoveries are poor for all samples (Table 5.1AA).

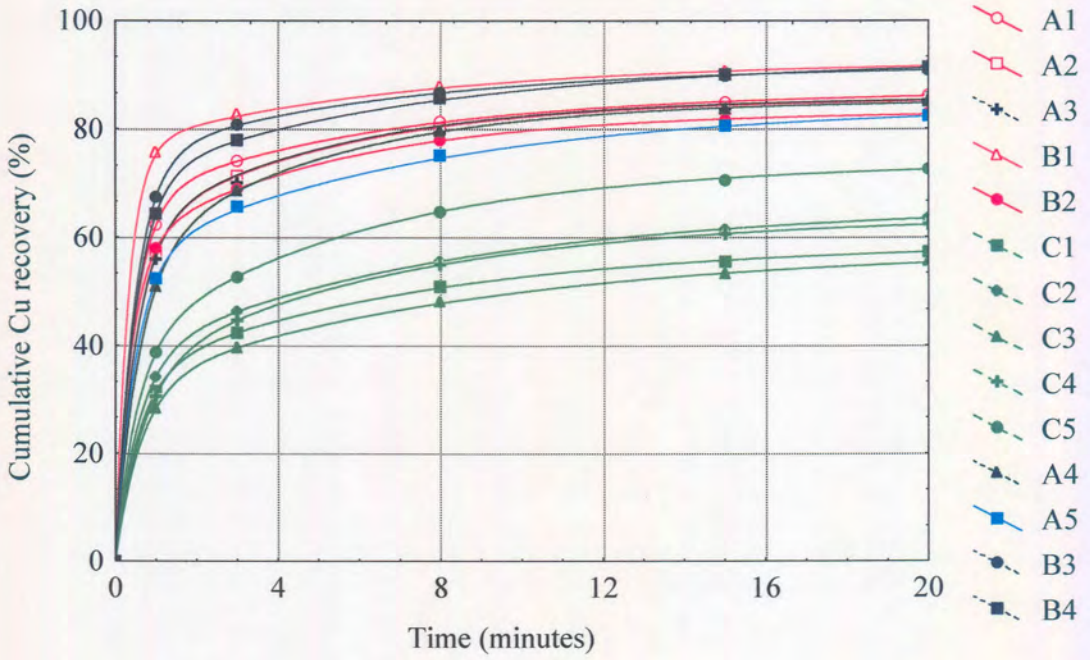

Figure 81 *Time-recovery curves for copper from fourteen samples of UG2 chromitite milled to 80% <75µm. A modified Kelsall model (Kelsall, 1961; Marais, 1989) was used to fit the data.*

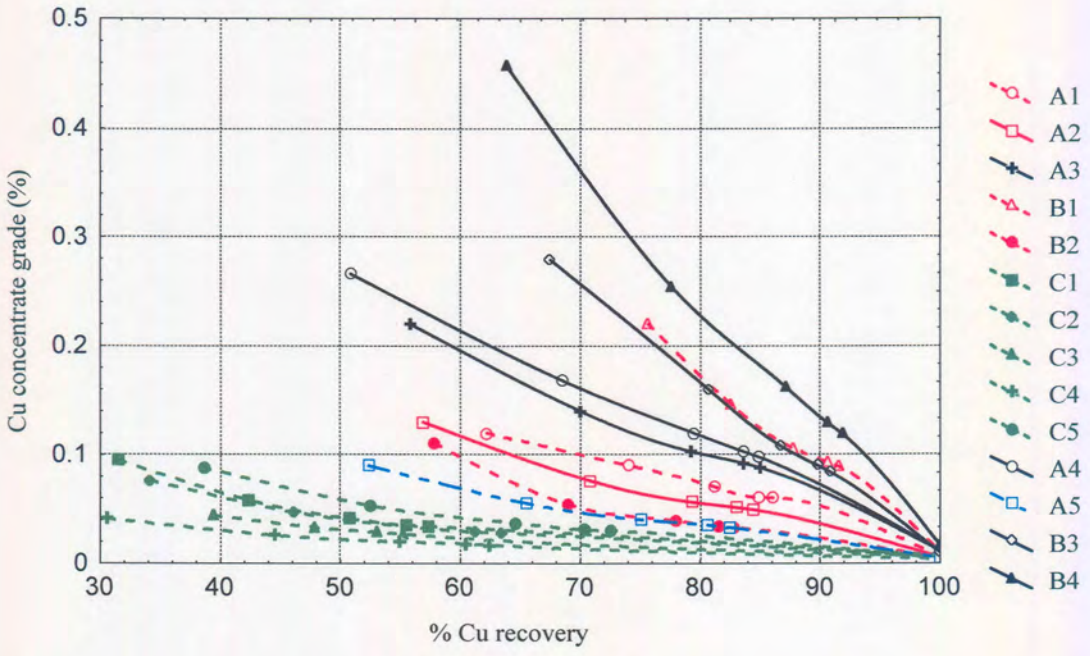

Figure 82 *Grade-recovery curves for copper for fourteen samples of UG2 chromitite milled to 80% <75µm.*

5.6.6 Total PGE+Au recovery

PGE+Au flotation results are given in Tables 8 and 9 of Appendix J and summarised in Table 5.1AB. Calculated and assayed PGE+Au values generally compare well. The Kelsall model fits the data exceptionally well with loss values of less than 0.1 for all samples. With the exception of sample A5, the ultimate PGE+Au recoveries predicted for all the samples are relatively high, ranging between 89 and 96 per cent (Figure 83). The non-floating fraction in sample A5 is 32 per cent with a 40 per cent recovery of fast-floating material. Samples A4 and B4 are characterised by relatively small recoveries of fast-floating material, 60 and 57 per cent respectively, compared to the rest of the samples at 63 to 80 per cent. Concentrate grades for all the samples are less than 80 g/t at 90% recovery (Figure 84).

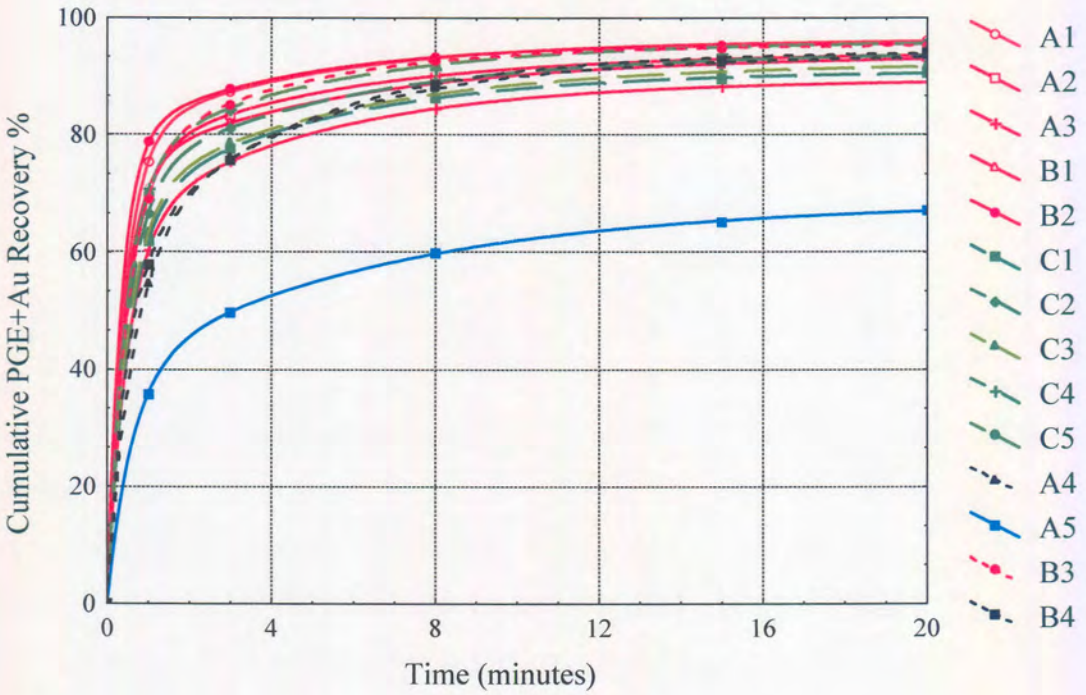

Figure 83 *PGE+Au time-recovery curves for fourteen UG2 chromitite samples milled to 80% <75µm. Data fitted according to a modified Kelsall model (Kelsall, 1961; Marais, 1989).*

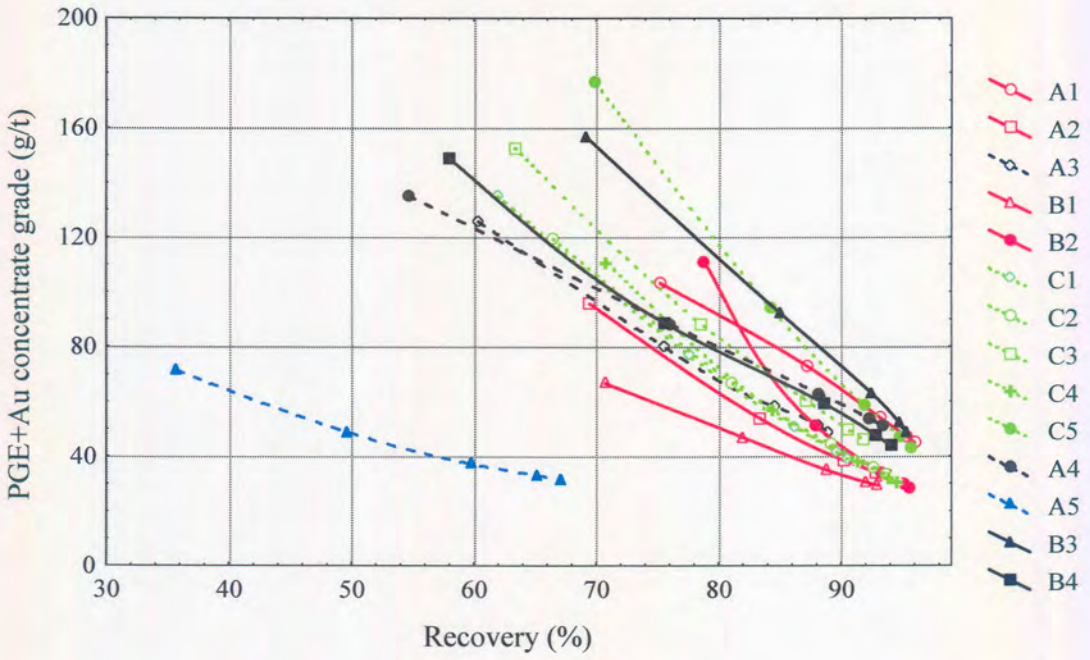

Figure 84 *Grade-recovery curves for PGE+Au for fourteen samples of UG2 chromitite milled to 80% <75μm.*

5.6.7 Platinum, palladium and rhodium

To generate enough material for individual PGE analysis, rougher concentrates 3, 4 and 5 were combined (Tables 10 to 15, Appendix J). Consequently only three data points were available for modelling of the flotation data. Assuming an ultimate recovery of 100 for platinum, palladium and rhodium makes it possible to obtain values for ϕ, k_f and k_s which can be used to compare the flotation behaviour of these elements. As PGE+Au recoveries after 20 minutes were very similar to ultimate recoveries, it was assumed that recoveries of the individual PGEs after 20 minutes approximate ultimate recoveries. These values, together with ϕ, were then used to calculate the values for R_f, R_s and 100-U reported in Table 5.1 AC to AE. The alternative approach of direct substitution of recovery after 20 minutes for U in the model equation, gave poor results.

For most samples, the amount of fast-floating platinum (Figure 85) is very similar to that for palladium (Figure 86). Notable exceptions are samples A4 and B4, which are characterised by very small fast-floating palladium fractions, with relatively large slow-floating palladium fractions. The non-floating fractions of platinum and

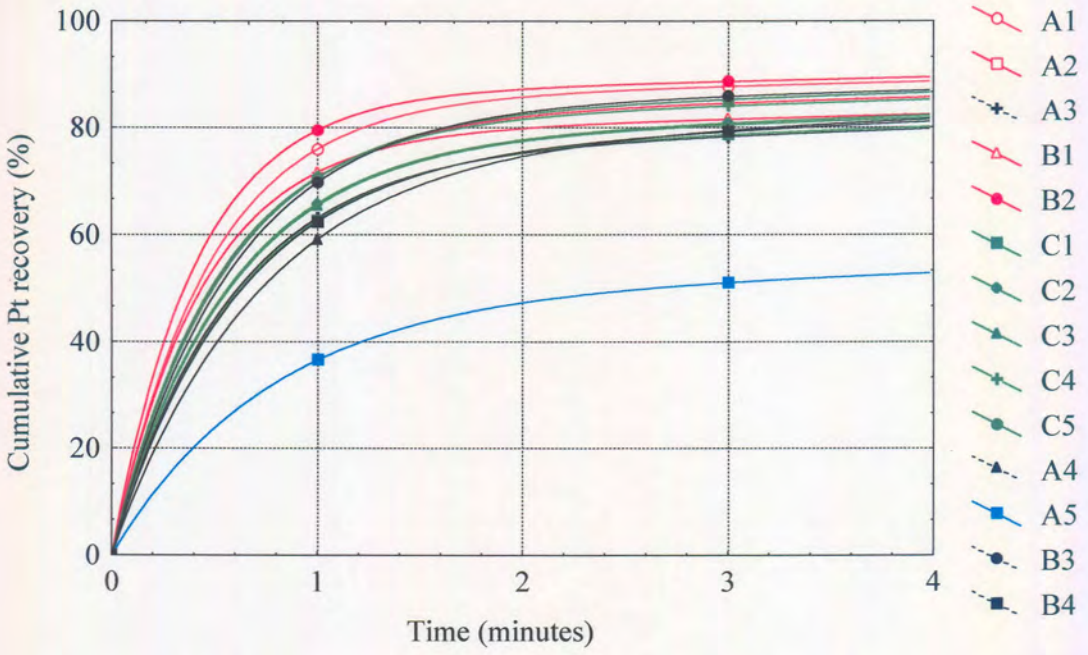

Figure 85 *Platinum time-recovery curves for fourteen UG2 chromitite samples milled to 80% <75µm. Data fitted using a modified Kelsall model (Kelsall, 1961; Marais, 1989) assuming an ultimate recovery of 100 per cent.*

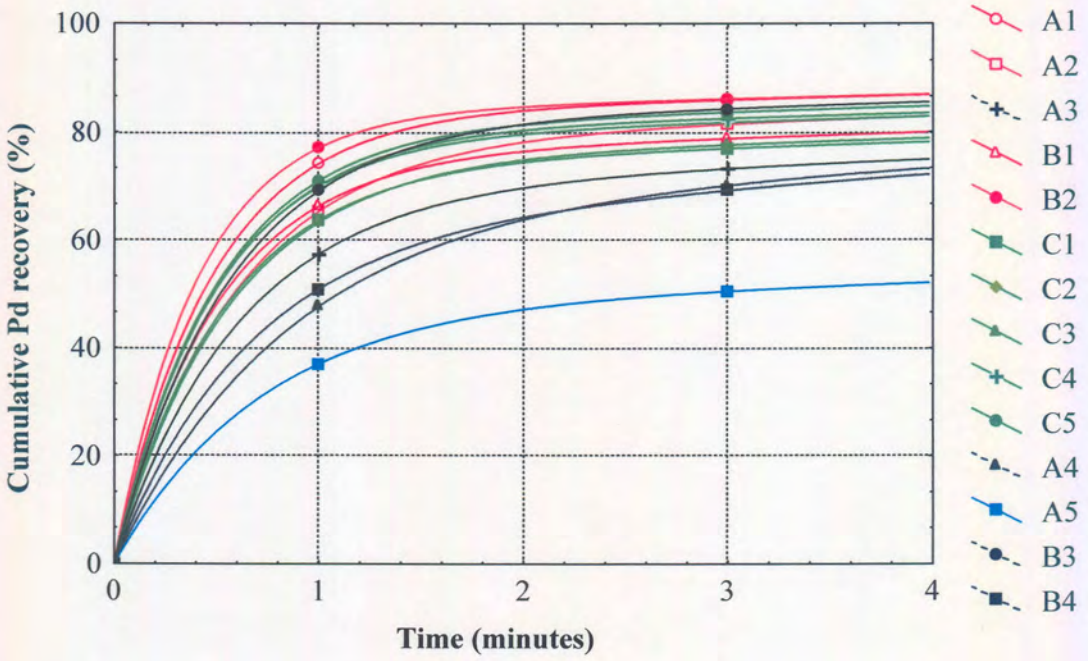

Figure 86 *Palladium time-recovery curves for fourteen UG2 chromitite samples milled to 80% <75µm. Data fitted using a modified Kelsall model (Kelsall, 1961; Marais, 1989) assuming an ultimate recovery of 100 per cent.*

palladium are very similar in all samples. Rhodium recoveries (Figure 87) seem to follow the same trend as palladium, but, as explained in section 4.4 there are large uncertainties associated with estimating rhodium recoveries.

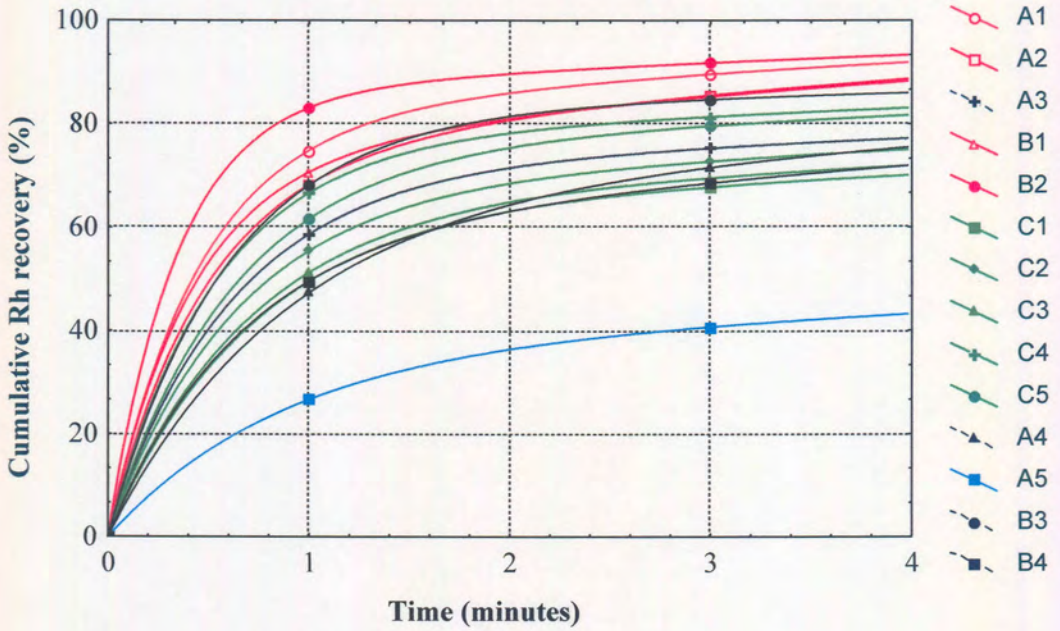

Figure 87 *Rhodium time-recovery curves for fourteen UG2 chromitite samples milled to 80% <75μm. Data fitted using a modified Kelsall model (Kelsall, 1961; Marais, 1989) assuming an ultimate recovery of 100 per cent.*